YARA LUIZA COELHO

CARACTERIZAÇÃO CINÉTICA E TERMODINÂMICA DE FORMAÇÃO DAS ESTRUTURAS SUPRAMOLECULARES: LACTOFERRINA-CORANTES FENOTIAZÍNICOS E LACTOFERRINA-POLISSACARÍDEOS

Tese apresentada à Universidade Federal de Viçosa, como parte das exigências do Programa de Pós-Graduação em Agroquímica, para obtenção do título de *Doctor Scientiae.*

Orientador: Luis Henrique Mendes da Silva

Coorientadoras: Ana Clarissa dos Santos Pires
Maria do Carmo Hespanhol

VIÇOSA - MINAS GERAIS
2020

Ficha catalográfica preparada pela Biblioteca Central da Universidade Federal de Viçosa - Câmpus Viçosa

T
C672c
2020

Coelho, Yara Luiza, 1990-
Caracterização cinética e termodinâmica de formação das estruturas supramoleculares : lactoferrina-corantes fenotiazínicos e lactoferrina-polissacarídeos / Yara Luiza Coelho. – Viçosa, MG, 2020.
183f. : il. (algumas color.) ; 29 cm.

Inclui apêndices.
Orientador: Luis Henrique Mendes da Silva.
Tese (doutorado) - Universidade Federal de Viçosa.
Inclui bibliografia.

1. Lactoferrina. 2. Corantes. 3. Polissacarídeos.
I. Universidade Federal de Viçosa. Departamento de Química. Programa de Pós-Graduação em Agroquímica. II. Título.

CDD 22 ed. 541.226

YARA LUIZA COELHO

CARACTERIZAÇÃO CINÉTICA E TERMODINÂMICA DE FORMAÇÃO DAS ESTRUTURAS SUPRAMOLECULARES: LACTOFERRINA-CORANTES FENOTIAZÍNICOS E LACTOFERRINA-POLISSACARÍDEOS

Tese apresentada à Universidade Federal de Viçosa, como parte das exigências do Programa de Pós-Graduação em Agroquímica, para obtenção do título de *Doctor Scientiae*.

APROVADA: 17 de fevereiro de 2020.

Assentimento:

Yara Luiza Coelho
Autora

Luis Henrique Mendes da Silva
Orientador

AGRADECIMENTOS

Agradeço à Universidade Federal de Viçosa (UFV), ao Departamento de Química, ao Programa de Pós-Graduação em Agroquímica e ao Laboratório Química Verde Coloidal e Macromolecular (QUIVECOM) pela oportunidade oferecida de desenvolvimento deste trabalho e ter proporcionado a minha formação em nível de doutorado.

Agradeço às agências de fomento. O presente trabalho foi realizado com apoio da Coordenação de Aperfeiçoamento de Pessoal de Nível Superior – Brasil (CAPES) – Código de Financiamento 001. Agradeço também ao Instituto Nacional de Ciências e Tecnologias Analíticas Avançadas (INCTAA), à Fundação de Amparo à Pesquisa do Estado de Minas Gerais (FAPEMIG), ao Conselho Nacional de Desenvolvimento Científico e Tecnológico (CNPq) e à Financiadora de Estudos e Projetos (FINEP) pelo apoio financeiro aos projetos.

Agradeço imensamente ao meu orientador Prof. Luis Henrique Mendes da Silva, que também é personagem central nessa história, que ultrapassa os quatro anos de doutorado. Obrigada pela oportunidade, orientação, incentivo e principalmente por me fazer acreditar. Sua dedicação e postura profissional é fonte de admiração e inspiração que fizeram deste trabalho uma atividade gratificante.

À Profª. Ana Clarissa dos Santos Pires por sua coorientação e amizade, sou imensamente grata por seu apoio e confiança durante todos esses anos.

Também não poderia deixar de destacar que todas as conquistas que alcancei em minha vida, sobretudo esta, tiveram como alicerces minha família: minha mãe Sonia, meu pai Fernando e minhas irmãs, em especial Márcia, Cláudia e Karla. Sem o apoio incondicional e incentivo deles, não teria forças para superar os desafios ao longo do processo. Aproveito novamente, para pedir desculpas pela ausência, pelas preocupações e angústias que os fiz passar durante essa jornada. Perdoem-me por tudo! E obrigada por tudo!

Agradeço também aos meus sobrinhos João e Luiz, pelo carinho, e por tantos favores prestados. A tia ama muito vocês!

Ao Ronan, pela dedicação, amor, paciência e por tantos momentos privados em prol das minhas realizações. Sem o seu apoio e incentivo jamais teria conseguido. Essa conquista é sua também, meu eterno incentivador!

Ao Álvaro, meu irmão de coração, agradeço por toda atenção, paciência, incentivo, ensinamentos e amizade. Obrigada pelo companheirismo, que tornou todo o esforço muito gratificante durante o processo doutoral.

À Isabela e ao Pedro, pelas fundamentais contribuições na realização deste trabalho, e por tantos ensinamentos profissionais e pessoais. A amizade e generosidade de vocês fizeram meus dias mais felizes!

À Jaqueline e à Eliara, do Departamento de Tecnologia de Alimentos da UFV, pela disponibilidade e generosidade sempre que precisei.

Às professoras Débora Guimarães de Oliveira e Márcia Cristina Teixeira Ribeiro Vidigal e ao professor Leandro Gutierrez Rizzi por aceitarem o convite para participar da defesa desta tese.

Por fim, agradeço infinitamente a Deus, por tudo!

BIOGRAFIA

Yara Luiza Coelho, filha de Fernando Luiz Coelho e Sonia Aparecida Leite Coelho, nasceu em 19 de novembro de 1990, na cidade de Guidoval, Minas Gerais.

Em fevereiro de 2009 ingressou no curso de Licenciatura em Química na Universidade do Estado de Minas Gerais (UEMG) e em fevereiro de 2013 obteve o título de Licenciada em Química. Nesta instituição foi bolsista de iniciação científica financiada pela FAPEMIG no período entre março de 2011 e janeiro de 2013.

No período de fevereiro de 2013 a março de 2014 atuou como professora de química para o ensino médio em escolas estaduais e como bolsista de apoio técnico nível II na UEMG.

Em março de 2014 iniciou o mestrado em Físico-Química no Programa de Pós-Graduação em Agroquímica, na Universidade Federal de Viçosa, obtendo seu título em fevereiro de 2016.

Em março de 2016 matriculou-se no doutorado em Físico-Química no Programa de Pós-Graduação em Agroquímica na Universidade Federal de Viçosa, submetendo-se à defesa de tese em fevereiro de 2020.

Durante o processo de mestrado e doutorado participou de vários projetos que resultaram em 13 publicações em periódicos, apresentadas no Apêndice D.

“Dizem que antes de um rio entrar no mar, ele treme de medo.
Olha para trás, para toda a jornada que percorreu, para os cumes,
as montanhas, para o longo caminho sinuoso que trilhou
através de florestas e povoados, e vê à sua frente um oceano tão vasto,
que entrar nele nada mais é do que desaparecer para sempre.
Mas não há outra maneira. O rio não pode voltar.
Ninguém pode voltar. Voltar é impossível na existência.
O rio precisa se arriscar e entrar no oceano.
E somente quando ele entra no oceano é que o medo desaparece,
porque apenas então o rio saberá que não se trata de
desaparecer no oceano, mas de tornar-se oceano."
(Osho)

RESUMO

COELHO, Yara Luiza, D.Sc., Universidade Federal de Viçosa, fevereiro de 2020. **Caracterização cinética e termodinâmica de formação das estruturas supramoleculares: lactoferrina-corantes fenotiazínicos e lactoferrina-polissacarídeos**. Orientador: Luis Henrique Mendes da Silva. Coorientadoras: Ana Clarissa dos Santos Pires e Maria do Carmo Hespanhol.

A manifestação da vida é baseada principalmente no reconhecimento molecular. Consequentemente, elucidar a cinética e a termodinâmica das interações proteína-ligante é estratégico para compreensão e modulação dos sistemas biológicos. Além disso, a formação de estruturas supramoleculares é muito importante em aplicações industriais, como processos de formação e estabilização de emulsões e encapsulamento. Assim, neste trabalho avaliou-se a termodinâmica e a cinética de interação entre a lactoferrina (BLF) e dois grupos de ligantes: corantes fenotiazínicos (azul de metileno (MB) e azure A (AZA)) e polissacarídeos (carboximetilcelulose (CMC) e kappa-carragena (κCG)), combinando dados de ressonância plasmônica de superfície (SPR), calorimetria de titulação isotérmica (ITC) e espectroscopia de fluorescência (EF). O trabalho foi dividido em três artigos: no primeiro, foi feito um estudo comparativo da interação entre a BLF e os corantes MB e AZA, utilizando múltiplas técnicas (SPR, EF e ITC), visando elucidar o mecanismo de ligação desses corantes à BLF e às contribuições dos grupos CH_3 para essa interação. No segundo, investigou-se a cinética e a termodinâmica da interação BLF-CMC, utilizando EF e SPR. Por fim, no terceiro artigo foi estudado a energética e a dinâmica de formação dos complexos BLF-κCG, na ausência e presença de KCl, por meio das técnicas de EF e SPR. Acerca da interação BLF-corantes fenotiazínicos, constatou-se que apesar das semelhanças estruturais entre os corantes, os parâmetros termodinâmicos de ligação BLF-AZA foram maiores em magnitude comparados ao sistema BLF-MB. Os resultados obtidos por SPR e EF indicaram que os fatores entrópicos eram as únicas forças motrizes da interação. No entanto, a ITC mostrou que há uma forte contribuição entálpica associada à interação com a holo-BLF. Embora a formação dos complexos de transição BLF-MB e BLF-AZA a partir da associação dos ligantes livres exigiu parâmetros energéticos muito semelhantes ($\Delta G^{\ddagger}_{\mathrm{a,MB}}$ = 51,84 e $\Delta G^{\ddagger}_{\mathrm{a,AZA}}$ = 50,7 kJ mol^{-1}), na dissociação estes parâmetros foram dependentes do número de grupos CH_3 na estrutura dos corantes ($\Delta G^{\ddagger}_{\mathrm{d,MB}}$ = 81,4 e $\Delta G^{\ddagger}_{\mathrm{d,AZA}}$ = 74,93 kJ mol^{-1}). Quanto à interação BLF-CMC, o estudo cinético sugeriu que a formação do complexo ativado a temperaturas ≤ 289,2 K foi dominada pela energia liberada pelas interações específicas entre a proteína e o polissacarídeo. Embora os dados de SPR

tenham demonstrado que a formação dos complexos BLF-CMC foi conduzida entropicamente ($57 \leq T\Delta S^{o}_{SPR} \leq 60$ kJ mol^{-1}), os ensaios de EF revelaram valores negativos ΔH^{o}_{EF} até 293,2 K e positivos em temperaturas ≥ 298,2 K, e $-58 \leq T\Delta S^{o}_{EF} \leq 230$ kJ mol^{-1}. Por fim, o estudo da interação BLF-κCG mostrou que a formação do complexo foi entalpicamente dirigida ($\Delta H^{o}_{SPR} = -81$ kJ mol^{-1}) e a comparação entre os dados termodinâmicos obtidos por SPR e EF revelou que a interação BLF-κCG ocorreu em vários sítios da BLF. Já os parâmetros cinéticos mostraram que a interação ocorreu através da formação de um complexo de transição e que esse processo foi mais rápido a partir da associação das moléculas livres. A mudança na força iônica alterou a forma como a BLF e a κCG interagem, tornando a ligação um processo de uma única etapa.

Palavras-chave: Lactoferrina. Corantes fenotiazínicos. Polissacarídeos.

ABSTRACT

COELHO, Yara Luiza, D.Sc., Universidade Federal de Viçosa, February, 2020. **Kinetic and thermodynamic characterization of the supramolecular structures formation: lactoferrin-phenothiazine dyes and lactoferrin-polysaccharides**. Adviser: Luis Henrique Mendes da Silva. Co-advisers: Ana Clarissa dos Santos Pires and Maria do Carmo Hespanhol.

Life manifestation is based mainly on molecular recognition. Consequently, the elucidation of the kinetics and thermodynamics of the protein-ligand interactions is strategic for the comprehension and modulation of biological systems. Besides that, the formation of supramolecular structures is very important to industrial applications, such as, formation and stabilization of emulsions, and encapsulation. Therefore, in this work, it was evaluated the thermodynamics and kinetics of the interaction between lactoferrin (BLF) and two groups of ligands: phenothiazine dyes (methylene blue (MB) and azure A (AZA)) and polysaccharides (carboxymethylcellulose (CMC) and κ-carrageenan (κCG)); combining surface plasmon resonance (SPR), isothermal titration calorimetry (ITC), and fluorescence spectroscopy (FS) data. The work was divided into three articles: in the first one, the comparative study of the interaction between the MB and AZA dyes were made, using multiple techniques (SPR, FS, and ITC), aiming the elucidation of the binding mechanism between these dyes and BLF, and contributions of the CH_3 groups to this interaction. In the second one, the kinetics and thermodynamics of the BLF-CMC interaction were investigated, using FS, and SPR. Finally, in the third article, it was studied the energetics and dynamics of the formation of BLF-κCG complexes, in the absence and presence of KCl, via FS and SPR techniques. Concerning the BLF-phenothiazine dyes interaction, it was verified that, although the similarity between the dyes structures, the thermodynamic parameters for the BLF-AZA binding was higher in magnitude when compared to the BLF-MB system. The results obtained from SPR and FS indicated the entropic factors were the only driving forces of the interaction. However, the ITC showed there is a strong enthalpic contribution associated with the interaction with the holo-BLF. Although the formation of the BLF-MB and BLF-AZA transition complexes, from the association of free ligands, requires similar energetic parameters ($\Delta G^{\ddagger}_{a,MB}$ = 51.84 and $\Delta G^{\ddagger}_{a,AZA}$= 50.7 kJ mol^{-1}), in the dissociation, these parameters depended on the number of CH_3 groups in the dye structure ($\Delta G^{\ddagger}_{d,MB}$ = 81.4 and $\Delta G^{\ddagger}_{d,AZA}$ = 74.93 kJ mol^{-1}). As for the BLF-CMC interaction, the kinetic study suggested the formation of the activated complex at temperatures ≤ 289.2 K was dominated by the energy released by specific interactions between the protein and polysaccharide. Although the SPR data have shown the formation of the BLF-CMC

complex was entropy-driven ($57 \leq T\Delta S^{o}_{SPR} \leq 60$ kJ mol^{-1}), the FS assays revealed negative ΔH^{o}_{FS} values until 293.2 K, and positive values in temperatures ≥298.2 K, and $-58 \leq T\Delta S^{o}_{FS} \leq 230$ kJ mol^{-1}. Finally, the study of the BLF-κCG interaction showed the complex formation was enthalpy-driven ($\Delta H^{o}_{SPR} = -81$ kJ mol^{-1}), and the comparison between the thermodynamic data obtained by SPR and FS revealed the interaction occurs in various sites of BLF. While the kinetic parameters showed the interaction occurs through the formation of a transition complex and this process is faster from the association of the free molecules. The change in the ionic strength altered the way BLF and κCG interact, making the binding a one-step process.

Keywords: Lactoferrin. Phenothiazine dyes. Polysaccharides.

LISTA DE FIGURAS

LISTA DE TABELAS

LISTA DE ABREVIATURAS E SÍMBOLOS

CAPÍTULO 1

$[A]$: concentração de analito

AZA: azure A

BLF: lactoferrina bovina

BSA: albuminas do soro bovino

CMC: carboximetilcelulose

ΔH^0: variação da entalpia padrão de interação

ΔH_{obs}: variação de entalpia observada

ΔH_{ap-int}: variação de entalpia aparente de interação

ΔG^0: variação da energia livre de Gibbs padrão de interação

ΔS^0: a variação da entropia padrão de interação

$\Delta H^{\ddagger}$: variação da entalpia de ativação

$\Delta H_a^{\ddagger}$: variação da entalpia de ativação para o processo de associação

$\Delta H_d^{\ddagger}$: variação da entalpia de ativação para o processo de dissociação

$\Delta G^{\ddagger}$: variação da energia livre de Gibbs de ativação

$\Delta G_a^{\ddagger}$: variação da energia livre de Gibbs de ativação para o processo de associação

$\Delta G_d^{\ddagger}$: variação da energia livre de Gibbs de ativação para o processo de dissociação

$\Delta S^{\ddagger}$: variação da entropia de ativação

$\Delta S_a^{\ddagger}$: variação da entropia de ativação para o processo de associação

$\Delta S_d^{\ddagger}$: variação da entropia de ativação para o processo de dissociação

dU: energia interna

$E^{\ddagger}$: energia de ativação

$E_a^{\ddagger}$: energia de ativação para o processo de associação

$E_d^{\ddagger}$: energia de ativação para o processo de dissociação

EF: espectroscopia de fluorescência

F_0: intensidades de fluorescência da proteína na ausência do ligante

F:intensidades de fluorescência da proteína na presença do ligante

h: constante de Planck

H: entalpia

HSA: albuminas do soro humano

ITC: calorimetria de titulação isotérmica

κCG: kappa-carragena

k_a: constante cinética de associação

K_B: constante de Boltzmann

K_b: constante termodinâmica de interação

k_d: constante cinéticas de dissociação

k_{obs}: constante cinética observada

k_q: constante de taxa de extinção

K_{SV}: constante de Stern-Volmer

$[L]$: concentração total do agente supressor

MB: azul de metileno

n: estequiometria dos complexos formados

P: pressão do sistema

$[P]$: concentração de proteína

$[P_t]$: concentração total de proteína

$[PA]$: concentração de complexos proteína-analito

P_{ext}: pressão externa

pI: ponto isoelétrico

Phe: fenilalanina

q: calor

$[Q]$: concentração do supressor

R: constante dos gases ideais

RU: unidades de ressonância

RU_{max}: capacidade máxima de ligação

SPR: ressonância plasmônica de superfície

t: tempo

T: temperatura

t_m: tempo em que se iniciou a etapa de dissociação

τ_0: tempo de meia vida da proteína na ausência do agente supressor

Trp: triptofano

Tyr: tirosina

U: energia interna

V_c: volume efetivo da cela

w: trabalho

χ: razão molar

CAPÍTULOS 2, 3 E 4

AZA: azure A

A_{ex}: measured change in absorbance value at the excitation wavelength

A_{em}: measured change in absorbance value at the emission wavelength

BLF: bovine lactoferrin

$[BLF]$: concentration of lactoferrin

$[BLF - Dye]$: complex concentration

$[\mathrm{BLF} - \kappa\mathrm{CG}]^{\ddagger}$: activated complex

BSA: serum albumin bovine

CMC: carboxymethylcellulose

d_{em}: cuvette pathlength in the emission direction

d_{ex}: cuvette pathlength in the excitation direction

$[Dye]$: free phenothiazine dyes concentration

$\Delta G^{\ddagger}$: activation free energy change

$\Delta G_a^{\ddagger}$: activation free energy change for association processes

$\Delta G_d^{\ddagger}$: activation free energy change for dissociation processes

$\Delta H^{\ddagger}$: activation enthalpy change

$\Delta H_a^{\ddagger}$: activation enthalpy change for association processes

$\Delta H_d^{\ddagger}$: activation enthalpy change for dissociation processes

$\Delta S^{\ddagger}$: activation entropy change

$\Delta S_a^{\ddagger}$: activation entropy change for association processes

$\Delta S_d^{\ddagger}$: activation entropy changes for dissociation processes

ΔG^o: standard Gibbs free energy change

$\Delta G^0_{BLF-dye}$: standard Gibbs free energy change associated with the protein-dye interaction

ΔG^0_{conf}: standard Gibbs free energy change associated with the protein and ligand conformational change

ΔG^o_{comp}: standard free Gibbs energy change in compensation

ΔG^0_{desol}: standard Gibbs free energy change associated with the BLF and ligand molecule desolvation

ΔCp^o: standard heat capacity change

ΔH^o: standard enthalpy change

$\Delta H_{\mathrm{app-int}}$: apparent enthalpy change

ΔH^o_{cal}: calorimetric standard enthalpy change

ΔH_{obs}: observed enthalpy change

ΔS^o: standard entropy change

$\Delta S^0_{BLF-dye}$: system entropy change associated with the protein-dye interaction

ΔS^0_{conf}: system entropy change associated with the protein and ligand conformational change

ΔS^0_{desol}: system entropy change associated with the release of water molecules from the ligand and protein solvation shell

$E^{\ddagger}$: activation energy

$E^{\ddagger}_a$: activation energy for association processes

$E^{\ddagger}_d$: activation energy for dissociation processes

$E^{\ddagger}_{des}$: energy absorbed during the transfer of water molecules from the ligand solvation shell to the bulk system

$E_{conf}^{\ddagger}$: energy absorbed when the biopolymer conformational changes are induced by the interactions

$E_{int}^{\ddagger}$: energy released due to the protein-ligand interactions

<E_k>: average molecular kinetic energy

EDC: N-ethyl-N′, N′-dimethylaminopropylcarbodiimide

F: emission intensities in the presence of dye

F_{corr}: fluorescence intensity after correction of inner-filter effect

F_0: emission intensities in the absence of dye

F_{obs}: measured fluorescence by spectrofluorometer

FS: fluorescence spectroscopy

h: Planck's constant

HSA: serum albumin human

IKC: isokinetic compensation

ITC: isothermal titration calorimetry

k_a: kinetic constants of association

K_b: binding constant

K_B: Boltzmann's constant

k_d: kinetic constants of dissociation

κCG: κ-carrageenan

$k_{q:}$ bimolecular quenching rate constant

K_{SV}: Stern-Volmer quenching constant

k_{obs}: observed kinetic constant

λ_{max}: maximum emission wavelength

MB: methylene blue

n: stoichiometry number

NHS: N-hydroxysuccinimide

PMT: photomultiplier tube

pI: isoelectric point

Q: total heat content

$[Q]$: concentration of the quencher

$[Q_T]$: total concentration of ligand

R: gas constant

RU: resonance-response

RU_{max}: maximum analyte binding capacity

SPR: Surface plasmon resonance

T: temperature

T_{comp}: temperature of compensation

t: time

t_m: resonance time

τ_0: lifetime of the fluorophore

Trp: tryptophan

V_c: cell volume

χ: molar ratio

SUMÁRIO

CAPÍTULO 1: INTRODUÇÃO E REVISÃO DE LITERATURA

1.1 Introdução

O reconhecimento molecular constitui a base de uma ampla variedade de processos biológicos. Macromoléculas biológicas interagem entre si ou com pequenas moléculas para formar complexos específicos, que desempenham funções fundamentais para a manutenção da vida como: autorreplicação, metabolismo e processamento de informações [1,2]. Além disso, o conhecimento detalhado das interações proteína-ligante tem se mostrado de grande importância na descoberta, *design* e desenvolvimento de novos fármacos [3]. Por estes aspectos, elucidar os mecanismos que governam a energética e dinâmica da interação entre proteínas, como a lactoferrina (BLF), e diferentes ligantes tem sido uma meta científica importante, pois permite o controle sobre as propriedades fundamentais desse tipo de sistema, bem como sua aplicação nos diversos campos das ciências.

A BLF, uma glicoproteína da família das transferinas, é geralmente encontrada na maioria dos fluidos corporais de mamíferos. Possui alto ponto isoelétrico (pI ≈8,9) e massa molar de aproximadamente 80 kDa [4,5]. Além de sua capacidade especial de ligação ao ferro, essa biomolécula possui um grande potencial terapêutico [6], incluindo atividades imunomoduladora [7], antibacterianas [8], antivirais [9], antifúngicas[10], antimicrobiana [11], anti-inflamatórias [12] e anticarcinogênicas [13]. No entanto, todas estas propriedades funcionais associadas a essa proteína podem ser moduladas e/ou intensificadas estrategicamente por meio da sua interação com diferentes analitos, tais como os corantes fenotiazínicos e os polissacarídeos [14].

Utilizados há mais de um século como fármacos, os corantes fenotiazínicos assim como a BLF possuem inúmeras aplicações biológicas [15]. Frequentemente, estes corantes vêm sendo empregados no diagnóstico de doenças neurodegenerativas [16], na cura de doenças virais [17], no tratamento de isquemia cerebral [18], em terapia fotodinâmica contra carcinomas [19] e como agentes antimalárico [20]. Estas características os tornam estratégicos para interação com a BLF. O conhecimento das interações entre estes analitos proporcionará uma base molecular para compreender as propriedades farmacológicas de complexos proteína-ligante e abrirá caminho para novas abordagens no planejamento de drogas terapêuticas.

Assim como a interação proteína-pequenas moléculas está criticamente envolvida na descoberta e desenvolvimento de novos fármacos, a ligação proteína-polissacarídeo tem sido considerada uma peça chave no desenvolvimento tecnológico das indústrias alimentícias e de

cosméticos [21,22]. Devido às interações intermoleculares entre estes dois biopolímeros, formam-se geralmente bionanoestruturas que são usadas como encapsuladoras e/ou liberadoras de componentes químicos funcionais visando principalmente à obtenção de sistemas coloidais com aplicações estratégicas [23–27]. No entanto, as forças motrizes que dirigem o processo de interações BLF-polissacarídeo ainda são pouco conhecidas, o que torna a funcionalidade destes agregados em sistemas complexos bastante limitada [14,24,28–31].

Muitas técnicas têm sido propostas para investigar o processo de interação proteína-ligante, e em geral estas são divididas em abordagens separativas e não separativas [3]. O primeiro grupo envolve a separação do ligante livre da espécie ligada e é utilizado para determinar diretamente a concentração do analito não ligado ou da espécie ligada. Enquanto o segundo grupo baseia-se na detecção de uma alteração em uma propriedade físico-química do ligante ou da proteína devido à interação, no qual se destacam as técnicas de ressonância plasmônica de superfície (SPR), calorimetria de titulação isotérmica (ITC) e espectroscopia de fluorescência (EF). Por meio destas técnicas os parâmetros cinéticos (SPR) e termodinâmicos (SPR, ITC e EF) de interação entre proteínas e diferentes ligantes podem ser obtidos, o que permite uma melhor compreensão dos processos moleculares envolvidos nestas interações. Diante disso, pretendeu-se com o presente estudo alcançar os objetivos que são descritos na próxima seção.

1.2 Objetivos

1.2.1 Objetivo geral

Elucidar a cinética e a termodinâmica das interações BLF-corantes fenotiazínicos e BLF-polissacarídeos, visando determinar as forças motrizes envolvidas nestes processos associativos.

1.2.2 Objetivos específicos

- Trabalho1
    - Determinar os parâmetros termodinâmicos (K_b, ΔG^o, ΔH^o e ΔS^o) associados a formação dos complexos BLF-corantes fenotiazínicos (azul de metileno e azure A), utilizando espectroscopia de fluorescência;

- Obter os parâmetros termodinâmicos (K_b, ΔG^o, ΔH^o e ΔS^o) associados à interação entre a BLF e os corantes fenotiazínicos (azul de metileno e azure A), utilizando calorimetria de titulação isotérmica;

- Determinar os parâmetros termodinâmicos (K_b, ΔG^o, ΔH^o e ΔS^o) e cinéticos (k_a, k_d, $E^{\ddagger}$, $\Delta G^{\ddagger}$, $\Delta H^{\ddagger}$ e $\Delta S^{\ddagger}$) associados à interação entre a BLF e os corantes fenotiazínicos (azul de metileno e azure A), utilizando ressonância plasmônica de superfície;

- Avaliar as contribuições dos grupos CH_3 presentes nas estruturas dos corantes para o processo de formação das estruturas supramoleculares BLF-corantes fenotiazínicos.

- Trabalho 2
  - Obter os parâmetros termodinâmicos (K_b, ΔG^o, ΔH^o e ΔS^o) associados a formação dos complexos entre a BLF e o polissacarídeo carboximetilcelulose, utilizando espectroscopia de fluorescência;

  - Determinar os parâmetros termodinâmicos (K_b, ΔG^o, ΔH^o e ΔS^o) e cinéticos (k_a, k_d, $E^{\ddagger}$, $\Delta G^{\ddagger}$, $\Delta H^{\ddagger}$ e $\Delta S^{\ddagger}$) associados à interação entre a BLF e o polissacarídeo carboximetilcelulose, utilizando ressonância plasmônica de superfície.

- Trabalho 3
  - Obter os parâmetros termodinâmicos (K_b, ΔG^o, ΔH^o e ΔS^o) associados a formação das estruturas supramoleculares entre a BLF e o polissacarídeo kappa-carragena, utilizando espectroscopia de fluorescência;

  - Determinar os parâmetros termodinâmicos (K_b, ΔG^o, ΔH^o e ΔS^o) e cinéticos (k_a, k_d, $E^{\ddagger}$, $\Delta G^{\ddagger}$, $\Delta H^{\ddagger}$ e $\Delta S^{\ddagger}$) da interação entre a BLF e o polissacarídeo kappa-carragena, utilizando ressonância plasmônica de superfície;

  - Avaliar o efeito da mudança da força iônica do meio sobre os parâmetros cinéticos e termodinâmicos da formação dos complexos BLF-kappa-carragena.

1.3 Revisão de Literatura

1.3.1 Proteínas

Proteínas são uma classe muito importante de macromoléculas devido à variedade de papéis biológicos que desempenham, incluindo funções estruturais (citoesqueleto), mecânicas (musculares), bioquímicas (enzimas) e de sinalização celular (hormônios) [32]. As proteínas de todos os organismos, incluindo dos mais simples como bactérias aos mais complexos como seres humanos, são formadas a partir de vinte aminoácidos distintos ligados covalentemente em sequências lineares. Todos estes aminoácidos contêm um átomo de carbono central (C), que está ligado a um átomo de hidrogênio, um grupo amino (NH_2) e um grupo carboxila (COOH), e se diferem uns dos outros em suas cadeias laterais, ou grupos R, que variam em estrutura, tamanho e carga elétrica, e que está diretamente relacionada a solubilidade destes em água [32,33].

Assim como as letras do alfabeto são combinadas para formar palavras e sentenças significativas, a natureza seleciona e combina resíduos de aminoácidos para formar cadeias proteicas com funções específicas. Dependendo da sua complexidade, as moléculas de proteína podem ser descritas por quatro níveis de estrutura: primário, secundário, terciário e quaternário.

A estrutura primária descreve a sequência linear dos resíduos de aminoácidos ligados covalentemente por ligações peptídicas em uma proteína. A estrutura secundária refere-se ao arranjo espacial regular e recorrente dos aminoácidos adjacentes em uma cadeia polipeptídica. As principais estruturas secundárias são a α-hélice e a folha-β pregueada. Enquanto a estrutura terciária é resultante principalmente das interações entre os grupos R dos aminoácidos que as compõem e descreve todos os aspectos do enovelamento tridimensional de uma proteína. Por fim, quando uma cadeia proteica tem duas ou mais subunidades polipeptídicas, seus arranjos no espaço são chamados de estrutura quaternária [33,34].

A estrutura tridimensional de uma proteína, ou sua conformação, governa suas funções em sistemas bioquímicos, que podem ser afetadas por sua autoagregação ou pela interação com outras moléculas, incluindo peptídeos, ácidos nucléicos, membranas, substratos, polissacarídeos e pequenas moléculas, como corantes. Por esse motivo, um pré-requisito para uma compreensão mais profunda das funções das proteínas é entender completamente os mecanismos responsáveis pelas interações proteína-ligante, para os quais a caracterização cinética e a quantificação das energias que conduzem a formação de um complexo são cruciais.

Nos últimos anos, o mecanismo de interação entre proteínas e diferentes ligantes tem sido um campo de pesquisa de grande interesse da comunidade científica, sendo a lactoferrina (BLF) uma das proteínas alvo, principalmente devido suas propriedades terapêuticas e tecnológicas [35].

1.3.1.1 Lactoferrina

A BLF é uma glicoproteína pertencente à família das transferinas, possui cerca de 690 resíduos de aminoácidos e massa molar de aproximadamente de 80 kDa [36,37]. Além disso, a superfície da molécula de BLF possui várias regiões com altas concentrações de carga positiva, dando-lhe um alto ponto isoelétrico (pI ≈8,9). É constituída por uma cadeia polipeptídica simples dobrada em dois lóbulos globulares homólogos, denominados N e C-terminais (Fig. 1.1). Cada lóbulo é composto por dois sub-lóbulos ou domínios, que pode se ligar a um átomo de metal em cooperação sinérgica com o ânion carbonato (CO_3^{2-}) [35,38]. O principal metal que se liga à BLF é íon férrico (Fe^{3+}), mas também foi observado ligação com os íons Cu^{2+}, Zn^{2+} e Mn^{2+} [39].

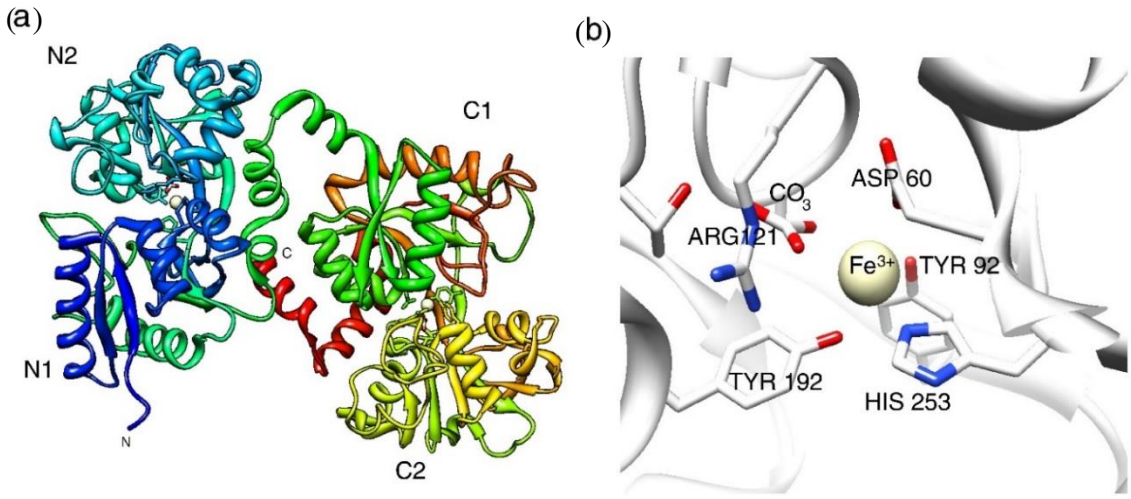

Fig. 1.1. Estrutura da lactoferrina: a) Lóbulos N e C e seus domínios N1, N2, C1 e C2. As esferas brancas representam os íons férricos em cada sítio de ligação. b) Local de ligação do Fe^{3+} no lóbulo N da lactoferrina [40].

Devido à sua capacidade de ligar reversivelmente com o íon ferríco, a BLF pode existir na sua forma livre (apolactoferrina) ou associado ao Fe^{3+} (hololactoferrina), possuindo uma conformação tridimensional diferente dependendo se está ou não ligada a este metal [36]. Em

sua "forma apo", livre de ferro, a conformação dos lóbulos dessa proteína muda, tornando a molécula mais aberta, enquanto que sua "forma holo" é mais compacta, o que lhe confere maior resistência à proteólise e desnaturação térmica [35,40]. Geralmente, a forma nativa da BLF compreende de uma mistura composta de apo (≈80%) e holo-lactoferrina (≈20%) [5].

Apesar de ser encontrada em maiores concentrações no leite de mamíferos, a BLF também está presente na maioria das secreções corporais, incluindo saliva, lágrimas e sêmen, além de um componente importante dos leucócitos [37]. Desde o seu isolamento a BLF tem sido objeto de muitos estudos, principalmente devido ao amplo espectro de propriedades funcionais para os seres humanos e animais, como regulação e diferenciação do crescimento celular[41], homeostase do ferro intestinal [42], capacidade antimicrobiana contra bactérias, parasitas, fungos e vírus [43], propriedades imunomoduladoras em relação às respostas imunes inatas e adaptativas [7], atividade antioxidante [44], anti-inflamatória [45] e proteção contra o câncer [46].

Todas essas características conferem à BLF um grande potencial terapêutico e tecnológico. Além disso, por ser um composto natural com alta biocompatibilidade, boa biodegradabilidade e baixa toxicidade, é particularmente atraente para aplicação em produtos alimentícios e farmacêuticos [47]. Nos últimos anos, esta proteína vem sendo adicionada como suplemento em vários produtos, incluindo medicamentos, fórmulas infantis, produtos lácteos, suplementos nutricionais, alimentos para animais e cosméticos [41]. No entanto, suas propriedades funcionais podem ser moduladas e/ou intensificadas estrategicamente com base na sua interação com diferentes ligantes [14].

A BLF pode interagir com muitas substâncias, entre elas, proteínas, polifenóis, fármacos, polissacarídeos e corantes, para formar complexos, que possuem propriedades físico-químicas e funcionais muito diferentes das moléculas isoladas. A formação destes complexos pode aumentar a estabilidade desta proteína a temperaturas elevadas, altas forças iônicas ou condições extremas de pH [48,49]. Além disso, pode ser usado para projetar bionanoestruturas para o encapsulamento, proteção ou liberação controlada de componentes químicos funcionais [23,27].

Nos últimos anos, pesquisas envolvendo a interação entre a BLF e moléculas bioativas foram conduzidas pelo setor farmacêutico e na área de alimentos. No entanto, estudos fundamentais que tratam tanto das características cinéticas e termodinâmicas, como da natureza das interações envolvidas na formação de complexos entre essas espécies ainda são escassos [14].

Estudos calorimétricos mostraram que a formação de complexos entre BLF e diferentes compostos fenólicos ocorre por meio de forças intermoleculares distintas [50–52]. Enquanto a interação da BLF com o ácido rosmarínico acontece principalmente via interações eletrostáticas [50], a associação entre a BLF e (-)-epigallocatechin-3-gallate é impulsionada predominantemente por ligações de hidrogênio [51]. Por outro lado, a complexação da BLF com ácido oleico ocorre sobretudo por meio de forças de van der Waals e ligações de hidrogênio [52].

A interação entre o fármaco lomefloxacina e a lactoferrina humana foi analisada por espectroscopia de fluorescência, dicroísmo circular e modelagem molecular. Verificou-se que a ligação da lomefloxacina à lactoferrina induziu mudanças conformacionais na estrutura da proteína que afetaram suas funções fisiológicas. Além disso os parâmetros termodinâmicos, ΔH^0 e ΔS^0, foram calculados como sendo 63,41 kJ mol^{-1} e 0,231 kJ mol^{-1} K^{-1}, respectivamente, mostrando que as interações hidrofóbicas foram as principais forças envolvidas na ligação [53].

Recentemente, as propriedades de ligação de dois fármacos isoméricos (ácido ursólico e ácido oleanólico) à BLF foram estudadas utilizando modelagem molecular, espectroscopia de fluorescência, espectroscopia no ultravioleta-visível e espectroscopia de infravermelho. Os autores constataram que as diferenças estruturais dos fármacos conduzem a mecanismos de ligação distintos, e que as principais forças envolvidas nestes processos são interações hidrofóbicas e ligações de hidrogênio [54].

Além de moléculas bioativas, a BLF pode interagir fortemente com polissacarídeos. Como mencionado, o ponto isoelétrico da BLF é alto (≈8,9), o que significa que possui carga positiva em uma ampla faixa de pH. Consequentemente, essa proteína pode tanto formar complexos eletrostáticos com polissacarídeos carregados negativamente, como interagir com biomoléculas de mesma carga. A natureza dos complexos formados depende principalmente do tipo e concentração dos polissacarídeos utilizados, pH, força iônica e temperatura [55].

Apesar de ser uma das questões fundamentais mais importantes na compreensão dos mecanismos de interação proteína-polissacarídeos, a energética e a dinâmica de formação dos complexos entre BLF e polissacarídeo tem recebido muito menos atenção nos últimos anos em comparação a estrutura e propriedades dos complexos formados [14,24,28–31]. Por exemplo, Bengoechea et al. [48] estudaram a interação da BLF (0,2% em peso) com pectina (0,005–0,15% em peso) em diferentes valores de pH (2-7) e temperaturas (30-90°C). Os autores mostraram que em pH 7 a carga elétrica da mistura passou de positiva para negativa quando quantidades crescentes de pectina foram adicionadas à solução de BLF, o que foi atribuído à formação de um complexo eletrostático entre estas macromoléculas. Estes complexos

permaneceram solúveis entre pH 3,5 e 7, mas tornaram-se turvos entre pH 2 e 3,5, devido a neutralização de carga e efeitos da ligação.

Peinado *et al*. [28] prepararam complexos de BLF-polissacarídeos baseados em interações eletrostáticas e estudaram o efeito do pH e força iônica em sua estabilidade. Este estudo apontou que o tipo e a concentração de polissacarídeos, a proporção BLF/polissacarídeo, o pH e a força iônica foram parâmetros-chave na formação, estabilidade e morfologia dos complexos formados. Os complexos BLF-pectina foram relatados como tendo maior estabilidade em presença de sais do que os complexos BLF-carragenina e BLF-alginato, que foi atribuído a diferenças estruturais entre esses polissacarídeos aniônicos: a pectina tem uma cadeia aniônica com ramificações neutras, enquanto a carragenina e o alginato possuem apenas cadeias aniônicas lineares.

Como pode ser visto, o número de estudos fundamentais de termodinâmica e cinética envolvendo a interação da BLF tanto com moléculas bioativas como com polissacarídeos ainda é muito reduzido. Mais especificamente, não existem trabalhos publicados até o momento que tratam das interações entre a BLF e os corantes fenotiazínicos, bem como, entre a BLF e os polissacarídeos carboximetilcelulose e kappa-carragena, o que fazem dessas pesquisas ainda mais relevantes. Essa escassez de trabalhos, mostra a necessidade da caracterização cinética e termodinâmica da interação entre a BLF e diferentes ligantes, visando principalmente, compreender e modular os processos moleculares responsáveis pela formação de complexos supramoleculares entre essas espécies, a fim de se obter sistemas coloidais com aplicações estratégicas.

Por reconhecer essa lacuna no conhecimento, neste trabalho buscou-se avaliar a cinética e a termodinâmica de interação entre a BLF e dois grupos de ligantes estratégicos: corantes fenotiazínicos (azul de metileno e azure A) e polissacarídeos (carboximetilcelulose e kappa-carragena).

1.3.2 Corantes fenotiazínicos

Os corantes fenotiazínicos possuem uma diversidade de atividades biológicas, e têm sido amplamente utilizados como agentes terapêuticos no tratamento de muitas doenças [56]. O mecanismo de atividade destes corantes já foi reconhecido e está ligado principalmente à sua estrutura química, devido seu alto potencial redox e sua capacidade de interagir com a luz visível [57,58].

Tanto o azul de metileno (MB) como o azure A (AZA) pertencem a classe dos fenotiazínicos, são corantes catiônicos estruturalmente semelhantes, e se diferem apenas nos grupos CH_3 presentes na posição 3 de suas estruturas químicas (Fig. 1.2). Esses corantes têm a capacidade de inativar vários tipos de patógenos e têm sido aplicados no tratamento de doenças neurodegenerativas [59], isquemia cerebral [18], malária [20], câncer [60] dentre outras. Portanto, estudar a interação entre os corantes fenotiazínicos e a BLF se torna de grande importância, considerando que a atividade desses corantes em aplicações terapêuticas pode ser potencializada baseado em sua ligação às proteínas.

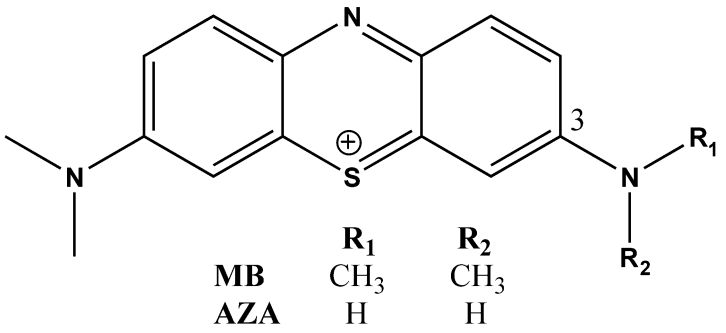

Fig. 1.2. Estrutura química dos corantes MB e AZA.

Nos últimos anos, foram estudadas apenas as interações dos corantes fenotiazínicos com as proteínas hemoglobina bovina [61] e as albuminas do soro bovino (BSA) e humano (HSA) [62–66]. Destes trabalhos somente dois investigaram a termodinâmica da formação dos complexos proteína-corantes fenotiazínicos. Li *et al.*[62] usando espectroscopia de fluorescência, encontraram que a interação entre BSA e MB era entropicamente dirigida, enquanto Das *et al.* [66] descobriram, utilizando calorimetria, que a ligação dos corantes fenotiazínicos, azure A, B e C à BSA ou HSA era entalpicamente favoráveis. Apesar das diferenças entre os parâmetros termodinâmicos, ambos os estudos confirmaram que as interações hidrofóbicas eram as principais forças envolvidas na formação dos complexos proteína-corantes fenotiazínicos. Além disso, como pode ser visto nos trabalhos acima citados, a cinética de interação proteína-corantes fenotiazínicos ainda não foi elucidada, tornando o estudo da dinâmica e energética da formação dos complexos entre corantes fenotiazínicos e BLF ainda mais relevante.

1.3.3 Polissacarídeos

Polissacarídeos são biopolímeros extraídos de plantas, algas, animais ou fungos, os quais podem ser formados por um único ou diferentes tipos de monossacarídeos ligados entre si por ligações glicosídicas [67,68]. As propriedades físicas destes polímeros, bem como a capacidade de se ligarem a outras moléculas, são em grande parte determinadas por sua conformação. A conformação dos polissacarídeos, por vez, depende de sua estrutura química (a natureza de suas unidades monoméricas, os arranjos sequenciais das diferentes unidades monoméricas dentro da cadeia polimérica, as ligações entre as unidades monoméricas e ramificações) e da natureza de seu meio (umidade; pH; temperatura e presença de outros solutos como sais) [67,69].

Na natureza os polissacarídeos desempenham uma variedade de funções, entre elas, fonte e reserva de energia, função estrutural e matéria prima para a síntese de outras biomoléculas. Na indústria são utilizados há décadas, sobretudo em produtos farmacêuticos (veículos de administração de medicamentos), biomateriais , alimentos e biocombustíveis [70]. Portanto, o entendimento e investigação mais profunda da interação entre a BLF e os polissacarídeos carboximetilcelulose e kappa-carragena são fundamentais tanto para a ciência da vida, como para o desenvolvimento de novas aplicações tecnológicas para essas bionanoestruturas.

1.3.3.1 Carboximetilcelulose

A carboximetilcelulose (CMC) é um biopolímero derivado da celulose que apresenta uma série de vantagens em relação aos demais polissacarídeos, sendo as mais importantes a disponibilidade em vários pesos moleculares e seu baixo custo, que permitem sua aplicação em diferentes campos industriais [71]. Na indústria de petróleo, a CMC é usada para aumentar a estabilidade da lama para fins de perfuração; em aplicações cosméticas, farmacêuticas e alimentícias é utilizada principalmente como agente espessante e/ou estabilizador de emulsões; já na indústria de papel, atua como fortalecedor e aglutinante e aumenta a retenção de água das misturas, entre outras inúmeras aplicações [72].

A CMC é formada por unidades β-(1→4)-D-glicopiranose, que possuem seus grupos hidroxilas substituídos por grupos carboximetil (Fig. 1.3) [73,74].

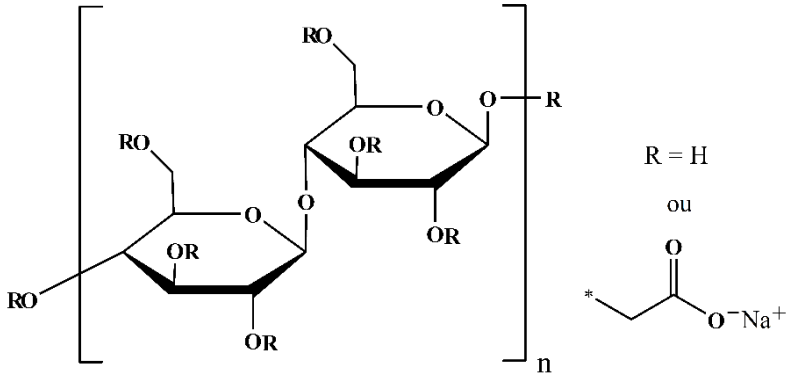

Fig. 1.3. Estrutura química da carboximetilcelulose.

Devido a presença do grupo carboxilato, as moléculas de CMC apresentam carga negativa, permitindo assim a interação com proteínas como a BLF, para formar complexos que possuem propriedades físico-químicas e funcionais distintas das macromoléculas isoladas [75–77]. No entanto, aspectos fundamentais, como a cinética e a termodinâmica de interação entre esses biopolímeros, ainda não foram esclarecidos [14,28–31].

1.3.3.2 Kappa-carragena

A kappa-carragena (κCG) é um polissacarídeo sulfatado extraído das paredes celulares de algas marinhas, comumente usada como aditivo alimentar para melhorar a textura de produtos alimentícios comerciais [78]. Devido a suas propriedades como compatibilidade, degradabilidade, solubilidade e não toxicidade, o uso desse polímero para encapsular moléculas nutracêuticas também vem ganhando atenção crescente [79–82]. Além dessas características, a κCG exibe muitas atividades biológicas e fisiológicas, incluindo atividades anticoagulante, antitrombótico, anti-inflamatório, antiviral e antitumoral [83,84].

Esse polissacarídeo é formado por unidades alternadas de (1–3)-α-D-galactose-4-sulfato e (1–4)-β-3,6-anidro-D-galactose (Fig. 1.4), e possui uma massa molar de cerca de 788,7 g mol^{-1} [85,86].

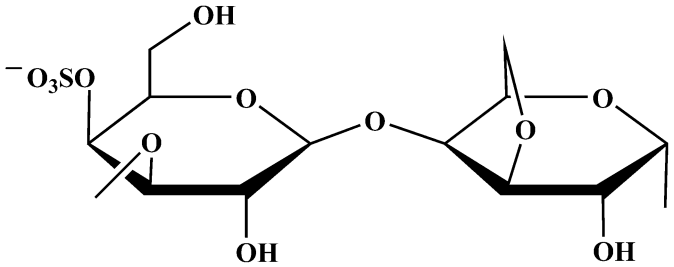

Fig. 1.4. Estrutura química da kappa-carragena.

Embora exista um grande número de estudos sobre a interação de várias proteínas com a kCG, por exemplo, albuminas do soro [87,88]; caseína [89–91]; beta-lactoglobulina [92,93]; lisozima [94,95], não há estudos sobre a interação da BLF com esse polissacarídeo, o que torna a caracterização cinética e termodinâmica deste sistema indispensável.

1.3.4 Técnicas experimentais utilizadas para o estudo da interação proteína-ligante

Para a determinação dos parâmetros cinéticos e termodinâmicos da interação entre a BLF e os corantes fenotiazínicos, bem como, entre a BLF e os polissacarídeos carboximetilcelulose e kappa-carragena foram utilizadas as seguintes técnicas experimentais: ressonância plasmônica de superfície (SPR), calorimetria de titulação isotérmica (ITC) e espectroscopia de fluorescência (EF). A seguir são apresentados os princípios gerais que norteiam estas técnicas e permitem que elas sejam utilizadas em estudos de interação intermolecular envolvendo proteínas e diferentes ligantes.

1.3.4.1 Ressonância Plasmônica de Superfície

Desde a sua primeira observação por Wood em 1902 [96], o fenômeno físico de ressonância plasmônica de superfície foi estudado e direcionado para aplicações práticas em instrumentos com detectores sensíveis, capazes de monitorar interações entre diferentes analitos em tempo real e utilizando pequenos volumes de amostra [97]. Por meio das medidas de SPR, não apenas a afinidade dos compostos, mas também os aspectos cinéticos e termodinâmicos da interação puderam ser determinados [98]. Características essas que fazem desta técnica cada vez mais presente em estudos biológicos fundamentais [99], pesquisas em ciências da saúde [100], descoberta de medicamentos [101], diagnóstico clínico [102] e monitoramento ambiental [103].

Em termos de princípios físicos de funcionamento, a ressonância plasmônica de superfície é um fenômeno que ocorre em um filme fino de metal depositado em uma interface separando duas fases com índices de refração distintos [104]. Um exemplo deste fenômeno ocorre numa fina camada de ouro depositada na superfície de um prisma de vidro, quando a mesma é colocada em contato com uma solução aquosa que tem um índice de refração menor que o do vidro (Fig. 1.5).

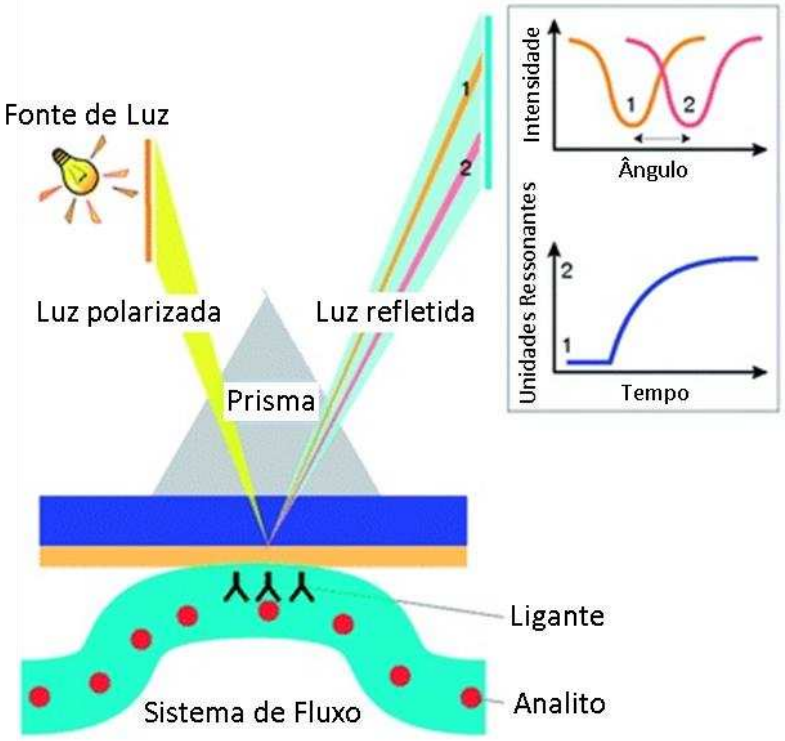

Fig. 1.5. Configuração esquemática de um detector SPR. O deslocamento do ângulo de reflexão da posição 1 para a posição 2 revela uma mudança na composição do meio próximo ao filme de ouro como resultado da ligação entre o ligante e o analito [65].

Quando a luz incidente passa pelo prisma e chega na interface metal/vidro, ela é refletida para o meio mais denso (vidro). No entanto, a reflexão interna total gera uma onda evanescente que penetra em uma fina camada do metal + solução, aproximadamente 100 nm. Quando o metal é submetido a radiação eletromagnética, o campo elétrico da luz induz uma oscilação coletiva de elétrons, denominado plasmons. Porém, em um determinado ângulo específico de incidência da luz, quando o vetor de onda do plasma é igual ao vetor de onda do campo evanescente, parte da radiação acopla com os elétrons livres oscilantes (plasmons) no filme metálico, chegando à condição de ressonância plasmônica de superfície. Como consequência, ocorre transferência da energia das ondas de luz para o plasma e sua subsequente dissipação no filme de metal, resultando em uma queda na intensidade da luz refletida [97,104,105]. Mostrando assim que a intensidade de luz refletida é dependente do ângulo de incidência e este ângulo é denominado ângulo de ressonância (Fig. 1.5).

O ângulo de ressonância é determinado pelas características ópticas do sistema, como o índice de refração da solução que flui acima da superfície do metal. Uma alteração no índice de refração do meio resulta em uma mudança da constante de propagação dos plasmons de

superfície, que por vez altera a condição de ressonância [105]. Por exemplo, quando na superfície do metal existem moléculas de proteína imobilizadas, em um determinado ângulo de incidência da radiação é atingido o ângulo de ressonância. E quando um analito interage com este ligante, é observado que o ângulo de ressonância varia. Isso informa que se o índice de refração acima da superfície do metal sofre alguma alteração, como a adsorção da proteína, ou interação com outra molécula, uma mudança no ângulo de incidência é requerida para que a excitação do plasmon de superfície possa ocorrer.

Basicamente, o detector de SPR monitora a variação no índice de refração de uma camada fina de solução que está em contato com o filme de ouro, cujo valor depende da concentração das espécies químicas presentes próximos à interface do metal, permitindo assim estudar interações específicas entre diferentes moléculas [98,106,107]. Quase todas as moléculas, de proteínas, DNA, RNA, lipídios e oligossacarídeos, podem ser imobilizadas na superfície do sensor e monitoradas quanto à ligação a analitos solúveis, variando em tamanho a partir de fármacos de baixa massa molecular para grandes moléculas como polissacarídeos, com afinidades de interação de milimolar a picomolar [102,107].

Um dos instrumentos utilizados para o estudo da ressonância plasmônica de superfície é o Biacore X100 da GE Healthcare Life Sciences. Nele, a superfície do sensor (sensorchip) é uma película fina de ouro (normalmente em torno de 50 nm) sobre um prisma de vidro de alto índice de refração, que forma o piso de uma célula de fluxo através do qual uma solução aquosa, geralmente tampão, flui continuamente. Em um experimento típico de SPR, o ligante (proteína) é imobilizado na superfície do sensor e uma solução contendo o analito é injetada no fluxo para detectar a interação. Inicialmente apenas tampão flui sobre a superfície do sensor, gerando uma linha base, como mostrado pela Região I da Fig. 1.6. Após, soluções de diferentes concentrações do analito são injetadas em fluxo, para que a formação de complexos possa ser investigada. Quando as moléculas de analito interagem com as moléculas receptoras imobilizadas, um aumento do índice de refração (expresso em unidades de ressonância RU) é observado (Fig. 1.6-Região II). Após um tempo de associação desejada, uma solução ausente de analito, geralmente tampão, é injetada através da célula de fluxo para dissociar os complexos proteína-ligante formados. À medida que o ligante se dissocia da proteína imobilizada, uma diminuição em RU é observada (Fig. 1.6-Região III). As variações angulares são registradas em unidades de ressonância (RU) e plotadas em função do tempo em um sensorgrama (RU *versus* tempo) (Fig. 1.6), a partir do qual os parâmetros cinéticos e a constante termodinâmica de interação podem ser determinados [98,108].

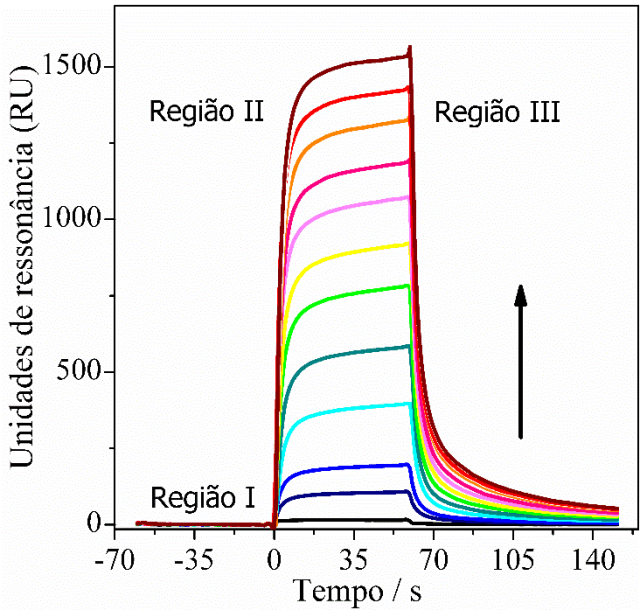

Fig. 1.6. Sensorgrama (RU *versus* tempo) obtido no SPR ilustrando a interação entre uma proteína imobilizada e o analito em solução. A seta indica o aumento da concentração do analito no sistema de fluxo.

A dinâmica de interação entre uma proteína e um analito específico pode ser avaliada aplicando um modelo de interação cinética 1:1 ao conjunto de dados obtidos pelo SPR [97,109]. Quando o analito interage com a proteína para formar um complexo 1:1 (Eq. 1), a taxa da formação deste complexo depende das concentrações do analito e proteína livres e da concentração dos complexos formados, que pode ser descrito pela Eq. 2.

$$P + A \rightleftharpoons PA \tag{1}$$

$$\frac{d[PA]}{dt} = k_a[A][P] - k_d[PA] \tag{2}$$

em que k_a e k_d são as constantes cinéticas de associação e dissociação, $[A]$, $[P]$ e PA são as concentrações de analito, proteína e complexos proteína-analito, respectivamente.

Na técnica de SPR, a concentração dos complexos formados será proporcional à resposta da ressonância (RU) no tempo (t), enquanto a concentração do ligante livre $[P]$ será a diferença entre a concentração total e complexada da proteína. Sabendo que a concentração total de proteína imobilizada é proporcional a sua capacidade máxima de ligação ao analito (RU_{max}), a concentração livre de proteína será, portanto, igual a $(RU_{max} - RU)$(t). Como a concentração do analito é mantida constante pelo sistema de fluxo, sua concentração livre pode

ser considerada idêntica à concentração total injetada. Deste modo, a interação entre a proteína imobilizada e o analito em solução seguirá uma cinética de pseudo primeira ordem, e a Eq. 2 poderá ser reescrita como Eq. 3.

$$\frac{dRU}{dt}(t) = k_a[A](t)(RU_{max} - RU(t)) - k_d RU(t) \tag{3}$$

Assim, para a fase de associação (Região II, Fig. 1.6), o sinal é dado por:

$$RU(t) = RU_{max}(t_\infty)[1 - e^{-k_{obs}(t)}] \tag{4}$$

em que k_{obs} é a constante cinética observada ($k_{obs} = k_a[A] + k_d$), e t é tempo. Já para a fase de dissociação (Região III, Fig. 1.6), o sinal pode ser compreendido como:

$$RU(t) = RU(t_m)e^{-k_d(t-t_m)} \tag{5}$$

em que t_m corresponde ao tempo em que se iniciou a etapa de dissociação.

Deste modo, os valores de k_{obs} e k_d podem ser obtidos a partir do ajuste não linear dos dados experimentais referentes as Regiões II e III do sensorgrama (Fig. 1.6) às Eqs. 4 e 5, respectivamente. Enquanto, o valor de k_a pode ser facilmente calculado a partir da inclinação da curva de k_{obs} em função de $[A]$.

Por meio do gráfico de Arrhenius ($ln\, k_a$ ou $ln\, k_d$ *versus* 1/T), as energias de ativação ($E_x^\ddagger$) para os processos de associação das espécies livres ($x = a$) ou dissociação dos complexos termodinamicamente estáveis ($x = d$), podem ser obtidas (Eq. 6). A partir dos valores de $E_x^\ddagger$, a variação da entalpia de ativação ($\Delta H_x^\ddagger$) pode ser calculada (Eq. 7), enquanto a variação da energia livre de Gibbs de ativação ($\Delta G_x^\ddagger$) e a variação da entropia de ativação ($\Delta S_x^\ddagger$), podem serem obtidas utilizando as Eqs. 8 e 9.

$$ln\left(\frac{k_x(T_2)}{k_x(T_1)}\right) = -\frac{E_x^\ddagger}{R}\left(\frac{1}{T_2} - \frac{1}{T_1}\right) \tag{6}$$

$$\Delta H_x^\ddagger = E_x^\ddagger - RT \tag{7}$$

$$\Delta G_x^{\ddagger} = -RTln\left(\frac{k_x h}{K_B T}\right) \quad (8)$$

$$T\Delta S_x^{\ddagger} = \Delta H_x^{\ddagger} - \Delta G_x^{\ddagger} \quad (9)$$

em que k_x representa a constante cinética de associação ($x = a$) ou dissociação ($x = d$), K_B é a constante de Boltzmann e h é a constante de Planck.

Além dos parâmetros cinéticos, a constante termodinâmica de interação (K_b) pode ser determinada utilizando a relação clássica ($K_b = k_a/k_d$), e a partir de seus valores a variação da energia livre de Gibbs padrão de interação (ΔG^0) pode ser obtida:

$$\Delta G^0 = -RTlnK_b \quad (10)$$

em que R é a constante universal dos gases (R = 8,314 J/mol K) e T a temperatura, em Kelvin.

Por apresentar a um controle de temperatura eficiente, a técnica de SPR permite a obtenção de K_b em diferentes temperaturas, o que possibilita determinar a variação da entalpia padrão (ΔH^0) de formação do complexo por meio da aproximação de van't Hoff (Eq. 11).

$$ln\left(\frac{K_b(T_2)}{K_b(T_1)}\right) = -\frac{\Delta H^0}{R}\left(\frac{1}{T_2} - \frac{1}{T_1}\right) \quad (11)$$

Na Eq. 11, R é a constante dos gases ideais (R = 8,314 $Jmol^{-1}K^{-1}$) e T_1 e T_2 são as temperaturas estudadas.

De posse dos valores de ΔG^0 e ΔH^0 a variação da entropia padrão (ΔS^0) associada ao processo de interação pode ser calculada utilizando a equação fundamental de Gibbs:

$$T\Delta S^0 = \Delta H^0 - \Delta G^0 \quad (12)$$

1.3.4.2 Calorimetria de Titulação Isotérmica

A associação molecular é um fenômeno fundamental em quase todos os aspectos dos processos biológicos, químicos e físicos [110]. Todos eles têm em comum mudanças energéticas que resultam na liberação ou no consumo de energia na forma de calor. Essas variações energéticas podem ser medidas e fornecem informações valiosas sobre as características específicas de um

processo de interação [111,112]. Embora diferentes técnicas tenham sido desenvolvidas para analisar eventos de associação molecular, como a SPR descrita anteriormente, a calorimetria de titulação isotérmica (ITC) é a única abordagem capaz de medir diretamente a troca de energia durante a formação de complexos a uma temperatura constante, se tornando referência na determinação das forças motrizes que impulsionam o processo de interações entre proteínas e diferentes ligantes [111,113].

Basicamente, um calorímetro de titulação isotérmica é composto por duas celas quase idênticas, uma de reação e outra de referência, de volume entre 1 e 4 mL, que se encontram em equilíbrio térmico em um ambiente de temperatura altamente controlada. A detecção da energia na forma de calor que é absorvida ou liberada pelos sistemas é realizada pelo uso de termopilhas semicondutoras interpostas entre as celas e um dissipador de calor (uma grande massa de metal em equilíbrio com um banho termostático revestido por uma câmara adiabática) [114]. Uma representação esquemática de um calorímetro de titulação isotérmica que opera por fluxo de calor é mostrada na Fig. 1.7.

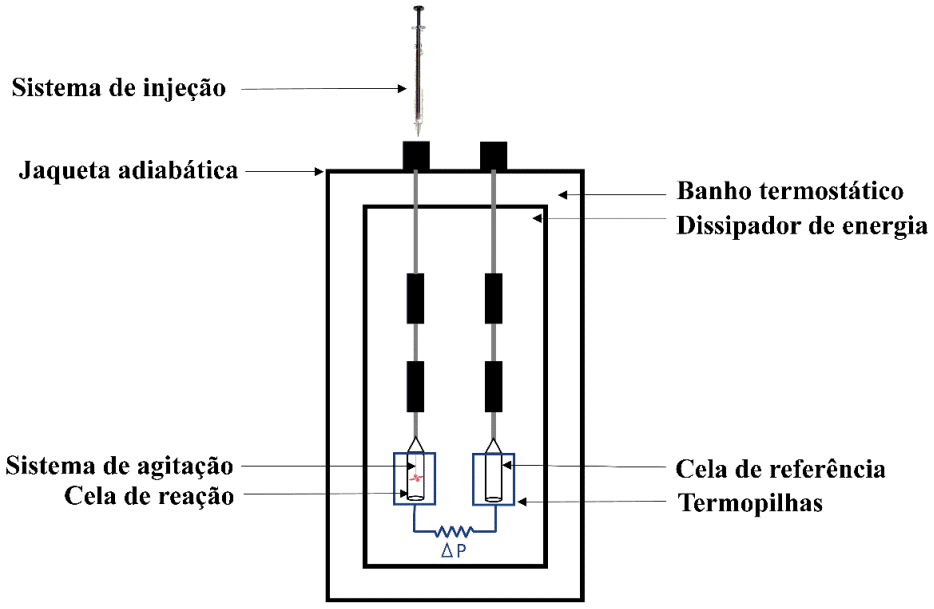

Fig. 1.7. Representação de um calorímetro de titulação isotérmica que opera por fluxo de calor.

Nos experimentos de ITC, a cela de reação é preenchida com uma solução de proteína e a cela de referência com tampão. Um sistema de titulação injeta o ligante na cela de reação em alíquotas consecutivas e precisamente conhecidas (1 a 15 μL), em um intervalo de tempo bem definido. Na cela de reação está presente um agitador que é utilizado para acelerar o processo de homogeneização do ligante na solução titulada (proteína). Quando as soluções de

proteína e ligante são misturadas, ocorre simultaneamente a ruptura e a formação de interações intermoleculares no sistema e a energia resultante absorbida ou liberada, na forma de calor, é detectada pelas termopilhas. Isto permite a obtenção de um gráfico de potência em função do tempo denominado termograma (Fig. 1.8), cuja integração resulta na energia na forma de calor (q) correspondente a cada injeção do ligante (Eq. 13). Para descontar a contribuição energética da interação do ligante com os componentes do tampão, um experimento semelhante é feito titulando o ligante na cela de amostra contendo apenas tampão.

$$q = \int_{t_1}^{t_2} P\, dt \tag{13}$$

em que t_1 é o tempo no início da injeção e t_2 o tempo no qual a linha base retorna ao seu valor inicial.

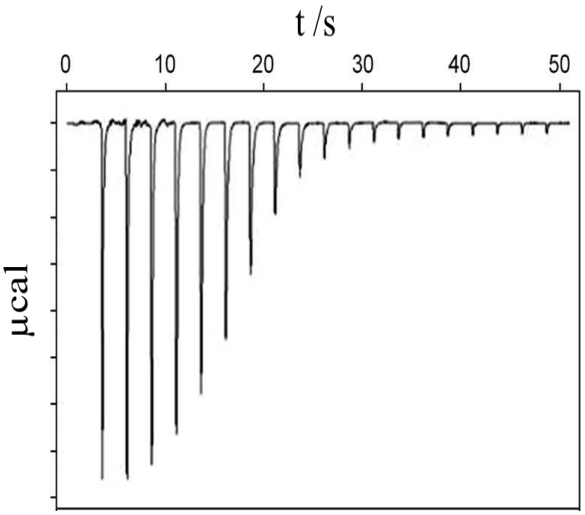

Fig. 1.8. Termograma (potência *versus* tempo) representativo obtido em um experimento de titulação calorimétrica isotérmica. Cada pico representa uma injeção de solução do ligante na cela de amostra que contém proteína.

Levando em consideração que os processos termodinâmicos que ocorrem no sistema são avaliados sob as condições termodinâmicas de temperatura e pressão constantes, o valor de q obtido corresponderá a variação de entalpia (ΔH), conforme será demonstrado a seguir.

De acordo com a primeira lei da termodinâmica em sua forma diferencial simplificada, tem-se:

$$dU = dq + dw \tag{14}$$

em que U é a energia interna do sistema e q e w são as quantidades de energia trocadas entre sistema e vizinhança nas formas de calor e trabalho, respectivamente.

Considerando que o processo analisado ocorra entre um estado inicial (i) e um estado final (f), integrando a Eq. 14 obtém-se:

$$\int_{\mathrm{i}}^{\mathrm{f}} \mathrm{dU} = \int_{\mathrm{i}}^{\mathrm{f}} \mathrm{dq} - \int_{\mathrm{i}}^{\mathrm{f}} \mathrm{dw} \tag{15}$$

Se neste processo apenas o trabalho de expansão contra uma pressão (P_{ext}) das vizinhanças for permitido, a Eq. 15 pode ser reescrita como:

$$dU = U_f - U_i = q - \int_i^f P_{ext} dV \tag{16}$$

em que, V é o volume.

Tendo em vista que o processo ocorre a pressão constate, tem-se:

$$U_f - U_i = q - P_{ext}\left(V_f - V_i\right) \tag{17}$$

Considerando que o sistema esteja em equilíbrio mecânico com suas vizinhanças, P_{ext} será igual a pressão do sistema (P), logo:

$$U_f - U_i = q - P\left(V_f - V_i\right) \tag{18}$$

Reordenando os termos na Eq. 18, obtém-se:

$$\left(U_f + PV_f\right) - \left(U_i + PV_i\right) = q \tag{19}$$

À soma $U + PV$ dá-se o nome de entalpia (H), obtendo-se:

$$\Delta H = H_f - H_i = q \tag{20}$$

Essa equação mostra que, para um dado sistema que esteja passando por um processo termodinâmico condicionado as características acima citadas (pressão constante, restrito a realizar apenas trabalho de expansão e em equilíbrio mecânico com suas vizinhanças), a quantidade de energia na forma de calor trocada entre sistema e vizinhança será numericamente igual à variação de entalpia associada a este processo.

Desta forma, em um experimento de interação proteína-ligante, a variação de entalpia por mol de ligante adicionado, também denominada de variação de entalpia observada (ΔH_{obs}) pode ser determinada. A fim de se obter a variação de entalpia aparente de interação (ΔH_{ap-int}), os valores ΔH_{obs} associados à mistura ligante-tampão são subtraídos da correspondente ΔH_{obs} ligante-proteína. Assim, os valores ΔH_{ap-int} são finalmente plotados em função da razão molar (χ) ligante/proteína e a curva ajustada ao modelo de "sítios de ligação independentes" [113] (Eq.21), para obtenção da constante termodinâmica de interação (K_b), a estequiometria dos complexos formados (n) e a variação da entalpia padrão de interação (ΔH°_{cal}) [115,116] (Fig. 1.9).

$$Q = \frac{V_c \Delta H^o_{cal}}{2K_b}\left[1 + K_b[L]_T + nK_b[P]_T - \sqrt{(1 + K_b[L]_T + nK_b[P]_T)^2 - 4n{K_b}^2[P]_T[L]_T}\right] \tag{21}$$

em que Q é o conteúdo total de calor, V_c é o volume efetivo da cela, K_b é a constante de interação, $[L]_T$ e $[P]_T$ são as concentrações totais de ligante e proteína no sistema, respectivamente, e n é o valor de estequiometria dos complexos formados.

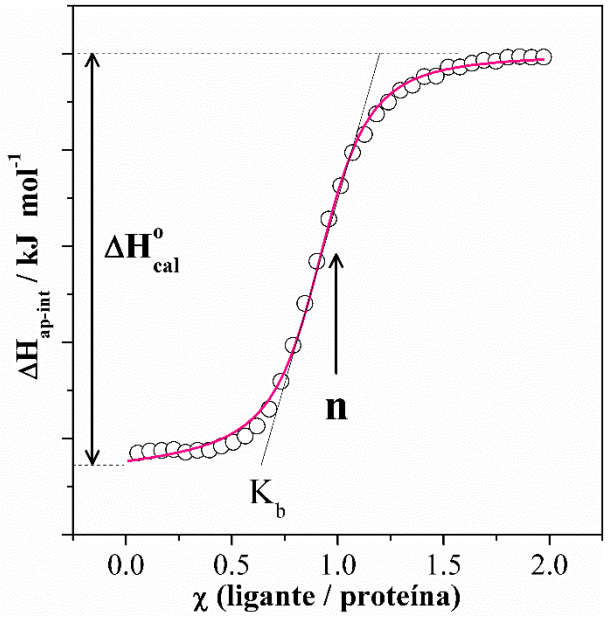

Fig. 1.9. Curvas ΔH_{ap-int} em função da razão molar ligante/proteína (χ).

A partir dos valores de K_b a variação da energia livre de Gibbs padrão (ΔG^0) pode ser calculada (Eq. 10), e a variação da entropia padrão de interação (ΔS^0) obtida pela Eq. 12.

1.3.4.3 Espectroscopia de Fluorescência

Das técnicas disponíveis para caracterização das interações proteína-ligante, a espectroscopia de fluorescência (EF) é uma das mais poderosas, pois permite várias abordagens para medir a interação [117,118]. É muito sensível, rápida, requer pouco material e geralmente envolve instrumentação relativamente barata [117,118]. Todas essas características fazem desta técnica uma das mais utilizadas para investigar os processos moleculares que regem a interação entre diferentes analitos [54,119–125].

O fenômeno de fluorescência envolve dois processos de interação molécula-fóton: i) absorção dos fótons pelas moléculas promovendo uma transição molecular do nível eletrônico fundamental para um nível roto-vibrônico excitado e ii) uma emissão subsequente, na qual a molécula sai de um nível eletrônico singlete excitado para o nível eletrônico fundamental [126,127]. A emissão ocorre em comprimento de onda maior devido à perda de energia que ocorre com a molécula excitada devido a colisões moleculares [128,129].

As proteínas possuem uma fluorescência intrínseca, devido à presença de resíduos de aminoácidos aromáticos, como triptofano (Trp), tirosina (Tyr) e fenilalanina (Phe). Dentre estes aminoácidos, o Trp é o mais utilizado em estudos de fluorescência de proteínas devido ao seu

elevado rendimento quântico, o qual permite a obtenção de um sinal mais intenso de emissão [130,131]. As propriedades de emissão deste aminoácido são extremamente sensíveis às interações intermoleculares que a proteína executa em sítios próximos ao mesmo [130]. Quando a proteína interage com ligantes, tais como corantes ou polissacarídeos, a sua fluorescência intrínseca, muitas vezes diminui à medida que aumenta a concentração do ligante [132,133].

A supressão de fluorescência é considerada uma ferramenta muito útil na determinação dos parâmetros termodinâmicos de interação proteína-ligante [134,135]. Os mecanismos de supressão são geralmente classificados como dinâmico ou estático. Na extinção estática, o ligante (agente supressor) forma um complexo não fluorescente com a proteína. Já na supressão dinâmica o ligante sofre colisões com a proteína, ocorrendo transferência de energia do fluoróforo para o agente supressor, com o consequente retorno do mesmo para o seu estado fundamental sem emissão de fluorescência [136]. Em geral, as têmperas dinâmicas e estáticas podem ser distinguidas pela sua diferente dependência com a temperatura e viscosidade, ou pela diferença do seu tempo de vida de fluorescência. Sendo assim, a determinação da constante de supressão é de grande importância para se verificar a formação ou não do complexo entre a proteína e o ligante.

A constante de supressão pode ser determinada utilizando a equação de Stern-Volmer (Eq. 22).

$$\frac{F_0}{F} = 1 + K_{SV}[Q] = 1 + \ k_q \tau_0 [Q] \tag{22}$$

em que F_0 e F são as intensidades de fluorescência da proteína na presença e na ausência do ligante; K_{SV} é a constante de Stern-Volmer (supressão); $[Q]$ é a concentração do supressor, k_q é a constante de taxa de extinção; e τ_0 é o tempo de meia vida da proteína na ausência do agente supressor.

Para o processo de têmpera estática, ou seja, quando ocorre a formação do complexo proteína-ligante, a constante de interação (K_b) e a estequiometria (n) dos complexos formados podem ser calculados por meio da Eq. 23 [135,137].

$$log\frac{F_0 - F}{F} = nLogK_b - nlog\left(\frac{1}{[L] - (F_0 - F)[P_t]/F_0}\right) \tag{23}$$

em que, $[L]$ é a concentração total do agente supressor, $[P_t]$ é a concentração total de proteína, n a estequiometria do complexo formado e K_b a constante de interação proteína-ligante.

O valor de K_b descreve a tendência do ligante de associar-se a um determinado sítio de ligação da proteína, sendo que quanto maior o valor desta constante, maior é a interação entre estas espécies. A partir da determinação de K_b em diferentes temperaturas, pode-se obter a variação da entalpia padrão de interação ΔH^0 por meio da aproximação de van't Hoff (Eq. 11).

Além de ΔH^0, os demais parâmetros termodinâmicos (ΔG^0 e $T\Delta S^0$) podem ser determinados, utilizando as Eqs. 10 e 12, respectivamente.

1.4 Organização da Tese

No primeiro capítulo, escrito em português, foi apresentada uma breve introdução ao tema estudado, foram descritos os objetivos gerais e específicos da tese e realizada uma revisão de literatura. No decorrer da revisão de literatura foram apresentadas ao leitor as principais características estruturais dos compostos estudados, bem como a importância de se elucidar a formação de estruturas supramoleculares entre as biomoléculas investigadas. Além disso, foram apresentados os princípios gerais que norteiam as técnicas experimentais utilizadas neste trabalho para caracterizar as interações proteína-ligante.

Os capítulos 2, 3 e 4 foram redigidos em inglês e apresentados na forma de artigos científicos. Na presente data, o trabalho apresentado no capítulo 2 encontra-se publicado no periódico *International Journal of Biological Macromolecules* (https://doi.org/10.1016/j.ijbiomac.2019.06.097), e se refere ao estudo da interação entre a proteína lactoferrina e dois corantes fenotiazínicos: o azure A e o azul de metileno. Já o artigo apresentado no capítulo 3 encontra-se submetido na revista *Food Chemistry* e trata da caracterização energética e dinâmica da formação de complexos supramoleculares entre a lactoferrina e o polissacarídeo carboximetilcelulose. O artigo apresentado no capítulo 4 está em fase de finalização para submissão em um periódico de relevância e se refere ao estudo da complexação entre a lactoferrina e o polissacarídeo kappa-carragena. Na última seção do trabalho é destinado um espaço para expor as conclusões gerais da tese.

Referências

[1] X. Du, Y. Li, Y. Xia, S. Ai, J. Liang, P. Sang, X. Ji, S.-Q. Liu, Insights into Protein – Ligand Interactions : Mechanisms, Models, and Methods, Interbational J. Mol. Sci. 17 (2016) 1–34. doi:10.3390/ijms17020144.

[2] J. Janin, PROTEIN-PROTEIN RECOGNITION, Prog. Biophys. Mol. Biol. 64 (1995) 145–166.

[3] K. Vuignier, J. Schappler, J.-L. Veuthey, P.-A. Carrupt, S. Martel, Drug–protein binding: a critical review of analytical tools, Anal. Bioanal. Chem. 398 (2010) 53–66. doi:10.1007/s00216-010-3737-1.

[4] P.P. Ward, E. Paz, O.M. Conneely, Multifunctional roles of lactoferrin: A critical overview, Cell. Mol. Life Sci. 62 (2005) 2540–2548. doi:10.1007/s00018-005-5369-8.

[5] H. Bokkhim, N. Bansal, L. Grndahl, B. Bhandari, Physico-chemical properties of different forms of bovine lactoferrin, Food Chem. 141 (2013) 3007–3013. doi:10.1016/j.foodchem.2013.05.139.

[6] L. Moreno-Expósito, R. Illescas-Montes, L. Melguizo-Rodríguez, C. Ruiz, J. Ramos-Torrecillas, E. de Luna-Bertos, Multifunctional capacity and therapeutic potential of lactoferrin, Life Sci. 195 (2018) 61–64. doi:10.1016/j.lfs.2018.01.002.

[7] J.K. Actor, S.-A. Hwang, M.L. Kruzel, Lactoferrin as a Natural Immune Modulator, Curr. Pharm. Des. 15 (2009) 1956–1973. doi:10.2174/138161209788453202.

[8] S. Teraguchi, H. Wakabayashi, H. Kuwata, K. Yamauchi, Y. Tamura, Protection against infections by oral lactoferrin: Evaluation in animal models, BioMetals. 17 (2004) 231–234. doi:10.1023/B:BIOM.0000027697.83706.32.

[9] H. Wakabayashi, H. Oda, K. Yamauchi, F. Abe, Lactoferrin for prevention of common viral infections, J. Infect. Chemother. 20 (2014) 666–671. doi:10.1016/j.jiac.2014.08.003.

[10] N. Takakura, H. Wakabayashi, H. Ishibashi, S. Teraguchi, Y. Tamura, H. Yamaguchi, S. Abe, Oral lactoferrin treatment of experimental oral candidiasis in mice, Antimicrob. Agents Chemother. 47 (2003) 2619–2623. doi:10.1128/AAC.47.8.2619-2623.2003.

[11] N.D. Embleton, J.E. Berrington, W. McGuire, C.J. Stewart, S.P. Cummings, Lactoferrin: Antimicrobial activity and therapeutic potential, Semin. Fetal Neonatal Med. 18 (2013) 143–1419. doi:10.1016/j.siny.2013.02.001.

[12] S. Baveye, E. Elass, J. Mazurier, G. Spik, D. Legrand, Lactoferrin : a mulitifunctional glycoprotein involved in the modulation of the inflammatory process, Clin.Chem.Lab.Med. 37 (1999) 281–286.

[13] M. Ligo, T. Kuhara, Y. Ushida, K. Sekine, M.. Moore, H. Tsuda, Inhibitory effects of bovine lactoferrin on colon carcinoma 26 lung metastasis in mice, Clin. Exp. Metastasis. 17 (1999) 35–40.

[14] F. Liu, S. Zhang, J. Li, D.J. McClements, X. Liu, Recent development of lactoferrin-based vehicles for the delivery of bioactive compounds: Complexes, emulsions, and nanoparticles, Trends Food Sci. Technol. 79 (2018) 1–43. doi:10.1016/J.TIFS.2018.06.013.

[15] M.J. Ohlow, B. Moosmann, Foundation review : Phenothiazine : the seven lives of pharmacology ' s first lead structure, Drug Discov. Today. 16 (2011) 119–131. doi:10.1016/j.drudis.2011.01.001.

[16] S.H. Yang, W. Li, N. Sumien, M. Forster, J.W. Simpkins, R. Liu, Alternative mitochondrial electron transfer for the treatment of neurodegenerative diseases and cancers: Methylene blue connects the dots, Prog. Neurobiol. 157 (2017) 273–291. doi:10.1016/j.pneurobio.2015.10.005.

[17] J. Stephen, Virus Inactivation in Blood Components by Photoactive Phenothiazine Dyes, Transfus. Med. Rev. 16 (2002) 61–66. doi:10.1053/tmrv.2002.29405.

[18] Z. Jiang, T.Q. Duong, Methylene blue treatment in experimental ischemic stroke: a mini review, Brain Circ. 2 (2016) 48–53. doi:10.4103/2394-8108.178548.

[19] R. Hosseinzadeh, K. Khorsandi, M. Jahanshiri, Combination photodynamic therapy of human breast cancer using salicylic acid and methylene blue, Spectrochim. Acta - Part A Mol. Biomol. Spectrosc. 184 (2017) 198–203. doi:10.1016/j.saa.2017.05.008.

[20] J.L. Vennerstrom, M.T. Makler, C.K. Angerhofer, J. a. Williams, Antimalarial Dyes Revisited: Xanthenes, Azines, Oxazines, and Thiazines, Antimicrob. Agents Chemother. 39 (1995) 2671–2677. doi:10.1128/AAC.39.12.2671.

[21] C. Schmitt, S.L. Turgeon, Protein-polysaccharide complexes and coacervates in food systems, Adv. Colloid Interface Sci. 167 (2011) 63–70. doi:10.1533/9781845695873.420.

[22] W. Wijaya, A.R. Patel, A.D. Setiowati, P. Van der Meeren, Functional colloids from proteins and polysaccharides for food applications, Trends Food Sci. Technol. 68 (2017) 56–69. doi:10.1016/j.tifs.2017.08.003.

[23] N. Devi, M. Sarmah, B. Khatun, T.K. Maji, Encapsulation of active ingredients in polysaccharide – protein complex coacervates, Adv. Colloid Interface Sci. 239 (2017) 136–145. doi:10.1016/j.cis.2016.05.009.

[24] E. da S. Gulão, C.J.F. de Souza, F.A.S. da Silva, JaneS.R.Coimbra, E.E. Garcia-Rojas, Complex coacervates obtained from lactoferrin and gum arabic : Formation and characterization, Food Res Int. 65 (2014) 367–374. doi:10.1016/j.foodres.2014.08.024.

[25] L. Zhang, J. Guo, X. Peng, Y. Jin, Preparation and Release Behavior of Carboxymethylated Chitosan/Alginate Microspheres Encapsulating Bovine Serum Albumin, J. Appl. Polym. Sci. 92 (2004) 878–882. doi:10.1002/app.13708.

[26] N. Eghbal, R. Choudhary, Complex coacervation : Encapsulation and controlled release of active agents in food systems, LWT - Food Sci. Technol. 90 (2018) 254–264. doi:10.1016/j.lwt.2017.12.036.

[27] A.I. Bourbon, M.A. Cerqueira, A.A. Vicente, Encapsulation and controlled release of bioactive compounds in lactoferrin-glycomacropeptide nanohydrogels: Curcumin and caffeine as model compounds, J. Food Eng. 180 (2016) 110–119.

doi:10.1016/j.jfoodeng.2016.02.016.

[28] I. Peinado, U. Lesmes, A. Andrés, J.D. McClements, Fabrication and morphological characterization of biopolymer particles formed by electrostatic complexation of heat treated lactoferrin and anionic polysaccharides, Langmuir. 26 (2010) 9827–9834. doi:10.1021/la1001013.

[29] C. Bengoechea, O.G. Jones, A. Guerrero, D.J. McClements, Formation and characterization of lactoferrin/pectin electrostatic complexes: Impact of composition, pH and thermal treatment, Food Hydrocoll. 25 (2011) 1227–1232. doi:doi:10.1016/j.foodhyd.2010.11.010.

[30] H. Bokkhim, N. Bansal, L. Grøndahl, B. Bhandari, Interactions between different forms of bovine lactoferrin and sodium alginate affect the properties of their mixtures, Food Hydrocoll. 48 (2015) 38–46. doi:10.1016/j.foodhyd.2014.12.036.

[31] B. Wang, E. Blanch, C.J. Barrow, B. Adhikari, Preparation and study of digestion behavior of lactoferrin-sodium alginate complex coacervates, J Funct Foods. 37 (2017) 97–106. doi:10.1016/j.jff.2017.07.044.

[32] B.E. Tropp, Protein Structure and Function, in: Mol. Biol. 4th Ed., 2012: pp. 27–74. doi:10.1021/ja209464f.

[33] D.L. Nelson, M.M. Cox, Lehninger Principles of Biochemistry 6th ed., 2013. doi:10.1016/j.jse.2011.03.016.

[34] M.M. Gromiha, Chapter 1 – Proteins, in: Protein Bioinforma., 2010: pp. 1–27. doi:10.1016/B978-8-1312-2297-3.50001-1.

[35] M. Tomita, H. Wakabayashi, K. Shin, K. Yamauchi, T. Yaeshima, K. Iwatsuki, Twenty-five years of research on bovine lactoferrin applications, Biochimie. 91 (2009) 52–57. doi:10.1016/j.biochi.2008.05.021.

[36] S.A. González-Chávez, S. Arévalo-Gallegos, Q. Rascón-Cruz, Lactoferrin: structure, function and applications, Int. J. Antimicrob. Agents. 33 (2009) 301.e1–301.e8.

doi:10.1016/j.ijantimicag.2008.07.020.

[37] E.N. Baker, H.M. Baker, Molecular structure, binding properties and dynamics of lactoferrin, Cell. Mol. Life Sci. 62 (2005) 2531–2539. doi:10.1007/s00018-005-5368-9.

[38] J.M. Steijns, A.C.M. van Hooijdonk, Occurrence, structure, biochemical properties and technological characteristics of lactoferrin, Br. J. Nutr. 84 (2000) 11–17. doi:10.1017/S0007114500002191.

[39] P.F. Levay, M. Viljoen, Lactoferrin: a general review., Haematologica. 80 (1995) 252–67. http://www.ncbi.nlm.nih.gov/pubmed/7672721.

[40] I.A. García-Montoya, T.S. Cendón, S. Arévalo-Gallegos, Q. Rascón-Cruz, Lactoferrin a multiple bioactive protein: An overview, Biochim. Biophys. Acta - Gen. Subj. 1820 (2012) 226–236. doi:10.1016/j.bbagen.2011.06.018.

[41] H. Wakabayashi, K. Yamauchi, M. Takase, Lactoferrin research, technology and applications, Int. Dairy J. 16 (2006) 1241–1251. doi:10.1016/j.idairyj.2006.06.013.

[42] J.H. Brock, The physiology of lactoferrin, Biochem. Cell Biol. 80 (2002) 1–6. doi:10.1139/o01-212.

[43] P. Valenti, G. Antonini, Lactoferrin: An important host defence against microbial and viral attack, Cell. Mol. Life Sci. 62 (2005) 2576–2587. doi:10.1007/s00018-005-5372-0.

[44] A.M. Mulder, P.A. Connellan, C.J. Oliver, C.A. Morris, L.M. Stevenson, Bovine lactoferrin supplementation supports immune and antioxidant status in healthy human males, Nutr. Res. 28 (2008) 583–589. doi:10.1016/j.nutres.2008.05.007.

[45] O.M. Conneely, Antiinflammatory Activities of Lactoferrin, J. Am. Coll. Nutr. 20 (2001) 389S–395S. doi:10.1080/07315724.2001.10719173.

[46] M. Arias, A.L. Hilchie, E.F. Haney, J.G.M. Bolscher, M.E. Hyndman, R.E.W. Hancock, and H.J. Vogel, Anticancer activities of bovine and human lactoferricin-

derived peptides, Biochem. Cell Biol. 95 (2016) 91–98.

[47] C. Conesa, M. Calvo, L. Sánchez, Recombinant human lactoferrin: A valuable protein for pharmaceutical products and functional foods, Biotechnol. Adv. 28 (2010) 831–838. doi:10.1016/j.biotechadv.2010.07.002.

[48] C. Bengoechea, O.G. Jones, A. Guerrero, D.J. McClements, Formation and characterization of lactoferrin / pectin electrostatic complexes : Impact of composition , pH and thermal treatment, Food Hydrocoll. 25 (2011) 1227–1232. doi:doi:10.1016/j.foodhyd.2010.11.010.

[49] F. Liu, D. Wang, C. Ma, Y. Gao, Conjugation of polyphenols prevents lactoferrin from thermal aggregation at neutral pH, Food Hydrocoll. 58 (2016) 49–59. doi:10.1016/j.foodhyd.2016.02.011.

[50] V. Ferraro, A.R. Madureira, B. Sarmento, A. Gomes, M.E. Pintado, Study of the interactions between rosmarinic acid and bovine milk whey protein α-Lactalbumin, β-Lactoglobulin and Lactoferrin, Food Res. Int. 77 (2015) 450–459. doi:10.1016/j.foodres.2015.08.024.

[51] W. Yang, F. Liu, C. Xu, F. Yuan, Y. Gao, Molecular interaction between (-)-epigallocatechin-3-gallate and bovine lactoferrin using multi-spectroscopic method and isothermal titration calorimetry, Food Res. Int. 64 (2014) 141–149. doi:10.1016/j.foodres.2014.06.001.

[52] B. Fang, M. Zhang, M. Tian, L. Jiang, H.Y. Guo, F.Z. Ren, Bovine lactoferrin binds oleic acid to form an anti-tumor complex similar to HAMLET, Biochim. Biophys. Acta - Mol. Cell Biol. Lipids. 1841 (2014) 535–543. doi:10.1016/j.bbalip.2013.12.008.

[53] J. Chamani, N. Tafrishi, M. Momen-Heravi, Characterization of the interaction between human lactoferrin and lomefloxacin at physiological condition: Multi-spectroscopic and modeling description, J. Lumin. 130 (2010) 1160–1168. doi:10.1016/j.jlumin.2010.02.014.

[54] M. Guo, X. Lu, Y. Wang, P.E. Brodelius, Comparison of the interaction between

lactoferrin and isomeric drugs, Spectrochim. Acta - Part A Mol. Biomol. Spectrosc. 173 (2017) 593–607. doi:10.1016/j.saa.2016.10.029.

[55] S.L. Turgeon, C. Schmitt, C. Sanchez, Protein–polysaccharide complexes and coacervates, Curr. Opin. Colloid Interface Sci. 12 (2007) 166–178. doi:10.1016/j.cocis.2007.07.007.

[56] M. Wainwright, The development of phenothiazinium photosensitisers, Photodiagnosis Photodyn. Ther. 2 (2005) 263–272. doi:10.1016/S1572-1000(05)00110-9.

[57] W. Wang, L. Yang, H. Sun, Z. Yang, Q. Du, C. Li, Improved photodynamic efficiency for methylene blue from silica-methylene blue@tannic acid-Fe(III) ions complexes in aqueous solutions, Adv. Powder Technol. 29 (2018) 341–348. doi:10.1016/j.apt.2017.11.021.

[58] A. Jaszczyszyn, K. Gqsiorowski, P. Swiqtek, W. Malinka, K. Cieslik-boczula, J. Petrus, B. Czarnik-matusewicz, biological activity, Pharmacol. Reports. 64 (2012) 16–23.

[59] S.C. How, Y.H. Cheng, C.H. Lo, J.T. Lai, T.H. Lin, Z. Bednarikova, A. Antosova, Z. Gazova, J.W. Wu, S.S.S. Wang, Exploring the effects of methylene blue on amyloid fibrillogenesis of lysozyme, Int. J. Biol. Macromol. 119 (2018) 1059–1067. doi:10.1016/j.ijbiomac.2018.08.038.

[60] D. Rajan, M. Ilanchelian, Exploring the interaction of Azure dyes with t-RNA by hybrid spectroscopic and computational approaches and its applications toward human lung cancer cell line, Int. J. Biol. Macromol. 113 (2018) 1052–1061. doi:10.1016/j.ijbiomac.2018.02.164.

[61] K. Shanmugaraj, S. Anandakumar, M. Ilanchelian, Exploring the biophysical aspects and binding mechanism of thionine with bovine hemoglobin by optical spectroscopic and molecular docking methods, J. Photochem. Photobiol. B Biol. 131 (2014) 43–52. doi:10.1016/j.jphotobiol.2014.01.001.

[62] Y. Li, Y. Zhang, S. Sun, A. Zhang, Y. Liu, Binding investigation on the interaction

between Methylene Blue (MB)/TiO2 nanocomposites and bovine serum albumin by resonance light-scattering (RLS) technique and fluorescence spectroscopy, J. Photochem. Photobiol. B Biol. 128 (2013) 12–19. doi:10.1016/j.jphotobiol.2013.07.027.

[63] A.S. Sharma, S. Anandakumar, M. Ilanchelian, In vitro investigation of domain specific interactions of phenothiazine dye with serum proteins by spectroscopic and molecular docking approaches, RSC Adv. 4 (2014) 36267. doi:10.1039/C4RA04630G.

[64] A. Selva, S. Anandakumar, M. Ilanchelian, A combined spectroscopic and molecular docking study on site selective binding interaction of Toluidine blue O with Human and Bovine serum albumins, J. Lumin. 151 (2014) 206–218. doi:10.1016/j.jlumin.2014.02.009.

[65] S.S. Arumugam, N. Subramanian, I. Malaichamy, New insights into the dimerization and site-specific cooperative interaction of Azure B with model transport proteins by spectroscopic and computational studies, J. Photochem. Photobiol. B Biol. 164 (2016) 212–225. doi:10.1016/j.jphotobiol.2016.09.011.

[66] S. Das, M.M. Islam, G.C. Jana, A. Patra, P.K. Jha, M. Hossain, Molecular binding of toxic phenothiazinium derivatives, azures to bovine serum albumin: A comparative spectroscopic, calorimetric, and in silico study, J. Mol. Recognit. 30 (2016) 1–11. doi:10.1002/jmr.2609.

[67] H. Arnon-Rips, E. Poverenov, 10 - Biopolymers-embedded nanoemulsions and other nanotechnological approaches for safety, quality, and storability enhancement of food products: active edible coatings and films, in: Emulsions, Elsevier Inc., 2016: pp. 329–363. doi:10.1016/B978-0-12-804306-6/00010-6.

[68] A.M. Donald, Polysaccharide Crystallization, in: Encycl. Mater. Sci. Technol., 2001: pp. 7714–7718. doi:10.1016/b0-08-043152-6/01385-1.

[69] James N.BeMiller, Polysaccharides: Properties, in: T. Edition (Ed.), Carbohydr. Chem. Food Sci., 2019: pp. 103–157. doi:10.1016/B978-0-12-812069-9.00005-4.

[70] V. Gopinath, S. Saravanan, A.R. Al-Maleki, M. Ramesh, J. Vadivelu, A review of natural polysaccharides for drug delivery applications: Special focus on cellulose, starch and glycogen, Biomed. Pharmacother. 107 (2018) 96–108. doi:10.1016/j.biopha.2018.07.136.

[71] A. Benchabane, K. Bekkour, Rheological properties of carboxymethyl cellulose (CMC) solutions, Colloid Polym. Sci. 286 (2008) 1173–1180. doi:10.1007/s00396-008-1882-2.

[72] M. Edali, M.N. Esmail, G.H. Vatistas, Rheological Properties of High Concentrations of Carboxymethyl Cellulose Solutions, J. Appl. Polym. Sci. 79 (2001) 1787–1801.

[73] K. Kamide, 2 - Characterization of Molecular Structure of Cellulose Derivatives, in: Cellul. Cellul. Deriv. Mol. Charact. Its Appl., 2005: p. 652. doi:10.1016/B978-0-444-82254-3.50004-7.

[74] A.M. Zhivkov, Electric Properties of Carboxymethyl Cellulose, in: Cellul. – Fundam. Asp., 2013: pp. 197–226.

[75] K. Kamide, 3 - Molecular Properties of Cellulose and Cellulose Derivatives, in: Cellul. Cellul. Deriv. Mol. Charact. Its Appl., 2005: p. 652. doi:10.1016/B978-044482254-3/50005-9.

[76] H. Zaleska, P. Tomasik, C.Y. Lii, Formation of carboxymethyl cellulose-casein complexes by electrosynthesis, Food Hydrocoll. 16 (2002) 215–224. doi:10.1016/S0268-005X(01)00085-6.

[77] L. Liu, Q. Zhao, T. Liu, J. Kong, Z. Long, M. Zhao, Sodium caseinate/carboxymethylcellulose interactions at oil-water interface: Relationship to emulsion stability, Food Chem. 132 (2012) 1822–1829. doi:10.1016/j.foodchem.2011.12.014.

[78] I.J. Haug, K.I. Draget, O. Smidsrød, Physical behaviour of fish gelatin-κ-carrageenan mixtures, Carbohydr. Polym. 56 (2004) 11–19. doi:10.1016/j.carbpol.2003.10.014.

[79] J. Liu, X. Zhan, J. Wan, Y. Wang, C. Wang, Review for carrageenan-based pharmaceutical biomaterials : Favourable physical features versus adverse biological effects, Carbohydr. Polym. 121 (2015) 27–36. doi:10.1016/j.carbpol.2014.11.063.

[80] W. Liang, X. Mao, X. Peng, S. Tang, Effects of sulfate group in red seaweed polysaccharides on anticoagulant activity and cytotoxicity, Carbohydr. Polym. 101 (2014) 776–785. doi:10.1016/j.carbpol.2013.10.010.

[81] L. Li, R. Ni, Y. Shao, S. Mao, Carrageenan and its applications in drug delivery, Carbohydr. Polym. 103 (2014) 1–11. doi:10.1016/j.carbpol.2013.12.008.

[82] S. Selvakumaran, I.I. Muhamad, S.I.A. Razak, Evaluation of kappa carrageenan as potential carrier for floating drug delivery system : Effect of pore forming agents, Carbohydr. Polym. 135 (2016) 207–214. doi:10.1016/j.carbpol.2015.08.051.

[83] S. Alban, A. Schauerte, G. Franz, Anticoagulant sulfated polysaccharides : Part I . Synthesis and structure-activity relationships of new pullulan sulfates, Carbohydr. Polym. 47 (2002) 267–276.

[84] H. Yuan, J. Song, X. Li, N. Li, J. Dai, Immunomodulation and antitumor activity of k -carrageenan oligosaccharides, Cancer Lett. 243 (2006) 228–234. doi:10.1016/j.canlet.2005.11.032.

[85] V.L. Campo, D.F. Kawano, D.B. da Silva Jr., I. Carvalho, Carrageenans : Biological properties , chemical modifications and structural analysis – A review, Carbohydr. Polym. 77 (2009) 167–180. doi:10.1016/j.carbpol.2009.01.020.

[86] J. Necas, L. Bartosikova, Carrageenan : a review, Vet. Med. (Praha). 4 (2013) 187–205.

[87] V.B. Galazka, D.A. Ledward, I.G. Sumner, E. Dickinson, Influence of High Pressure on Bovine Serum Albumin and Its Complex with Dextran Sulfate, J. Agric. Food Chem. 45 (1997) 3465–3471. doi:10.1021/jf9700642.

[88] E.S. Gul, M.F. De Campos, E.E. Garcia-rojas, Polymeric complexes obtained from the interaction of bovine serum albumin and k -carrageenan, Food Hydrocoll. 45 (2015)

286–290. doi:10.1016/j.foodhyd.2014.10.023.

[89] S. Bourriot, C. Garnier, J. Doublier, Micellar-casein – k -carrageenan mixtures . I . Phase separation and ultrastructure, Carbohydr. Polym. 40 (1999) 145–157.

[90] C. Garnier, C. Michon, S. Durand, G. Cuvelier, J.-L. Doublier, B. Launay, Iota-carrageenan / casein micelles interactions : e v idence at different scales, Colloids Surfaces B Biointerfaces. 31 (2003) 177–184. doi:10.1016/S0927-7765(03)00137-1.

[91] K. Ozawa, R. Niki, S. Arima, Interaction of β -Casein and κ-Carrageenan . I . Viscosity and Turbidity under Non-gelling Conditions, Agric. Bioi. Chern. 48 (1984) 627–632. doi:10.1080/00021369.1984.10866195.

[92] M.M.O. Eleya, S.L. Turgeon, The effects of pH on the rheology of b -lactoglobulin / k -carrageenan mixed gels, Food Hydrocoll. 14 (2000) 245–251.

[93] M.M.O. Eleya, S.L. Turgeon, Rheology of k -carrageenan and b -lactoglobulin mixed gels, Food Hydrocoll. 14 (2000) 29–40.

[94] Y.A. Antonov, I.L. Zhuravleva, R. Cardinaels, P. Moldenaers, Food Hydrocolloids Speci fi c effect of the linear charge density of the acid polysaccharide on thermal aggregation / disaggregation processes in complex carrageenan / lysozyme systems, Food Hydrocoll. 70 (2017) 8–13. doi:10.1016/j.foodhyd.2017.03.017.

[95] Y.A. Antonov, I.L. Zhuravleva, R. Cardinaels, P. Moldenaers, Food Hydrocolloids Macromolecular complexes of lysozyme with kappa carrageenan, Food Hydrocoll. 74 (2018) 227–238. doi:10.1016/j.foodhyd.2017.07.022.

[96] R. W. Wood, On a remarkable case of uneven distribution of light in a diffraction grating spectrum, Philos. Mag. 4 (1902) 396–402. doi:10.1080/14786440209462857.

[97] A.J. Tudos, R.B.M. Schasfoort, Introduction to surface plasmon resonance, in: Handb. Surf. Plasmon Reson., 2008: pp. 1–14. doi:10.1039/9781847558220.

[98] R.L. Rich, D.G. Myszka, Why you should be using more SPR biosensor technology,

Drug Discov. Today Technol. 1 (2004) 301–308. doi:10.1016/j.ddtec.2004.09.009.

[99] H.F. Teh, W.Y.X. Peh, X. Su, J.S. Thomsen, Characterization of protein-DNA interactions using surface plasmon resonance spectroscopy with various assay schemes, Biochemistry. 46 (2007) 2127–2135. doi:10.1021/bi061903t.

[100] A. Juhász, E. Csapo, D. Ungor, G. Tóth, L. Vécsei, I. Dékány, Kinetic and Thermodynamic Evaluation of Kynurenic Acid Binding to GluR1 270 − 300 Polypeptide by Surface Plasmon Resonance Experiments, J. Phys. Chem. B. 120 (2016) 7844–7850. doi:10.1021/acs.jpcb.6b05682.

[101] A. Olaru, C. Bala, N. Jaffrezic-Renault, H.Y. Aboul-Enein, Surface Plasmon Resonance (SPR) Biosensors in Pharmaceutical Analysis, Crit. Rev. Anal. Chem. 45 (2015) 97–105. doi:10.1080/10408347.2014.881250.

[102] K.L.M. Moran, D. Lemass, R. O'Kennedy, Surface Plasmon Resonance–Based Immunoassays: Approaches, Performance, and Applications, in: Handb. Immunoass. Technol., Elsevier Inc., 2018: pp. 129–156. doi:10.1016/B978-0-12-811762-0.00006-2.

[103] Y. Hirakawa, T. Yamasaki, A. Harada, T. Ohtake, K. Adachi, S. Iwasa, H. Narita, S. Miyake, Analysis of the Fungicide Boscalid in Horticultural Crops Using an Enzyme-Linked Immunosorbent Assay and an Immunosensor Based on Surface Plasmon Resonance, J. Agric. Food Chem. 63 (2015) 8075–8082. doi:10.1021/acs.jafc.5b03637.

[104] R.M. De Carvalho, S. Rath, L.T. Kubota, SPR - Uma nova ferramenta para biossensores, Quim. Nova. 26 (2003) 97–104. doi:10.1590/S0100-40422003000100017.

[105] E. Wijaya, C. Lenaerts, S. Maricot, J. Hastanin, S. Habraken, J.P. Vilcot, R. Boukherroub, S. Szunerits, Surface plasmon resonance-based biosensors: From the development of different SPR structures to novel surface functionalization strategies, Curr. Opin. Solid State Mater. Sci. 15 (2011) 208–224. doi:10.1016/j.cossms.2011.05.001.

[106] M. Beseničar, P. Maček, J.H. Lakey, G. Anderluh, Surface plasmon resonance in

protein-membrane interactions, Chem. Phys. Lipids. 141 (2006) 169–178. doi:10.1016/j.chemphyslip.2006.02.010.

[107] M.A. Cooper, Advances in membrane receptor screening and analysis, J. Mol. Recognit. 17 (2004) 286–315. doi:10.1002/jmr.675.

[108] S.G. Patching, Surface plasmon resonance spectroscopy for characterisation of membrane protein-ligand interactions and its potential for drug discovery, Biochim. Biophys. Acta - Biomembr. 1838 (2014) 43–55. doi:10.1016/j.bbamem.2013.04.028.

[109] J.M. Casasnovas, T.A. Springer, Kinetics and Thermodynamics of Virus Binding to Receptor, J. Biol. Chem. 270 (1995) 13216–13224. doi:10.1074/jbc.270.22.13216.

[110] J.E. Ladbury, B.Z. Chowdhry, Sensing the heat: The application of isothermal titration calorimetry to thermodynamic studies of biomolecular interactions, Chem. Biol. 3 (1996) 791–801. doi:10.1016/S1074-5521(96)90063-0.

[111] S. Leavitt, E. Freire, Direct measurement of protein binding energetics by isothermal titration calorimetry, Curr. Opin. Struct. Biol. 11 (2001) 560–566. doi:10.1016/S0959-440X(00)00248-7.

[112] I. Jelesarov, H.R. Bosshard, Isothermal titration calorimetry and differential scanning calorimetry as complementary tools to invesitigate the energetics of biomolecular recognition, J. Mol. Recognit. 12 (1999) 3–18.

[113] J.C. Martinez, J. Murciano-calles, E.S. Cobos, M. Iglesias-bexiga, I. Luque, J. Ruiz-sanz, Isothermal Titration Calorimetry : Thermodynamic Analysis of the Binding Thermograms of Molecular Recognition Events by Using Equilibrium Models, in: Appl. Calorim. a Wide Context – Differ. Scanning Calorimetry, Isothermal Titration Calorim. Microcalorim., 2013: pp. 73–104. doi:http://dx.doi.org/10.5772/53311.

[114] E. Freire, O.L. Mayorga, M. Straume, Isothermal Titration, Anal. Chem. 62 (1990) 950A–959A. doi:10.1021/ac00217a002.

[115] J.B. Chaires, Calorimetry and Thermodynamics in Drug Design, Annu. Rev. Biophys.

37 (2008) 135–151. doi:10.1146/annurev.biophys.36.040306.132812.

[116] M.W. Freyer, E.A. Lewis, Isothermal Titration Calorimetry: Experimental Design, Data Analysis, and Probing Macromolecule/Ligand Binding and Kinetic Interactions, in: Methods Cell Biol., 2008: pp. 79–113. doi:10.1016/S0091-679X(07)84004-0.

[117] L.D. Ward, Measurement of Ligand-Binding to Proteins by Fluorescence Spectroscopy, in: Methods Enzymol., 1985: pp. 400–414.

[118] P. Brown, C. Royer, Fluorescence spectroscopy as a tool to investigate protein interactions, Curr. Opin. Biotechnol. 8 (1997) 45–49. doi:10.1016/S0958-1669(97)80156-5.

[119] M. Guo, L. Zhang, W.-J. Lu, H. Cao, Analysis of the spectroscopic characteristics on the binding interaction between tosufloxacin and bovine lactoferrin, J. Lumin. 131 (2011) 768–775. doi:10.1016/j.jlumin.2010.11.036.

[120] C.A. Lelis, E.A. Hudson, G.M.D. Ferreira, G.M.D. Ferreira, L.H.M. da Silva, M. do C.H. da Silva, M.S. Pinto, A.C. dos S. Pires, Binding thermodynamics of synthetic dye Allura Red with bovine serum albumin, Food Chem. 217 (2017) 52–58. doi:10.1016/j.foodchem.2016.08.080.

[121] N. Barbero, E. Barni, C. Barolo, P. Quagliotto, G. Viscardi, L. Napione, S. Pavan, F. Bussolino, A study of the interaction between fluorescein sodium salt and bovine serum albumin by steady-state fluorescence, Dye. Pigment. 80 (2009) 307–313. doi:10.1016/j.dyepig.2008.08.006.

[122] L. Satish, S. Millan, H. Sahoo, Spectroscopic insight into the interaction of bovine serum albumin with imidazolium-based ionic liquids in aqueous solution, Luminescence. 32 (2017) 695–705. doi:10.1002/bio.3239.

[123] A.Y. Khan, G. Suresh Kumar, Spectroscopic studies on the binding interaction of phenothiazinium dyes, azure A and azure B to double stranded RNA polynucleotides, Spectrochim. Acta Part A Mol. Biomol. Spectrosc. 152 (2016) 417–425. doi:10.1016/j.saa.2015.07.091.

[124] P. Paul, G. Suresh Kumar, Spectroscopic studies on the binding interaction of phenothiazinium dyes toluidine blue O, azure A and azure B to DNA., Spectrochim. Acta. A. Mol. Biomol. Spectrosc. 107 (2013) 303–10. doi:10.1016/j.saa.2013.01.063.

[125] A. Orstan, J.F. Wojcik, Spectroscopic determination of protein: Ligand binding constants, J. Chem. Educ. 64 (1987) 814. doi:10.1021/ed064p814.

[126] J.R. Lakowicz, Principles of Fluorescence Spectroscopy, Trird edit, Maryland, USA, 2006. doi:10.1007/978-0-387-46312-4.

[127] P.R. Callis, Binding phenomena and fluorescence quenching. I: Descriptive quantum principles of fluorescence quenching using a supermolecule approach, J. Mol. Struct. 1077 (2014) 14–21. doi:10.1016/j.molstruc.2014.04.050.

[128] M.Y. Berezin, S. Achilefu, Fluorescence lifetime measurements and biological imaging, Chem. Rev. 110 (2010) 2641–2684. doi:10.1021/cr900343z.

[129] I.J. Joye, G. Davidov-Pardo, R.D. Ludescher, D.J. McClements, Fluorescence quenching study of resveratrol binding to zein and gliadin: Towards a more rational approach to resveratrol encapsulation using water-insoluble proteins, Food Chem. 185 (2015) 261–267. doi:10.1016/j.foodchem.2015.03.128.

[130] P.R. Callis, Binding phenomena and fluorescence quenching. II: Photophysics of aromatic residues and dependence of fluorescence spectra on protein conformation, J. Mol. Struct. 1077 (2014) 22–29. doi:10.1016/j.molstruc.2014.04.051.

[131] H. Liu, H. Zhang, B. Jin, Fluorescence of tryptophan in aqueous solution, Spectrochim. Acta - Part A Mol. Biomol. Spectrosc. 106 (2013) 54–59. doi:10.1016/j.saa.2012.12.065.

[132] M. Yang, Y. Wu, J. Li, H. Zhou, X. Wang, Binding of curcumin with bovine serum albumin in the presence of k-carrageenan and implications on the stability and antioxidant activity of curcumin, J. Agric. Food Chem. 61 (2013) 7150–7155. doi:10.1021/jf401827x.

[133] A.A. Rhodes, B.L. Swartz, E.R. Hosler, D.L. Snyder, K.M. Benitez, B.S. Chohan, S. Basu, Static quenching of tryptophan fluorescence in proteins by a dioxomolybdenum(VI) thiolate complex, J. Photochem. Photobiol. A Chem. 293 (2014) 81–87. doi:10.1016/j.jphotochem.2014.07.023.

[134] D. Bose, D. Sarkar, N. Chattopadhyay, Probing the binding interaction of a phenazinium dye with serum transport proteins: A combined fluorometric and circular dichroism study, Photochem. Photobiol. 86 (2010) 538–544. doi:10.1111/j.1751-1097.2009.00688.x.

[135] L. Wang, G. Zhang, Y. Wang, Binding properties of food colorant allura red with human serum albumin in vitro, Mol. Biol. Rep. 41 (2014) 3381–3391. doi:10.1007/s11033-014-3200-z.

[136] N. Ghosh, R. Mondal, S. Mukherjee, Hydrophobicity is the governing factor in the interaction of human serum albumin with bile salts, Langmuir. 31 (2015) 1095–1104. doi:10.1021/la504270a.

[137] S. Bi, L. Ding, Y. Tian, D. Song, X. Zhou, X. Liu, H. Zhang, Investigation of the interaction between flavonoids and human serum albumin, J. Mol. Struct. 703 (2004) 37–45. doi:10.1016/j.molstruc.2004.05.026.

CAPÍTULO 2: LACTOFERRIN-PHENOTHIAZINE DYE INTERACTIONS: THERMODYNAMIC AND KINETIC APPROACH

Abstract

Life manifestation is mainly based on biopolymer-ligand molecular recognition; therefore, the elucidation of energy and speed associated with protein-ligand binding is strategic in understanding and modulating biological systems. In this study, the interactions between methylene blue (MB) or azure A (AZA) dyes and bovine lactoferrin (BLF) were investigated by surface plasmon resonance, fluorescence spectroscopy, and isothermal titration calorimetry. Despite the molecular similarities between the dyes, the BLF-AZA binding thermodynamic parameters (ΔG^{o}_{AZA} = -30.50 and ΔH^{o}_{AZA} = 10.8 (kJ mol^{-1})) were higher in magnitude than those of the BLF-MB systems (ΔG^{o}_{MB} = -27.3 and ΔH^{o}_{MB} = 5.72 (kJ mol^{-1})). To increase the systems' entropy ($T\Delta S^{o}_{AZA}$ = 41.3 and $T\Delta S^{o}_{MB}$ = 33.0 (kJ mol^{-1})), the hydrophobic interactions must outweigh the electrostatic repulsion, thereby promoting BLF-dye binding. The activation complex formation ($E^{\ddagger}_{a,MB}$ = 33, $E^{\ddagger}_{a,AZA}$ = 32, $\Delta H^{\ddagger}_{a,MB}$ = 31, $\Delta H^{\ddagger}_{a,AZA}$ = 30, $\Delta G^{\ddagger}_{a,MB}$ = 51.84, $\Delta G^{\ddagger}_{a,AZA}$ = 50.7, $T\Delta S^{\ddagger}_{a,MB}$ = -21, $T\Delta S^{\ddagger}_{a,AZA}$ = -21 (kJ mol^{-1})), owing to free BLF and MB (or AZA) associations, was not affected by the dye chemical structure, while for the thermodynamically stable BLF-dye complex dissociation, the same energetic parameters ($E^{\ddagger}_{d,MB}$= 16, $E^{\ddagger}_{d,AZA}$= 6.4, $\Delta H^{\ddagger}_{d,MB}$ = 14, $\Delta H^{\ddagger}_{d,AZA}$ = 3.9, $\Delta G^{\ddagger}_{d,MB}$ = 81.4, $\Delta G^{\ddagger}_{d,AZA}$ = 74.93, $T\Delta S^{\ddagger}_{d,MB}$ = -68, $T\Delta S^{\ddagger}_{d,AZA}$ = -71.0 (kJ mol^{-1})) were considerably affected by the number of methyl groups. Our results may be very useful to determine binding processes controlled by kinetic parameters, as well as to optimize the application of these photosensitive dyes in biological systems.

Keywords: interaction, kinetics, thermodynamic, phenothiazine dyes, protein, lactoferrin.

2.1 Introduction

Different types of molecular interactions drive or modulate life machinery, including the interactions between proteins [1], proteins and DNA polynucleotides [2] , proteins and RNA polynucleotides [3], and proteins and small molecules [4]. Understanding the kinetics and thermodynamics of the interactions between small molecules and proteins has been a great challenge, although it is highly important in the research of life sciences, clinical medicine, and chemistry, particularly to employ proteins, such as bovine lactoferrin (BLF), as nanocarriers for different drugs [5].

BLF is an 80 kDa glycosylated protein with about 690 aminoacid residues, 13 of which are tryptophan (Trp) residues, comprised of a simple polypeptide chain folded into two symmetrical lobes, each possessing one site capable of reversibly and concomitantly binding to a ferric ion and a carbonate anion [6,7]. BLF can exist freely (apo-BLF) or associated with Fe^{3+} (holo-BLF) because of its ability to reversibly bind to ferric ions, affording different three-dimensional conformations depending on the number of bound Fe [8]. The properties ascribed to this protein include immunomodulatory activity, anti-inflammatory responses, antimicrobial activity linked to the Fe-binding capacity, disease prevention and other important physiological functions [9,10].

The investigation of the interaction between phenothiazine dyes and lactoferrin is a strategic topic, considering that the effectiveness and efficacy of these dyes in therapeutic applications may be improved based on their interactions with lactoferrin. Azure A (AZA) and Methylene Blue (MB) are phenothiazine dyes with the same basic phenothiazine skeleton, however, differing in the CH_3 groups present at position 3 (Fig. 2.1) [11]. These dyes have the capacity to inactivate several kinds of pathogens, and have been applied in the treatment of many diseases, including neurodegenerative diseases [12], cerebral ischemia [13], malaria [14], and cancer [15], owing to their high redox potential and their ability to effectively interact with visible light [16]. However, to the best of our knowledge, the kinetics and thermodynamics of the interactions between phenothiazine dyes and bovine lactoferrin have not been investigated, which makes this study even more relevant.

In recent years, only the interactions of phenothiazine dyes with bovine hemoglobin and serum albumins, bovine (BSA) and human (HSA), have been studied [17–22]. Only two of these works investigated the formation thermodynamics of these complexes. Li *et al*. [17] using fluorescence spectroscopy, reported the interaction between BSA and MB nanocomposites to be entropy-driven, while Das et al., [22] found, by calorimetry, that the bindings of three azure

dyes (A, B, and C) to BSA or HSA are enthalpically favorable. Despite the differences between the thermodynamic parameters, both reports confirmed that hydrophobic interactions were the main forces involved in the serum albumin-phenothiazine dye complex formation. However, as can be seen, the kinetics of proteins-phenothiazine dye interactions have not been elucidated yet. In addition, no elucidation was provided about a possible site-conformational fitting induced by protein-dye interactions.

Many methods have been proposed to assess the intermolecular interactions involving proteins and drug molecules, and they can be divided into separative and non-separative approaches [23]. The non-separative methods include the techniques of fluorescence spectroscopy, nanocalorimetry, ultraviolet-visible spectroscopy, circular dichroism, nuclear magnetic resonance, infrared spectroscopy, Raman spectroscopy, and surface plasmon resonance.

Surface plasmon resonance (SPR) is an appropriate technique for investigating the interaction between small molecule ligands and bio-macromolecules in real time [24]. The major advantage of SPR is that the interaction process can be kinetically [association (k_a) and dissociation (k_d) kinetic constants] and thermodynamically [binding constant (K_b)] characterized. The temperature dependence of the kinetic parameters (k_a and k_d) can be used to calculate the activation energy ($E^{\ddagger}$), variations in Gibbs free energy ($\Delta G^{\ddagger}$), and enthalpy ($\Delta H^{\ddagger}$) and entropy ($T\Delta S^{\ddagger}$) of activation, associated with a possible intermediate complex formation, which occurs during the association of free species or stable complex dissociation. In particular, the K_b values and their temperature dependence allow the determination of the standard Gibbs free energy change (ΔG^o), standard enthalpy change (ΔH^o), and standard entropy change (ΔS^o) of complex formation.

Despite the significant amount of information obtained by SPR, which could not be acquired by other methods, the use of complementary techniques such as fluorescence spectroscopy and calorimetry is of fundamental importance for obtaining binding parameters. Therefore, in the present paper, we report a complete comparative study of the interaction between BLF and the phenothiazine dyes, MB and AZA, using multiple techniques, aiming at the elucidation of the binding mechanism of these dyes to BLF and the contributions of CH_3 groups to the interactions.

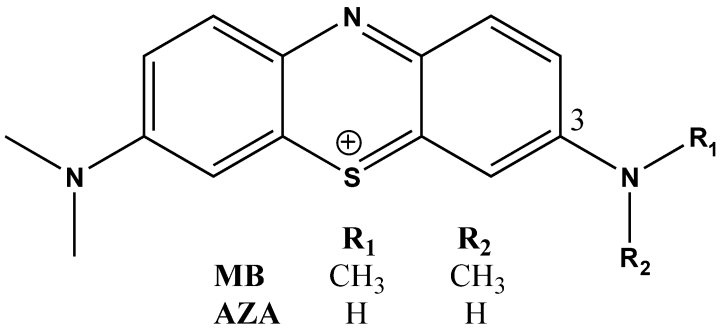

Fig. 2.1. Chemical structures of MB and AZA.

2.2 Materials and methods

2.2.1 Materials

Methylene blue (>99 wt%), Azure A (>98 wt%), BLF (>99 wt%), dibasic sodium phosphate (Na_2HPO_4) (reagent grade), and monohydrated sodium phosphate ($NaH_2PO_4 \cdot H_2O$) (reagent grade) were purchased from Sigma-Aldrich (St. Louis, MO, USA). Research-grade CM5 sensor chips and coupling reagents (N-ethyl-N′, N′-dimethylaminopropylcarbodiimide, EDC; N-hydroxysuccinimide, NHS; and 1-M ethanolamine hydrochloride, pH= 8.5) were purchased from GE Healthcare (Pittsburgh, PA, USA).

2.2.2 BLF-phenothiazine dye interactions studied by fluorescence spectroscopy

To determine the BLF-phenothiazine dyes binding parameters, fluorescence spectroscopy was employed. The appropriate spectra were obtained using a Cary Eclipse fluorescence spectrophotometer (Agilent, Santa Clara, CA, USA) equipped with a thermostat bath, using quartz cells having a 1-cm path length. In each cell, 2.5 mL of the BLF solution (20 μM) at a pH of 7.4, was titrated by successive additions of MB (15.93-67.82 μM) and AZA (18.61-60.09 μM). The fluorescence spectra were obtained over the 283-323 K temperature range, at wavelengths between 296 and 500 nm, excited at 295 nm.

2.2.3 BLF-phenothiazine dye interactions studied by surface plasmon resonance (SPR)

The kinetic and thermodynamic parameters for the interactions between the phenothiazine dyes (MB and AZA) and BLF were obtained by SPR using a Biacore X100

instrument (GE Healthcare, Pittsburgh, PA, USA). Initially, BLF was immobilized (3890 RU) on a CM5 sensor chip (GE Healthcare Company) by amine coupling according to the protocol recommended by the Biacore X100 handbook BR-1008-10 edition AC. For this, the CM5 chips were activated for 7 min with EDC/NHS, after which the excess activated carboxyl groups were blocked with ethanolamine for 7 min. Subsequently, BLF was immobilized on the chip (15 $\mu g \cdot mL^{-1}$) in 10 mM sodium acetate, at a pH of 4.0, resulting in low-density BLF immobilization (3890 RU), which reduces any potential mass transport and crowding artifacts (Fig. S.A.1). In the experiments with immobilized BLF, one flow cell was used as a reference surface; this surface was prepared as described above, however, without BLF immobilization.

The BLF-phenothiazine dyes binding experiments were carried out at a pH of 7.4, at temperatures ranging from 285.2 to 301.2 K. The solutions of MB (2-6 µM) and AZA (8-12 µM) were prepared in a flowing buffer at a pH of 7.4. For each binding experiment, the phenothiazine dyes solutions at a determined concentration were injected to increase their concentration on the sample (immobilized BLF) and reference (without BLF) surfaces, in order to correct the systematic noise and instrument drift. Before the binding cycle of each phenothiazine dye, a buffer was injected to establish the baseline.

2.2.4 BLF-phenothiazine dye interactions studied by isothermal titration calorimetry (ITC)

The enthalpy changes associated with the BLF-phenothiazine dye interactions at 298.1500 ± 0.0001 K were obtained in a TAM III isothermal titration nanocalorimeter (TA instruments, EUA), controlled by TAM dedicated assistant^{TM} software. Initially, solutions of BLF (0.50 mM) and dye [MB (4.99 mM) or AZA (5.01 mM)], at a pH of 7.4, were prepared and degassed before titration. Afterward, the sample and reference cells were loaded with 2.7 mL of protein solution and buffer, respectively, while the dye (MB or AZA) solution was injected using a syringe. After baseline stability was achieved, 50 aliquots of the dye solution (10 µL each) were injected to the BLF solution. A dilution experiment was carried out, replacing the BLF solution with a pH 7.4 buffer. The samples were stirred constantly at 180 rpm to ensure uniform mixing. The duration of each injection was fixed at 10 s, and the delay time between successive injections was 15 min. Raw data were obtained as a plot of potency (µW) against time. These data were integrated to obtain a plot of observed enthalpy change (ΔH_{obs}) per mole of the injected dye. The ΔH_{obs} associated with the dye-buffer mixing was subtracted from the corresponding ΔH_{obs} dye-protein binding to obtain the real, apparent enthalpy change ($\Delta H_{\mathrm{app-int}}$) of the BLF-phenothiazine dye interactions. The $\Delta H_{\mathrm{app-int}}$ values

for BLF-phenothiazine dye interactions were finally plotted as a function of the molar ratio (χ) of dye/BLF and fitted to an "independent binding sites" model to obtain the binding constant (K_b), the binding stoichiometry number (n), and the calorimetric standard enthalpy change (ΔH^o_{cal}) for the BLF-phenothiazine dyes complex formation.

2.3 Results and discussion

2.3.1 Binding of phenothiazine dyes on BLF studied by fluorescence spectroscopy

T The intrinsic fluorescence of BLF excited at 295 nm is mainly an effect of its tryptophan (Trp) residues and may be affected by the binding of a ligand to the protein [25]. By measuring the intrinsic fluorescence quenching of BLF, important information on the binding parameters and the change in the microenvironment of the fluorophore in the macromolecules can be provided [26,27].

To elucidate the interaction thermodynamics of the phenothiazine dyes (MB and AZA) with BLF, the emission spectra of BLF in the absence and presence of different concentrations of two distinct phenothiazine dyes were recorded at 298.2 K, upon excitation at 295 nm, as shown in Fig. 2.2, for the BLF-MB interaction. A similar plot was obtained for the BLF-AZA interaction (Fig. S.A.2).

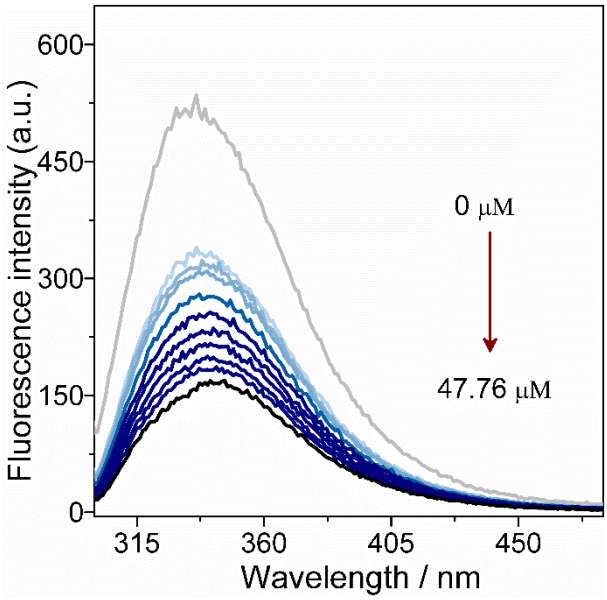

Fig. 2.2. Steady-state fluorescence emission spectra of BLF (20 μM) titrated with MB (0-47.76 μM). All experiments were carried out in a pH 7.4 phosphate buffer, at 298.2 K.

The emission spectra of BLF in the absence of phenothiazine dyes show an emission maximum at 332 nm when excited at 295 nm. Upon adding increasing concentrations of MB, the emission intensity of BLF decreased gradually with a slight red shift at the maximum emission wavelength ($\Delta\lambda_{max}$ = 9.00 nm), particularly at high dye concentrations. The shift in λ_{max} of BLF to a higher wavelength occurs due to the exposure of Trp residues to the more polar microenvoriment upon conformational changes of the protein, probably owing to the complexation with phenothiazine dyes.

Fluorescence quenching may be observed for various molecular interactions, such as excited state reactions, molecular rearrangements, collisional quenching, or static quenching [28]. To confirm the quenching mechanism that occurs in the BLF-phenothiazine dyes systems, emission quenching data were obtained at several temperatures, and the Stern-Volmer model was applied (Eq. 1).

$$\frac{F_0}{F} = 1 + k_q\tau_0[Q] = 1 + K_{SV}[Q] \quad (1)$$

where F_0 and F are the emission intensities in the absence and presence of dye, respectively. K_{SV} is the Stern-Volmer quenching constant; k_q, the bimolecular quenching rate constant; τ_0, the average lifetime of the biomolecule fluorescence without the quencher (for native BLF, τ_0 is about 1.06 ns [29]); and $[Q]$, the concentration of the quencher (phenothiazine dyes).

The Stern-Volmer plot for the BLF fluorescence quenching by MB at different temperatures is shown in Fig. 2.3. A similar profile was found for AZA (Fig. S.A.2).

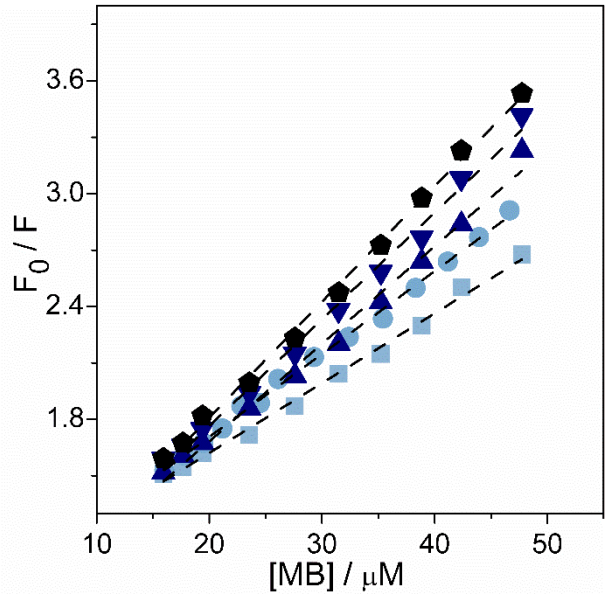

Fig. 2.3. Stern-Volmer plots of BLF fluorescence quenching due to binding with MB, λ_{ex} = 295 nm: (■) 283.15 K; (●) 293.15 K; (▲) 298.15 K; (▼) 303.15 K; (◀) 313.15 K, and pH7.4.

The values of K_{SV} for both ligands were obtained from the slopes of the linear Stern-Volmer plots (Fig. 2.3), and using the relation $k_q = K_{SV}/\tau_0$, k_q was determined. The K_{SV} and k_q values were determined for the temperature range of 283.2-313.2 K; these values are presented in Table 2.1.

Table 2.1. K_{SV} and k_q values for BLF-MB and BLF-AZA binding at five different temperatures and pH 7.4.

T	LF-MB			LF-AZA		
	K_{SV}	r^2	k_q	K_{SV}	r^2	k_q
K	10^4 M^{-1}		10^{13} M^{-1} s^{-1}	10^4 M^{-1}		10^{13} M^{-1} s^{-1}
283.2	3.7 ± 0.1	0.99	3.5 ± 0.1	13.7 ± 0.4	0.99	12.9 ± 0.4
293.2	4.4 ± 0.1	0.99	4.2 ± 0.1	15.1 ± 0.5	0.99	14.3 ± 0.4
298.2	5.2 ± 0.2	0.99	4.9 ± 0.2	15.6 ± 0.4	0.99	14.7 ± 0.4
303.2	5.7 ± 0.2	0.99	5.4 ± 0.2	17.1 ± 0.6	0.99	16.1 ± 0.5
313.2	6.1 ± 0.1	0.99	5.8 ± 0.1	18.9 ± 0.7	0.98	17.8 ± 0.7

For the two studied dyes, the K_{SV} values increased with temperature. In general, the formation of protein-ligand complexes is characterized by the decrease in K_{SV} with increasing temperature [30]. However, for the complex formation associated with the endothermic process, K_{SV} can increase with increasing temperature [31]. In addition, the k_q values were 3

orders in magnitude higher than the maximum value for the diffusion-limited collisional quenching (2.0 x 10^{10} M^{-1} s^{-1}) [28], indicating that the fluorescence quenching mechanism of BLF was static, and the formation of complexes was probably an entropy-driven process [31]. Furthermore, another evidence for BLF-phenothiazine dyes complex formation processes is that the differences in the dye molecular structures generate differences in the intensity of the BLF fluorescence quenching. The k_q and K_{SV} values of the BLF-AZA system were higher than those of the BLF-MB system (Table 2.1), which suggested that AZA molecules play a great role in the fluorescence quenching effect of BLF.

For a static quenching process, the modified double logarithm equation (Eq. 2) can be used to calculate the binding constant (K_b) and the stoichiometry number (n) of the formed complexes [32].

$$log\frac{(F_0 - F)}{F} = nlogK_b - nlog\frac{1}{\left([Q_T] - \frac{(F_0 - F)[BLF]}{F_0}\right)} \quad (2)$$

where F_0 and F are the fluorescence intensities of BLF in the absence and presence of phenothiazine dyes; n, the stoichiometry number of formed complexes; K_b, the binding constant; and $[Q_T]$ and $[BLF]$, the total concentration of dyes and protein, respectively.

The values of K_b and n for the complexes formed by BLF and phenothiazine dyes were obtained from the slope and intercept of linear regressions of the double-logarithm model curve (Eq. 2) at five different temperatures (Fig. S.A.4), and their values are shown in Table 2.2.

Table 2.2. Values of K_b and n associated with the complexation of phenothiazine dyes with BLF at different temperatures (T) and pH 7.4.

T	BLF-MB			BLF-AZA		
	K_b	r^2	n	K_b	r^2	n
K	10^4 M^{-1}			10^4 M^{-1}		
283.2	4.8 ± 0.1	0.99	0.92 ± 0.02	15.0 ± 0.4	0.99	1.04 ± 0.02
293.2	5.7 ± 0.2	0.99	1.00 ± 0.02	20.3 ± 0.5	0.99	0.91 ± 0.02
298.2	6.0 ± 0.2	0.99	1.06 ± 0.01	22.1 ± 0.8	0.99	0.93 ± 0.03
303.2	6.2 ± 0.2	0.99	1.03 ± 0.02	23.6 ± 0.7	0.99	0.98 ± 0.03
313.2	6.4 ± 0.3	0.99	0.97 ± 0.03	25.0 ± 0.8	0.99	0.94 ± 0.03

The binding constant (K_b) values for BLF-phenothiazine dye interactions show that, despite structural similarities between MB and AZA, they do not bind to BLF in an equivalent manner. For all the temperatures investigated, the BLF-AZA binding affinity was higher, showing that dye molecules with fewer methyl substituents have a relatively high tendency to bind to BLF. This CH_3 group effect should be associated with steric and rotational impediment. Regardless of the dye chemical structure, the stoichiometry (n) values were calculated to be approximately 1, demonstrating the presence of only one dye molecule in the binding site near the Trp residue of BLF.

From the literature, it was found that the binding affinity of phenothiazine dyes toward BSA increased with the number of methyl substitution of the dye, with $K_b = 3.64 \pm 0.04 \times 10^4$ M^{-1} for azure C, $4.88 \pm 0.05 \times 10^4$ M^{-1} for azure A, and $9.19 \pm 0.09 \times 10^4$ M^{-1} for azure B [113], whereas our study revealed an opposite binding order. This result can be explained by the difference between the binding sites of the dyes in the proteins. Site-selective binding studies revealed that the phenothiazine dyes interact in site I (subdomain IIA) of BSA, while our results suggest that the BLF-phenothiazine dye interactions probably occur in the less hydrophobic sites of the BLF.

The intermolecular forces involved in the complex formation between the dyes and protein may include hydrophobic forces, van der Waals interactions, electrostatic interactions, and hydrogen bonds [33]. To distinguish the contribution of each intermolecular energy to the dye-BLF complex formation, the standard Gibbs free energy change (ΔG^o), the standard enthalpy change (ΔH^o), the standard heat capacity change (ΔCp^o), and the standard entropy change (ΔS^o) of phenothiazine dye-BLF interaction were determined.

The ΔG^o values were directly calculated from the K_b values at each temperature (Eq. 3).

$$\Delta G^0 = -RT ln\, K_b \tag{3}$$

where K_b is the binding constant at temperature T, and R is the gas constant.

ΔH^o values were determined by fitting the data of the $ln\, K_b$ *versus* $1/T$ curves (Fig. S.A.5) to a polynomial expression (Eq. 4) [34], after which the constants, a, b, c, and d, were obtained. With these constants, the ΔH^o values were calculated using Eq. 5.

$$ln\, K_b = a + b\left(\frac{1}{T}\right) + c\left(\frac{1}{T}\right)^2 + d\left(\frac{1}{T}\right)^3 \tag{4}$$

$$\Delta H^0 = -R\left[b + 2c\left(\frac{1}{T}\right) + 3d\left(\frac{1}{T}\right)^2\right] \quad (5)$$

The ΔCp^o values can be calculated from the temperature dependence of the ΔH^o plot Fig. 2.4 using Eq. 6.

$$\Delta Cp^0 = \frac{\partial \Delta H^0}{\partial T} \quad (6)$$

The entropic term ($T\Delta S^o$) was obtained using the fundamental Gibbs equation (Eq. 7).

$$T\Delta S^0 = \Delta H^0 - \Delta G^0 \quad (7)$$

The values of ΔG^o, ΔH^o, ΔCp^o, and $T\Delta S^o$ are shown in Table 2.3.

Table 2.3. Values of ΔG^o, ΔH^o, ΔCp^o, and $T\Delta S^o$ for the BLF-MB and BLF-AZA complexes formation, at different temperatures and pH 7.4. Data obtained from fluorescence measurements.

T	BLF-MB				BLF-AZA			
	ΔH^o	ΔG^o	$T\Delta S^o$	ΔCp^o	ΔH^o	ΔG^o	$T\Delta S^o$	ΔCp^o
K	kJ mol^{-1}			kJ mol^{-1} K^{-1}	kJ mol^{-1}			kJ mol^{-1} K^{-1}
283.2	15.97 ± 0.02	-25.37 ± 0.05	41.34 ± 0.05	-0.83 ± 0.01	26.8 ± 0.1	-28.06 ± 0.07	54.9 ± 0.1	-1.08 ± 0.01
293.2	8.33 ± 0.02	-26.7 ± 0.1	35.0 ± 0.1	-0.66 ± 0.01	15.2 ± 0.1	-29.79 ± 0.05	45.0 ± 0.1	-0.98 ± 0.01
298.2	5.72 ± 0.01	-27.3 ± 0.1	33.0 ± 0.1	-0.40 ± 0.00	10.84 ± 0.08	-30.50 ± 0.08	41.3 ± 0.1	-0.78 ± 0.01
303.2	3.81 ± 0.02	-27.8 ± 0.1	31.6 ± 0.1	-0.18 ± 0.00	7.38 ± 0.06	-31.18 ± 0.08	38.6 ± 0.1	-0.57 ± 0.01
313.2	1.86 ± 0.03	-28.8 ± 0.1	30.7 ± 0.1	-0.05 ± 0.00	2.81 ± 0.03	-32.36 ± 0.08	35.17 ± 0.09	-0.46 ± 0.00

The ΔG^o values were negative for BLF binding with both phenothiazine dyes investigated, indicating that, in spite of the charge-charge repulsion that occurred between the positive charges present on the phenothiazine dyes and BLF molecules, attractive interactions such as hydrophobic interactions, hydrogen bonding, London-van der Waals forces, and π-π stacking outweigh the electrostatic repulsion. In addition, the ΔG^o values for the BLF interacts with the different dyes were very close, because the BLF-dye complex formation occurs mainly via interactions of the aromatic rings with aminoacid residues. However, despite the similarities in the MB and AZA chemical structures, all the interaction thermodynamic parameters depended on the number of methyl groups on the dye structure. The decrease in the number of methyl groups in the dye structure increased the stabilities of the BLF-dye complexes. The ΔG^o values can be rationalized as the contribution of three molecular processes, as described by Eq. 8:

$$\Delta G^0 = \Delta G^0_{desol} + \Delta G^0_{BLF-dye} + \Delta G^0_{conf} \quad (8)$$

where ΔG^0_{desol} is the standard Gibbs free energy change associated with the BLF and dye molecule desolvation upon complex formation; $\Delta G^0_{BLF-dye}$, the standard Gibbs free energy change associated with the protein-dye interaction; and ΔG^0_{conf}, the standard Gibbs free energy change associated with the protein and dye conformational change upon complex formation.

The number of CH_3 groups in the phenothiazine structures may be influencing the values of ΔG^0_{desol}, $\Delta G^0_{BLF-dye}$, and ΔG^0_{conf} in a complicated way. Therefore, to better understand the effect of the CH_3 group on the BLF-phenothiazine dye interactions, evaluating how the methyl substituent affects the ΔG^o components, i.e., ΔH^o and $T\Delta S^o$, is a strategic step.

For all the temperatures, the ΔH^o values (Table 2.3) were more positive for the BLF-AZA interaction than for the BLF-MB complex formation. In a similar way to ΔG^o (Eq. 8), ΔH^o can be rationalized as the sum of the terms ΔG^0_{desol}, $\Delta G^0_{BLF-dye}$, and ΔG^0_{conf}. The positive ΔH^o values indicate that less energy is released in the BLF-phenothiazine dye interaction processes than that absorbed during: (i) breaking the BLF-solvent and dyes-solvent interactions and (ii) BLF and dyes conformational changes. Therefore, $\left|\Delta G^0_{BLF-dye}\right| < \left|\Delta G^0_{desol} + \Delta G^0_{conf}\right|$, because the desolvation processes imply the break of strong hydrogen bonds associated with water molecules near two hydrophobic surfaces, and the formation of relatively weak H_2O-H_2O

hydrogen bonds in the bulk of the system (hydrophobic effect). In addition, conformational changes in the biopolymer site requires absorption of energy [35].

The increase in ΔH^o values when the number of methyl groups in the dye structure decreases from 4 (MB) to 2 (AZA), suggests that the relatively high number of CH_3 groups in the MB structure induces a high electron density on its aromatic ring that favors BLF-MB complex formation and results in the release of more energy than in the BLF-AZA association processes, thereby overcoming the higher enthalpic gain from the desolvation of 4 CH_3 groups in the MB structure as well as the conformational changes of BLF and MB. Moreover, since the dyes and protein molecules were positively charged at a pH of 7.4, there is an electrostatic repulsion component in the interaction between them. Furthermore, for all BLF-dye interactions, as the temperature increased, the ΔH^o values decreased monotonically, as showed in Fig. 2.4.

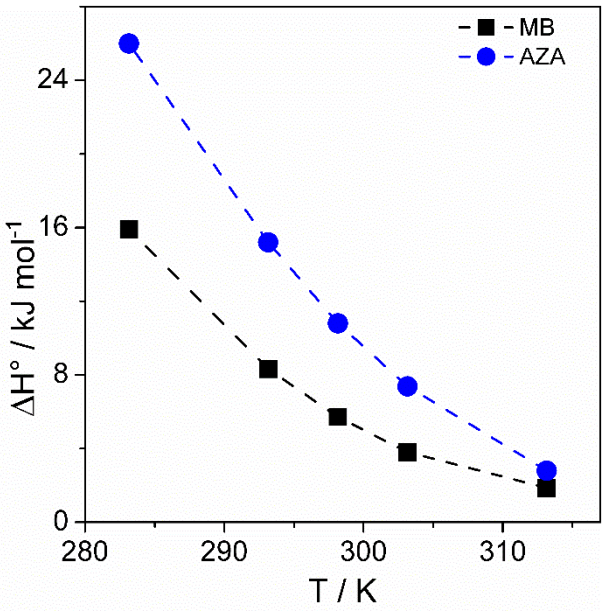

Fig. 2.4. Temperature dependence of ΔH^o values for (■) BLF-MB and (●) BLF-AZA binding.

From the plot of ΔH^o *versus* temperature (Fig. 2.4), the ΔCp^o data for BLF with MB or AZA interactions can be calculated ($\Delta Cp^0 = \partial \Delta H^o / \partial T$), and their values are given in Table 2.3.

The ΔCp^o values may provide valuable insights into the type and magnitude of the forces involved in the protein-dyes binding process [36]. The standard heat capacity change values of the BLF-dye interactions were negative throughout the evaluated temperature range;

however, these values differ according to the number of CH_3 substituents in the dye structure. ΔCp^o is more negative for the BLF-AZA interaction than for BLF-MB association processes.

Although a number of factors can influence the ΔCp^o value of the protein-ligand complex formation such as changes in the secondary protein structure and ionization of interacting species [37], the ΔCp^o negative values mainly suggest changes in the hydration of the hydrophobic groups of both interacting molecules; it can be considered as an indicator of a dominant hydrophobic effect in the binding process. Consequently, since AZA is more hydrophobic than MB [38], a larger number of ordered water molecules solvating the dye hydrophobic region will be released in the BLF-AZA interaction processes; hence, ΔCp^o will be more negative. This result shows that the hydrophobicity of dye has a role in the BLF-phenothiazine dyes interactions.

Despite the more accurate direct measurements of ΔCp^o, compared to those obtained by the van't Hoff approximation [39], our heat capacity values for the BLF-phenothiazine dyes bindings, are of the same signal and magnitude of the ΔCp^o determined for the interaction of phenothiazine dyes with DNA (-0.32 to -0.23 kJ mol^{-1} K^{-1}) [40] or RNA (-0.86 to -0.44 kJ mol^{-1} K^{-1}) [41,42] determined by calorimetric measurements.

Besides ΔCp^o, another thermodynamic parameter which aptly expresses the hydrophobic effect, is the entropy change associated with the protein-dye interaction. Within the temperature range, the $T\Delta S^o$ values were positive for the interaction process of both studied phenothiazine dyes with BLF and became more positive when the number of CH_3 groups in the dye structure decreased from 4 (MB) to 2 (AZA) (Table 2.3). In addition, with increasing the temperature, the $T\Delta S^o$ parameter decreased.

As discussed for ΔH^o, the entropic term ($T\Delta S^o$) is also the result of the contribution of three molecular processes (Eq. 9):

$$T\Delta S^0 = T\Delta S^0_{desol} + T\Delta S^0_{BLF-dye} + T\Delta S^0_{conf} \quad (9)$$

where $T\Delta S^0_{desol}$ is the system entropy change associated with the release of water molecules from the dye and protein solvation shell, when the BLF-dye complex is formed, which results in an increase in the molecular configurational number of the system. The $T\Delta S^0_{BLF-dye}$ term refers to the loss of translational entropy owing to the decrease in the spatial number of freedom degrees of the interacting molecules when BLF is translated together with

the dyes. $T\Delta S^0_{conf}$ is mainly attributed to the gain and, sometimes, loss in entropy owing to the conformational changes of the protein site and dye molecules.

The $T\Delta S^o$ values were positive because the entropic gain owing to the $T\Delta S^0_{desol}$ and $T\Delta S^0_{conf}$ outweighs the entropic loss from the $T\Delta S^0_{BLF-dye}$ term. The same thermodynamic analysis used to explain the positive values of $T\Delta S^o$ could be applied to explain the difference between $T\Delta S^o$ (MB) and $T\Delta S^o$ (AZA). Since both dyes interact with BLF forming a 1:1 complex, the loss in translational entropy is the same for both dyes. Thus, the different $T\Delta S^o$ values found for both phenothiazine dyes result from the desolvation of interacting solutes, as well as the dye and protein conformational changes. However, since the MB and AZA dyes have very similar molecular geometry, the contribution from $T\Delta S^0_{conf}$ to $T\Delta S^o$ is probably approximately the same for both dyes. Thus, the difference in the $T\Delta S^o$ values between both dyes is due to the relatively higher hydrophobicity of AZA [38], compared to that of MB, which consequently releases a higher number of hydration water molecules, as corroborated by the ΔH^o and ΔCp^o measurements obtained in this work.

In years past, a great number of researches on protein-ligand interactions have demonstrated a proportional change between ΔH^o and ΔS^o, mainly when these parameters are measured in similar systems or in the same systems at different temperatures [43]. Fig. 2.5 depicts the variation in ΔH^o, as a function of ΔS^o for the BLF bindings to both of the investigated dyes.

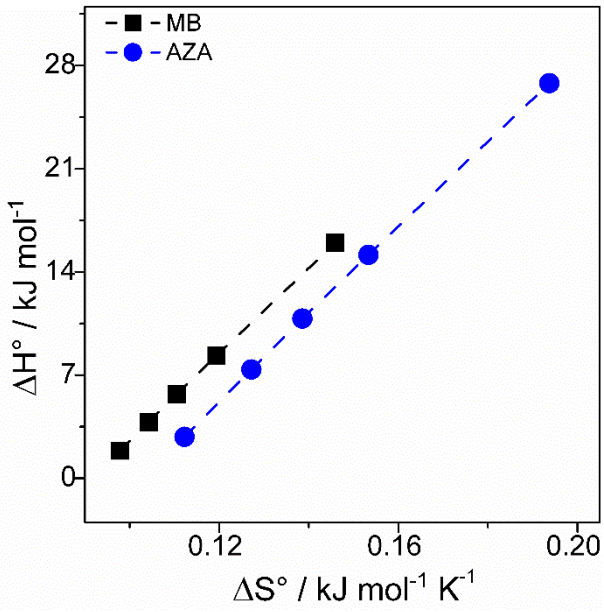

Fig. 2.5. Plot of ΔH^o versus ΔS^o for the interaction of (■) MB and (●) AZA with BLF.

ΔH^o increases linearly with ΔS^o, allowing the fitting of ΔH^o *versus* ΔS^o curve data with Eq. 10.

$$\Delta H^0 = \alpha + \beta \Delta S^0 \quad (10)$$

with α = -26.7 ± 0.3 kJ mol^{-1} and β = 293 ± 2 K, for BLF-MB interactions; and α = -30.0 ± 0.4 kJ mol^{-1} and β = 294 ± 3 K for BLF-AZA interactions.

Besides the protein-ligand system, the compensation between ΔH^o and ΔS^o is also observed in many processes and systems involving micellization [44], microemulsions [45], Langmuir monolayers [46], solution thermodynamics [47] and molecular recognition [48]; the molecular basis for such compensating behavior has attracted much interest [43]. As showed by all these works, the enthalpy-entropy compensation effect is an important tool for understanding the different thermodynamic aspects involved in dye-protein interactions [43].

To interpret the thermodynamic meaning of α and β constants, we need to use the fundamental Gibbs equations (Eq. 11):

$$\Delta H^0 = \Delta G^0 + T\Delta S^0 \quad (11)$$

By comparing Eq. 10 and 11, we can conclude that $\alpha = \Delta G^o_{comp}$ and $\beta = T_{comp}$, and they denote the standard free Gibbs energy change in compensation and the temperature of compensation, respectively.

The enthalpy-entropy compensation in the protein–ligand binding phenomenon could be related to two molecular mechanisms: (i) free ligand desolvation, and (ii) binding site fittings induced by the interactions. The binding of a ligand to a protein initially involves the release of H_2O molecules, which were solvating free molecules of the ligand and/or protein. This step of desolvation fundamentally affects the thermodynamic binding signature with respect to enthalpic and entropic contributions. The more water molecules are released, the more energy is spent to break the protein-H_2O, ligand-H_2O, and H_2O-H_2O interactions present in the interacting molecules solvation shell. However, this positive enthalpy change penalty is offset by an equivalent gain in entropy, associated with the increase in translational freedom degrees of the water molecules, resulting in a small variation in ΔG^o. Furthermore, the induced conformational fitting mechanism in the site assumes that the binding site in the protein is flexible, and that the interacting ligand induces a conformational change at the binding site.

This process, on one hand, leads to an enthalpic gain due to the break of intramolecular interactions among the protein aminoacids, and, on the other hand, results in an entropy gain due to the increase in conformational freedom degrees of protein segments, rendering ΔG^o almost invariant.

In spite of conventionality of fluorescence spectroscopy for investigating protein-dye interactions, it is restricted to the determination of the binding on the sites close to the Trp residues. Therefore, to better understand the BLF-phenothiazine dyes binding, complementary techniques that allow the elucidation of the interactions occurring at different sites, such as isothermal titration microcalorimetry (ITC) and surface plasmon resonance (SPR), are required.

2.3.2 Surface plasmon resonance (SPR) analysis

Exploiting the versatility of the experimental setup provided by SPR-based biosensors, evaluation of the kinetic and thermodynamic binding properties of different phenothiazine dyes to immobilized lactoferrin, can be achieved, and the results compared with data obtained from other solution-based affinity techniques.

2.3.2.1 Kinetics of BLF-phenothiazine dyes interaction

Analysis of protein-ligand binding kinetics by SPR can provide unique insights into the complex molecular recognition mechanisms [49,50]. With the purpose of determining the kinetic parameters of the BLF-phenothiazine dye interaction, the resonance-response (RU) profiles, as functions of time, known as sensorgrams, were recorded at 298.2 K and at a pH of 7.4, as illustrated in Fig. 2.6. Similar sensorgrams were obtained for the BLF-AZA interaction and are shown in Fig. S.A.6.

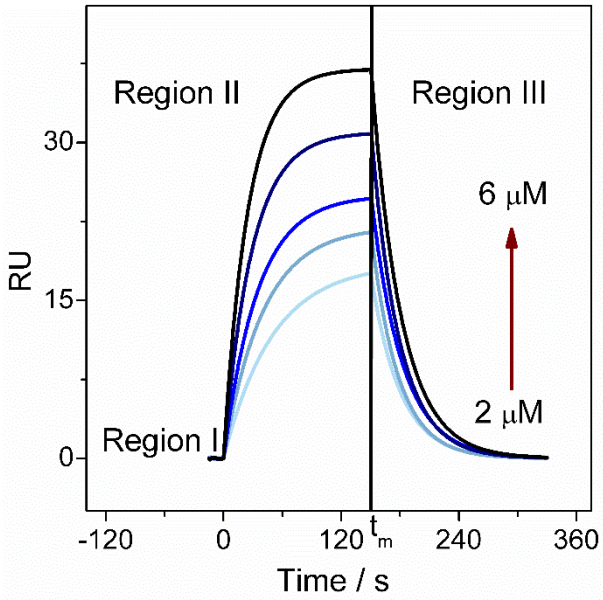

Fig. 2.6. Sensorgram (RU x time) obtained by the injection of MB (2-6 μM) flowing over a CM5 low-density BLF-immobilized sensor-chip surface (3890 RU), at 298.2 K and a pH of 7.4. The arrow indicates the increasing concentration of the MB solution.

In Region I, the RPS signals for all dyes were approximately zero because only the buffer flowed over the reference (without BLF immobilized) and sample cells (with BLF immobilized). Afterward, from 0 s, increasing concentrations of MB (or AZA) were injected into both cells (Region II). At each dye concentration, the SPR signal increased with the contact time between the dye solution and the BLF-immobilized phase (association/dissociation phase), achieving a maximum experimental value ($RU_{(tm)}$) at the resonance time (t_m) of 151 s and 11 s for MB and AZA, respectively. These profiles were determined for the BLF and phenothiazine dye free molecule association processes and BLF-phenothiazine dye complex dissociation.

However, after t_m (Region III), the RU values decreased because only the buffer fluxed on the sensor-chip surface, leading to the spontaneous dissociation of the complex, and return to baseline (dissociation phase). Similar profiles were found for the temperatures, 285.2 K, 289.2 K, 293.2 K, 297.2 K, 298.2 K, and 301.2 K (Fig. S.A.7 and Fig. S.A.8).

The kinetics of the binding between BLF and phenothiazine dyes was subsequently evaluated by applying a 1:1 kinetic interaction model to the SPR datasets. When phenothiazine dyes interact with BLF to form a 1:1 complex, the rate of the complex formation depends on the concentrations of the free dye molecules, free BLF adsorbed on the chip surface, and formed complexes, which can be described by Eq. 12:

$$\frac{d[BLF-Dye]}{dt} = k_a[Dye][BLF] - k_d[BLF-Dye] \quad (12)$$

where k_a and k_d are the association and dissociation rate constants, respectively; $[BLF-Dye]$, $[Dye]$, and $[BLF]$ are the complex, free phenothiazine dyes, and lactoferrin concentrations, respectively.

Considering the specification of the applied SPR technique, the concentration of formed complexes is proportional to the resonance response (RU) at time (t), while the free ligand concentration [BLF] will be the difference between total and bound protein concentrations. Knowing that the total concentration of immobilized BLF is proportional to the maximum analyte binding capacity (RU_{max}), the free BLF concentration will, therefore, be proportional to (RU_{max}-RU) (t). Since the dye concentration is constantly maintained by the flow system (absence of mass transport interference), its free concentration may be considered identical to the total dye concentration. The interaction between immobilized BLF and phenothiazine dyes in solution can, therefore, be assumed to follow pseudo-first order kinetics, and Eq. 12 can be rewritten as Eq. 13.

$$\frac{dRU}{dt}(t) = k_a[Dye](t)\big((RU_{max}-RU)(t)\big) - k_dRU(t) \quad (13)$$

Therefore, for the association phase (Region II, Fig. 2.6), the signal is given by:

$$RU(t) = RU_{max}(t_\infty)\left[1-e^{-k_{obs}(t)}\right] \quad (14)$$

where k_{obs} is the observed kinetic constant ($k_{obs}= k_a[Dye] + k_d$), and t is time. For the dissociation phase (Region III, Fig. 2.6), the signal is given by Eq. 15.

$$RU(t) = RU(t_m)e^{-k_d(t-t_m)} \quad (15)$$

where t_m is the initial time when the dissociation occurs.

The k_{obs} and k_d values were obtained by global fitting the experimental data of Region II and Region III of the sensorgrams to Eq. 14 and 15, respectively, using a nonlinear regression approach [51]. The k_a values were easily calculated from the slope of the k_{obs} *versus* $[Dye]$ curves (Fig. S.A.9). The association (k_a) and dissociation (k_d) kinetic rate constants for

interactions between BLF with MB or AZA, determined at different temperatures, are reported in Table 2.4.

Table 2.4. Values of k_a and k_d for the BLF-MB and BLF-AZA interactions at different temperatures obtained from SPR experiments.

T	BLF-MB		BLF-AZA	
	k_a	k_d	k_a	k_d
K	10^3 M^{-1} s^{-1}	s^{-1}	10^3 M^{-1} s^{-1}	s^{-1}
285.2	2.7 ± 0.1	0.025 ± 0.001	4.2 ± 0.3	0.42 ± 0.03
289.2	3.4 ± 0.3	0.027 ± 0.002	5.6 ± 0.1	0.42 ± 0.01
293.2	4.1 ± 0.1	0.03 ± 0.00	6.4 ± 0.3	0.44 ± 0.03
297.2	4.6 ± 0.1	0.032 ± 0.001	8.0 ± 0.5	0.46 ± 0.02
298.2	5.1 ± 0.1	0.034 ± 0.002	8.1 ± 0.6	0.46 ± 0.02
301.2	5.7 ± 0.3	0.036 ± 0.003	8.5 ± 0.6	0.47 ± 0.03

The k_a and k_d values for the BLF-MB and BLF-AZA systems were significantly different. The BLF-AZA complex formation process is about 1.6-fold faster ($4.2 \times 10^3 \pm 0.3 \leq k_a \geq 8.5 \times 10^3 \pm 0.6$ M^{-1} s^{-1}) than the BLF and MB molecule association ($2.7 \times 10^3 \pm 0.1 \leq k_a \geq 5.7 \times 10^3 \pm 0.3$ M^{-1} s^{-1}), while the k_d values for the BLF-AZA binding were approximately 13- to 16-fold higher than the rate constants of the BLF-MB complex dissociation, indicating that the BLF-phenothiazine dye interaction kinetics is dependent on the number of methyl substituents in the dye structure. Furthermore, it was found that an increase in temperature resulted in increased k_a and k_d values for the interactions of BLF with MB or AZA.

There are very few kinetic data on dye-protein interactions in the literature; however, recently, our group determined these parameters for the interaction of BSA with Congo red [52] or with curcumin [53] dyes. It was found that the Congo red binding to BSA is 5.7-fold faster than the formation of the BLF-MB complexes and 3.6-fold faster than the BLF-AZA association, while the BSA-curcumin interaction process is 2.9 and 1.8-fold faster than BLF-MB and BLF-AZA complex formation, respectively. Conversely, while the dissociation of the BLF-MB complex (0.034 ± 0.002 s^{-1}) is slower than BSA-Congo red (0.050 s^{-1}) and BSA-curcumin dissociation processes (0.677 s^{-1}), the BLF-AZA complex dissociation (0.46 ± 0.02 s^{-1}) is faster than the dissociation of BSA-Congo red complex and slower than that of BSA-curcumin. These discrepancies in the magnitude of k_a and k_d values between these dyes can

be attributed to possible differences in the interaction sites, structures, and charges of dye molecules (Congo red is an anion; curcumin is neutral; and phenothiazine dyes are cations).

Based on the Arrhenius plots for the temperature dependence of $ln\mathrm{k_a}$ and $ln\mathrm{k_d}$ (Fig. 2.7), the activation parameters values can be calculated via the linear regression.

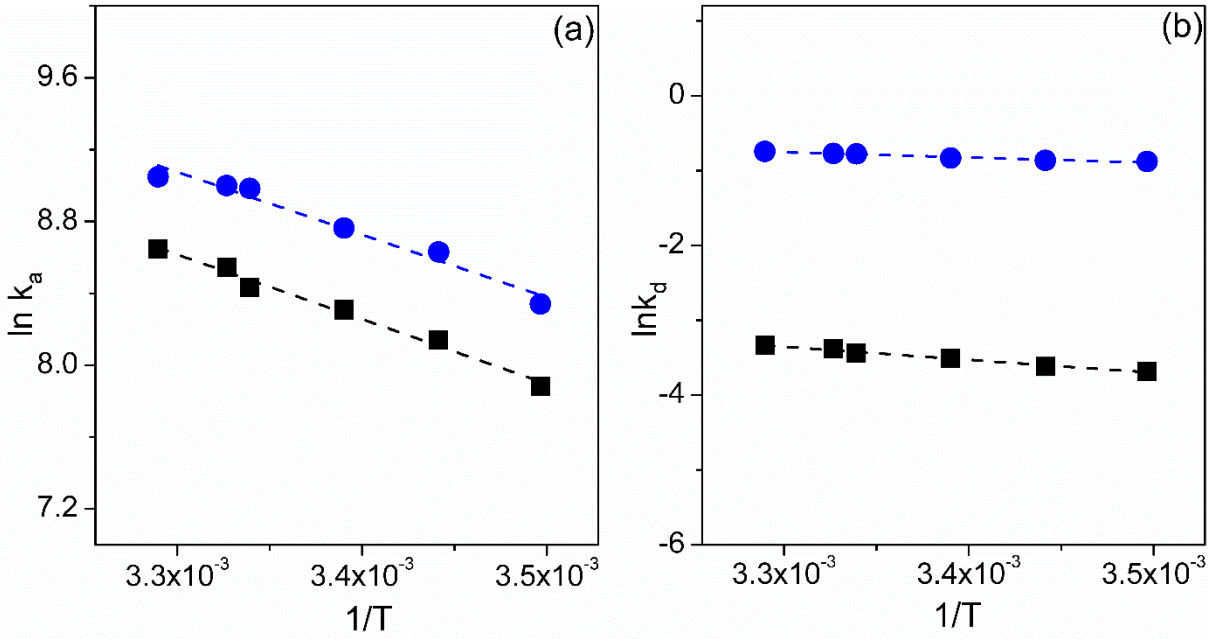

Fig. 2.7. Arrhenius plots of (a) $ln\ k_a$ and (b) $ln\ k_d$ associated with (■) BLF-MB and (●) BLF-AZA interactions, respectively, as functions of reciprocal temperature, obtained by SPR experiments.

From the slope of the $ln\ k_x$ *versus* $1/T$ ($x = a$ or d) curves, the activation energies ($E_x^{\ddagger}$) were obtained (Eq. 16). Similarly, the activation enthalpy ($\Delta H_x^{\ddagger}$), activation entropy ($\Delta S_x^{\ddagger}$), and activation free energy ($\Delta G_x^{\ddagger}$) changes associated with the activation complex formation processes were calculated with Eq. 17-19.

$$ln\left(\frac{k_x(T_2)}{k_x(T_1)}\right) = -\frac{E_x^{\ddagger}}{R}\left(\frac{1}{T_2} - \frac{1}{T_1}\right) \tag{16}$$

$$\Delta H_x^{\ddagger} = E_x^{\ddagger} - RT \tag{17}$$

$$\Delta G_x^{\ddagger} = -RTln\left(\frac{k_x h}{K_B T}\right) \tag{18}$$

$$T\Delta S_x^{\ddagger} = \Delta H_x^{\ddagger} - \Delta G_x^{\ddagger} \quad (19)$$

where k_x is the appropriate rate constant ($x = a$ for association, and $x = d$ for dissociation); K_B, Boltzmann's constant; and h, Planck's constant. The thermodynamic parameters of the activation derived from the Arrhenius plots are given in Table 2.5.

Table 2.5. Energy parameters of transition complex formation from the association of BLF and dye free molecules or from BLF-phenothiazine thermodynamic stable complex dissociation at 298.2 K.

Energy parameters	BLF-MB		BLF-AZA	
	Association	Dissociation	Association	Dissociation
$E^{\ddagger}$ (kJ mol^{-1})	33 ± 2	16 ± 1	32 ± 2	6.4 ± 0.6
$\Delta H^{\ddagger}$ (kJ mol^{-1})	31 ± 2	14 ± 1	30 ± 2	3.9 ± 0.6
$T\Delta S^{\ddagger}$ (kJ mol^{-1})	-21 ± 2	-68 ± 1	-21 ± 2	-71.0 ± 0.6
$\Delta G^{\ddagger}$ (kJ mol^{-1})	51.84 ± 0.05	81.4 ± 0.2	50.7 ± 0.2	74.93 ± 0.08

The intermediate complex is formed by the association of phenothiazine dyes and BLF free molecules or through the dissociation of thermodynamically stable BLF-phenothiazine dyes complexes. The activation energies related to the association ($E_a^{\ddagger}$) or dissociation ($E_d^{\ddagger}$) processes represent the energy that is required to overcome a hypothetical energy barrier that prevents the association of free ligands or dissociation of thermodynamically stable complexes [54].

Regardless of the dye chemical structure, the activation energy values for the association processes ($E_{a,MB}^{\ddagger}$ = 33 ± 2 kJ mol^{-1} and $E_{a,AZA}^{\ddagger}$ = 32 ± 2 kJ mol^{-1}) of the free ligands were higher than those for the complex dissociation processes ($E_{d,MB}^{\ddagger}$ = 16 ± 1 kJ mol^{-1} and $E_{d,AZA}^{\ddagger}$ = 6.4 ± 0.6 kJ mol^{-1}). These results show that the molecular dynamic of breaking and formation of biopolymer intramolecular interactions and ligand solvation shell are different when the activated complex is formed from the free ligands or from the dissociation of stable complexes. In addition, although the formation of the BLF-MB and BLF-AZA transition complexes from the free ligand association requires very similar $E_a^{\ddagger}$, the conformation change of the BLF-MB stable complex to the intermediate complex demands 2.5 times more energy ($E_{d,MB}^{\ddagger}$ = 16 ±1 kJ mol^{-1}) than that demanded by the BLF-AZA change process ($E_{d,AZA}^{\ddagger}$= 6.4 ±0.6 kJ mol^{-1}). This

difference in the $E_d^{\ddagger}$ values suggests that AZA, which has fewer CH_3 groups in its structure, promotes lesser intense BLF conformational change than MB does, resulting in less energy expenditure.

The $\Delta G^{\ddagger}$ values for the association ($\Delta G_a^{\ddagger}$) and dissociation ($\Delta G_d^{\ddagger}$) processes for each investigated temperature were not affected by the dye structure (Table S.A.1). This behavior occurs because in an association process, there are enthalpic and entropic variations that are different from those found in a dissociation process. Consequently, it is interesting to analyze the $\Delta G^{\ddagger}$ components, i.e., $\Delta H^{\ddagger}$ and $T\Delta S^{\ddagger}$.

In both systems, the $\Delta H^{\ddagger}$ values for the association processes were higher than for the dissociation processes (Table S.A.2), which can be explained with the same arguments proposed above for the activation energy. However, the greatest discrepancy between the association and dissociation processes is manifested in $T\Delta S^{\ddagger}$, whose difference ($T\Delta S_d^{\ddagger} - T\Delta S_a^{\ddagger}$) is -47 ± 2 kJ mol^{-1} for BLF-MB interaction, and -50 ± 2 kJ mol^{-1} for the BLF-AZA binding. This difference comes mainly from three contributions: (i) conformational changes that occur at the protein interaction site; (ii) release of free ligand solvation shell molecules; and (iii) loss of translational entropy of the free dye and protein molecules, which does not occur in the dissociation process of the thermodynamically stable complexes that form the activated complex.

2.3.2.2 Thermodynamic parameters for BLF-phenothiazine dyes interaction

Using the classical relation, $K_b = k_a/k_d$, the binding constant values (K_b) for the bindings of BLF to MB or AZA dyes were calculated. From the K_b values and their temperature dependence (Fig. S.A.10), the ΔG^o (Eq. 3), ΔH^o (Eq. 16, considering that k_x must be replaced by K_b, and $E_x^{\ddagger}$ by ΔH^o), and $T\Delta S^o$ (Eq. 7) values were obtained, as showed in Table 2.6.

Table 2.6. K_b, ΔG^o, ΔH^o, and $T\Delta S^o$ values for the BLF-MB and BLF-AZA complex formation at different temperatures and at a pH of 7.4. Data obtained by SPR measurements.

T	BLF-MB				BLF-AZA			
	K_b	ΔG^o	ΔH^o	$T\Delta S^o$	K_b	ΔG^o	ΔH^o	$T\Delta S^o$
K	10^4 M^{-1}	kJ mol^{-1}			10^4 M^{-1}	kJ mol^{-1}		
285.2	10.5 ± 0.3	-27.41 ± 0.01		45 ± 2	1.01 ± 0.04	-21.85 ± 0.01		48 ± 1
289.2	12.7 ± 0.3	-28.28 ± 0.00		46 ± 2	1.33 ± 0.06	-22.84 ± 0.01		49 ± 1
293.2	13.5 ± 0.9	-28.80 ± 0.01	17 ± 2	46 ± 2	1.47 ± 0.07	-23.39 ± 0.01	26 ± 1	49 ± 1
297.2	14.4 ± 0.6	-29.34 ± 0.01		47 ± 2	1.73 ± 0.09	-24.11 ± 0.01		50 ± 1
298.2	15.1 ± 0.8	-29.56 ± 0.01		47 ± 2	1.75 ± 0.06	-24.22 ± 0.01		50 ± 1
301.2	16.0 ± 0.2	-30.00 ± 0.00		47 ± 2	1.79 ± 0.03	-24.52 ± 0.00		50 ± 1

For all the investigated temperatures, the K_b values obtained by SPR were in the order of 10^4, and the ΔG^o values were negative, demonstrating that the equilibrium favors the BLF-phenothiazine dyes complex formation. In addition, the positive values of ΔH^o and $T\Delta S^o$ indicated that the binding of both phenothiazine dyes to BLF is entropy driven.

While fluorescence only monitors the interactions occurring near the Trp residues, SPR can determine the K_b values for all the sites present on the protein, even so, the values of the thermodynamic parameters for BLF-phenothiazine dye interactions obtained by both techniques were very similar. The exception was with the ΔH^o values, which, in spite of being positive, were larger in magnitude for SPR compared to those from the other technique, probably due to the contributions of other sites to the BLF-dye interaction. Despite of the BLF immobilization on the SPR chip surface, which in principle decrease the protein translational degree of freedom, $T\Delta S^o$ values determined by SPR were higher than those obtained by fluorescence, indicating that the biopolymer spatial restriction was not enough to reduce the entropic contribution to the BLF-dye interaction.

2.3.3 Thermodynamic binding parameters for BLF-phenothiazine dyes complex formation determined by isothermal titration calorimetry (ITC)

Although different techniques such as SPR and fluorescence spectroscopy have been developed to analyze the molecular interaction phenomena, calorimetry is the only technique which directly measures enthalpy changes, and therefore eliminates the need for the van't Hoff

analysis, which can lead to uncertainty in the values of this thermodynamic parameter [55]. Based on this, the binding of phenothiazine dyes to BLF was also investigated by ITC.

The plots of apparent molar enthalpy change ($\Delta H_{\mathrm{app-int}}$) of MB-BLF and AZA-BLF bindings against the molar ratio (χ) of dye/BLF, obtained at 298.15 K and at a pH of 7.4, are shown in Fig. 2.8.

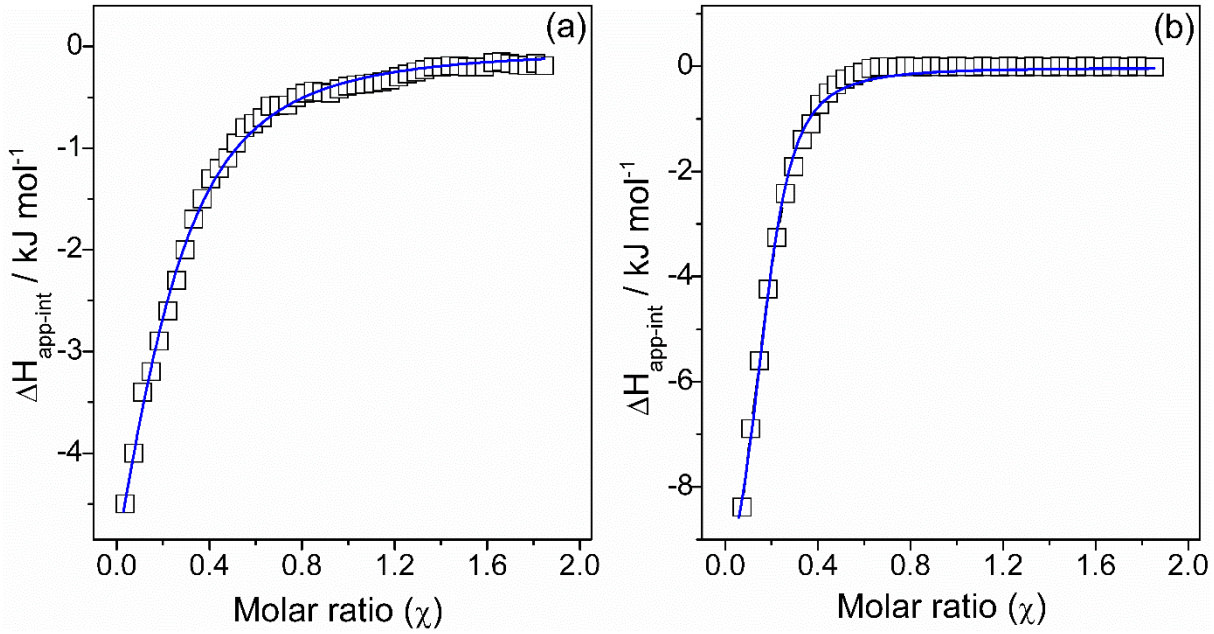

Fig. 2.8. $\Delta H_{\mathrm{app-int}}$ *versus* molar ratio (χ) plots for: (a) MB-BLF and (b) AZA-BLF interactions. Data points (□) reflect the experimental injection heat after correction for the heat of dilution, while the solid line represents the calculated fit of the data.

By fitting the $\Delta H_{\mathrm{app-int}}$ *versus* molar ratio (χ) curves (Fig. 2.8) to the independent binding sites model [56] described by Eq. 20, the K_b, n, and $\Delta H^{\circ}_{\mathrm{cal}}$ values for complex formation could be calculated, and from these parameters, it was possible to determine the ΔG^o (Eq. 3) and $T\Delta S^o$ (Eq. 7) values.

$$Q = \frac{V_c \Delta H^o_{cal}}{2K_b}\left[1 + K_b[dye]_T + nK_b[BLF]_T - \sqrt{(1 + K_b[dye]_T + nK_b[BLF]_T)^2 - 4nK_b{}^2[BLF]_T[dye]_T}\right] \quad (20)$$

where Q is the total heat content; V_c, the cell volume; K_b, the binding constant; $[dye]_T$ and $[BLF]_T$, the total dye and lactoferin concentrations in the system, respectively; and n, the stoichiometric number of formed complexes.

Fig. ***2.9*** shows the thermodynamic parameters for the BLF-phenothiazine dye interaction determined by ITC at 298.15 K and at a pH of 7.4.

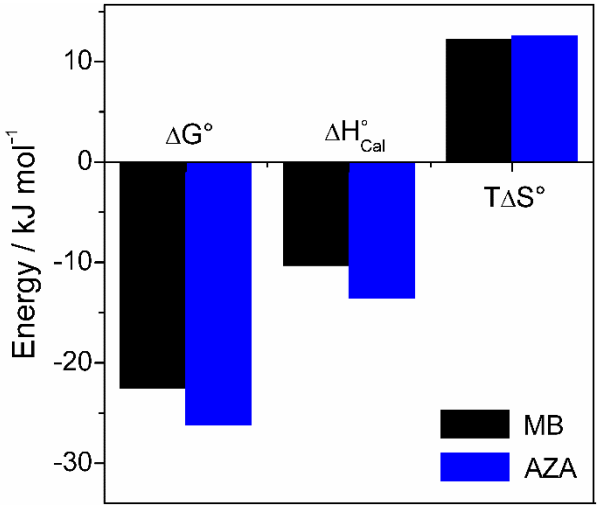

Fig. 2.9. Thermodynamic parameters for the bindings of BLF to MB and AZA at 298.15 K and at a pH of 7.4, obtained by ITC.

The K_b values obtained by ITC analysis for the BLF-phenothiazine dyes complexation [K_b^{MB} = 0.89 ± 0.05 × 10^4 M^{-1} and K_b^{AZA} = 3.8 ± 0.3 × 10^4 M^{-1}], as well as the calculated ΔG^o values (ΔG^o_{MB} = -22.5 ± 0.1 kJ·mol^{-1} and ΔG^o_{AZA} = -26.1 ± 0.2 kJ mol^{-1}), are in agreement with the values obtained by the fluorescence spectroscopy and SPR studies, revealing that the binding affinity of these dyes with BLF was higher for AZA than for MB. However, the *n* and $\Delta H^\circ_{\text{cal}}$ values determined by ITC were very different from those found in the fluorescence and SPR experiments; the n values obtained by calorimetry were about 5 times lower (n^{MB} = 0.19 ± 0.01 and n^{AZA} = 0.17 ± 0.01) and the $\Delta H^\circ_{\text{cal}}$ values were negative instead of positive as previously determined by the fluorescence and SPR techniques. This difference occurs because, although the phenothiazine dyes interact with both lactoferrin species (apo-BLF and holo-BLF), the interaction is more enthalpically intense and exothermic for the binding with holo-BLF (20% of native-BLF) [8], thereby dominating the energy values owing to the interaction with apo-BLF. Furthermore, similar to the fluorescence and SPR techniques, the $T\Delta S^o$ values determined by ITC were also positive, although lower in magnitude ($T\Delta S^o_{MB}$ = 12.2 ± 0.8

kJ·mol^{-1} and $T\Delta S^{o}_{AZA}$ = 12.6 ± 0.8 kJ mol^{-1}), which was expected, since the values of $T\Delta S^{o}$ were obtained from the ΔG^{o} and $\Delta H^{\circ}_{\mathrm{cal}}$ values that were previously determined.

2.4 Conclusions

The thermodynamics and kinetics of the interactions between lactoferrin and two phenothiazine dyes (MB or AZA) were investigated by surface plasmon resonance, fluorescence spectroscopy, and isothermal titration calorimetry techniques. Both dyes interact with lactoferrin, forming a complex; however, this interaction is stronger with AZA than with MB. The results obtained with techniques that involve the van't Hoff approximation (SPR and fluorescence) indicated that entropic factors were the only driving forces of the BLF-phenothiazine dye interactions. However, calorimetry indicated that there is a strong enthalpic contribution associated with the interaction of these dye with holo-BLF. Interestingly, although the formation of the BLF-MB and BLF-AZA transition complexes from the association of the free ligands requires very similar activation parameters, the dissociation of the thermodynamically stable complexes to form the intermediate complexes is very dependent on the dye chemical structure. This study provides a detailed insight into the interactions of AZA and MB dyes with lactoferrin, which may be very useful in understanding how these drug candidates interact with their macromolecular targets.

References

[1] A.L. Chapeau, G.M. Tavares, P. Hamon, T. Croguennec, D. Poncelet, S. Bouhallab, Spontaneous co-assembly of lactoferrin and β-lactoglobulin as a promising biocarrier for vitamin B9, Food Hydrocoll. 57 (2016) 280–290. doi:10.1016/j.foodhyd.2016.02.003.

[2] C.J. Baltazar, R. Mun, H.A. Tajmir-Riahi, J. Bariyanga, Spectroscopic studies on the interaction of mimosine with BSA and DNA, J. Mol. Struct. 1161 (2018) 273–278. doi:10.1016/j.molstruc.2018.01.039.

[3] R. Raj, S. Mitra, B. Gopal, Characterization of Staphylococcus epidermidis Polynucleotide phosphorylase and its interactions with ribonucleases RNase J1 and RNase J2, Biochem. Biophys. Res. Commun. 495 (2018) 2078–2084.

doi:10.1016/j.bbrc.2017.12.056.

[4] F. Poureshghi, P. Ghandforoushan, A. Safarnejad, S. Soltani, Interaction of an antiepileptic drug, lamotrigine with human serum albumin (HSA): Application of spectroscopic techniques and molecular modeling methods, J. Photochem. Photobiol. B Biol. 166 (2017) 187–192. doi:10.1016/j.jphotobiol.2016.09.046.

[5] F. Liu, S. Zhang, J. Li, D.J. McClements, X. Liu, Recent development of lactoferrin-based vehicles for the delivery of bioactive compounds: Complexes, emulsions, and nanoparticles, Trends Food Sci. Technol. 79 (2018) 1–43. doi:10.1016/J.TIFS.2018.06.013.

[6] S.A. González-Chávez, S. Arévalo-Gallegos, Q. Rascón-Cruz, Lactoferrin: structure, function and applications, Int. J. Antimicrob. Agents. 33 (2009) 301.e1–301.e8. doi:10.1016/j.ijantimicag.2008.07.020.

[7] E.N. Baker, H.M. Baker, Molecular structure, binding properties and dynamics of lactoferrin, Cell. Mol. Life Sci. 62 (2005) 2531–2539. doi:10.1007/s00018-005-5368-9.

[8] H. Bokkhim, N. Bansal, L. Grndahl, B. Bhandari, Physico-chemical properties of different forms of bovine lactoferrin, Food Chem. 141 (2013) 3007–3013. doi:10.1016/j.foodchem.2013.05.139.

[9] M.A. Coutinho da Silva, C.R. Darr, L.E. Moraes, B.S. Forshey, Lactoferrin Modulates Uterine Inflammation Postbreeding in the Mare, J. Equine Vet. Sci. 56 (2017) 63–67. doi:10.1016/j.jevs.2017.05.007.

[10] J. Padrão, R. Machado, M. Casal, S. Lanceros-Méndez, L.R. Rodrigues, F. Dourado, V. Sencadas, Antibacterial performance of bovine lactoferrin-fish gelatine electrospun membranes, Int. J. Biol. Macromol. 81 (2015) 608–614. doi:10.1016/j.ijbiomac.2015.08.047.

[11] P. Paul, S.S. Mati, S.C. Bhattacharya, G.S. Kumar, Exploring the interaction of phenothiazinium dyes methylene blue, new methylene blue, azure A and azure B with

tRNAPhe: spectroscopic, thermodynamic, voltammetric and molecular modeling approach, Phys.Chem.Chem.Phys. 19 (2017) 6636–6653. doi:10.1039/c6cp07888e.

[12] S.C. How, Y.H. Cheng, C.H. Lo, J.T. Lai, T.H. Lin, Z. Bednarikova, A. Antosova, Z. Gazova, J.W. Wu, S.S.S. Wang, Exploring the effects of methylene blue on amyloid fibrillogenesis of lysozyme, Int. J. Biol. Macromol. 119 (2018) 1059–1067. doi:10.1016/j.ijbiomac.2018.08.038.

[13] Z. Jiang, T.Q. Duong, Methylene blue treatment in experimental ischemic stroke: a mini review, Brain Circ. 2 (2016) 48–53. doi:10.4103/2394-8108.178548.

[14] J.L. Vennerstrom, M.T. Makler, C.K. Angerhofer, J. a. Williams, Antimalarial Dyes Revisited: Xanthenes, Azines, Oxazines, and Thiazines, Antimicrob. Agents Chemother. 39 (1995) 2671–2677. doi:10.1128/AAC.39.12.2671.

[15] D. Rajan, M. Ilanchelian, Exploring the interaction of Azure dyes with t-RNA by hybrid spectroscopic and computational approaches and its applications toward human lung cancer cell line, Int. J. Biol. Macromol. 113 (2018) 1052–1061. doi:10.1016/j.ijbiomac.2018.02.164.

[16] W. Wang, L. Yang, H. Sun, Z. Yang, Q. Du, C. Li, Improved photodynamic efficiency for methylene blue from silica-methylene blue@tannic acid-Fe(III) ions complexes in aqueous solutions, Adv. Powder Technol. 29 (2018) 341–348. doi:10.1016/j.apt.2017.11.021.

[17] Y. Li, Y. Zhang, S. Sun, A. Zhang, Y. Liu, Binding investigation on the interaction between Methylene Blue (MB)/TiO2 nanocomposites and bovine serum albumin by resonance light-scattering (RLS) technique and fluorescence spectroscopy, J. Photochem. Photobiol. B Biol. 128 (2013) 12–19. doi:10.1016/j.jphotobiol.2013.07.027.

[18] K. Shanmugaraj, S. Anandakumar, M. Ilanchelian, Exploring the biophysical aspects and binding mechanism of thionine with bovine hemoglobin by optical spectroscopic and molecular docking methods, J. Photochem. Photobiol. B Biol. 131 (2014) 43–52.

doi:10.1016/j.jphotobiol.2014.01.001.

[19] A.S. Sharma, S. Anandakumar, M. Ilanchelian, In vitro investigation of domain specific interactions of phenothiazine dye with serum proteins by spectroscopic and molecular docking approaches, RSC Adv. 4 (2014) 36267. doi:10.1039/C4RA04630G.

[20] A. Selva, S. Anandakumar, M. Ilanchelian, A combined spectroscopic and molecular docking study on site selective binding interaction of Toluidine blue O with Human and Bovine serum albumins, J. Lumin. 151 (2014) 206–218. doi:10.1016/j.jlumin.2014.02.009.

[21] S.S. Arumugam, N. Subramanian, I. Malaichamy, New insights into the dimerization and site-specific cooperative interaction of Azure B with model transport proteins by spectroscopic and computational studies, J. Photochem. Photobiol. B Biol. 164 (2016) 212–225. doi:10.1016/j.jphotobiol.2016.09.011.

[22] S. Das, M.M. Islam, G.C. Jana, A. Patra, P.K. Jha, M. Hossain, Molecular binding of toxic phenothiazinium derivatives, azures to bovine serum albumin: A comparative spectroscopic, calorimetric, and in silico study, J. Mol. Recognit. 30 (2016) 1–11. doi:10.1002/jmr.2609.

[23] K. Vuignier, J. Schappler, J.-L. Veuthey, P.-A. Carrupt, S. Martel, Drug–protein binding: a critical review of analytical tools, Anal. Bioanal. Chem. 398 (2010) 53–66. doi:10.1007/s00216-010-3737-1.

[24] H.H. Nguyen, J. Park, S. Kang, M. Kim, Surface plasmon resonance: A versatile technique for biosensor applications, Sensors. 15 (2015) 10481–10510. doi:10.3390/s150510481.

[25] M. Guo, L.-Y. Zhang, W.-J. Lü, H.-R. Cao, Analysis of the spectroscopic characteristics on the binding interaction between tosufloxacin and bovine lactoferrin, J. Lumin. 131 (2011) 768–775. doi:10.1016/j.jlumin.2010.11.036.

[26] W. Yang, F. Liu, C. Xu, F. Yuan, Y. Gao, Molecular interaction between (−)-

epigallocatechin-3-gallate and bovine lactoferrin using multi-spectroscopic method and isothermal titration calorimetry, Food Res. Int. 64 (2014) 141–149. doi:10.1016/j.foodres.2014.06.001.

[27] J. Jayabharathi, V. Thanikachalam, M.V. Perumal, A study on the binding interaction between the imidazole derivative and bovine serum albumin by fluorescence spectroscopy, J. Lumin. 132 (2012) 707–712. doi:10.1016/j.jlumin.2011.10.023.

[28] J.R. Lakowicz, Principles of Fluorescence Spectroscopy, Trird edit, Maryland, USA, 2006. doi:10.1007/978-0-387-46312-4.

[29] P.L. Xavier, K. Chaudhari, P.K. Verma, S.K. Pal, T. Pradeep, Luminescent quantum clusters of gold in transferrin family protein, lactoferrin exhibiting FRET, Nanoscale. 2 (2010) 2769–2776. doi:10.1039/c0nr00377h.

[30] M. Van De Weert, L. Stella, Fluorescence quenching and ligand binding: A critical discussion of a popular methodology, J. Mol. Struct. 998 (2011) 144–150. doi:10.1016/j.molstruc.2011.05.023.

[31] P.R. Callis, Binding phenomena and fluorescence quenching. I: Descriptive quantum principles of fluorescence quenching using a supermolecule approach, J. Mol. Struct. 1077 (2014) 14–21. doi:10.1016/j.molstruc.2014.04.050.

[32] X.L. Wei, J.B. Xiao, Y. Wang, Y. Bai, Which model based on fluorescence quenching is suitable to study the interaction between trans -resveratrol and BSA ?, Spectrochim. Acta Part A Mol. Biomol. Spectrosc. 75 (2010) 299–304. doi:10.1016/j.saa.2009.10.027.

[33] P.D. Ross, S. Subramanian, Thermodynamics of Protein Association Reactions: Forces Contributing to Stability, Biochemistry. 20 (1981) 3096–3102. doi:10.1021/bi00514a017.

[34] R.I. Boysen, Y. Wang, H.H. Keah, M.T.W. Hearn, Observations on the origin of the non-linear van’t Hoff behaviour of polypeptides in hydrophobic environments,

Biophys. Chem. 77 (1999) 79–97. doi:10.1016/S0301-4622(99)00002-2.

[35] G.M.D. Ferreira, G.M.D. Ferreira, Á.J.P. Agudelo, E.A. Hudson, A.C. dos S. Pires, L.H.M. Da Silva, Lactoferrin denaturation induced by anionic surfactants: The role of the ferric ion in the protein stabilization, Int. J. Biol. Macromol. 117 (2018) 1039–1049. doi:10.1016/j.ijbiomac.2018.05.058.

[36] K. Gallagher, K. Sharp, Electrostatic contributions to heat capacity changes of DNA-ligand binding, Biophys. J. 75 (1998) 769–776. doi:10.1016/S0006-3495(98)77566-6.

[37] J. Gómez, E. Freire, Thermodynamic Mapping of the Inhibitor Site of the Aspartic Protease Endothiapepsin, J. Mol. Biol. 252 (1995) 337–350. doi:10.1006/jmbi.1995.0501.

[38] J.S. da Silva, H.C. Junqueira, T.L. Ferreira, Effect of pH and dye concentration on the n-octanol/water distribution ratio of phenothiazine dyes: a microelectrode voltammetry study, Electrochim. Acta. 144 (2014) 154–160. doi:10.1016/j.electacta.2014.08.094.

[39] J.B. Chaires, Possible origin of differences between van't Hoff and calorimetric enthalpy estimates, Biophys. Chem. 64 (1997) 15–23. doi:10.1016/S0301-4622(96)02205-3.

[40] P. Paul, G.S. Kumar, Thermodynamics of the DNA binding of phenothiazinium dyes toluidine blue O, azure A and azure B, J. Chem. Thermodyn. 64 (2013) 50–57. doi:10.1016/j.jct.2013.04.023.

[41] B. Saha, G.S. Kumar, Binding interaction of phenothiazinium dyes with double stranded RNAs: Spectroscopic and calorimetric investigation, J. Photochem. Photobiol. B Biol. 167 (2017) 99–110. doi:10.1016/j.jphotobiol.2016.12.022.

[42] A.Y. Khan, G. Suresh Kumar, A thermodynamic investigation on the binding of phenothiazinium dyes azure A and azure B to double stranded RNA polynucleotides, J. Chem. Thermodyn. 91 (2015) 225–233. doi:10.1016/j.jct.2015.07.021.

[43] J.D. Chodera, D.L. Mobley, Entropy-Enthalpy Compensation: Role and Ramifications

in Biomolecular Ligand Recognition and Design, Annu Rev Biophys. 42 (2013) 121–142. doi:10.1146/annurev-biophys-083012-130318.

[44] L.-J. Chen, S.-Y. Lin, C.-C. Huang, Effect of Hydrophobic Chain Length of Surfactants on Enthalpy−Entropy Compensation of Micellization, J. Phys. Chem. B. 102 (1998) 4350–4356. doi:10.1021/jp9804345.

[45] S.K. Hait, S.P. Moulik, M.P. Rodgers, S.E. Burke, R. Palepu, Physicochemical Studies on Microemulsions. 7. Dynamics of Percolation and Energetics of Clustering in Water/AOT/Isooctane and Water/AOT/Decane w/o Microemulsions in Presence of Hydrotopes (Sodium Salicylate, a-Naphthol, b-Naphthol, Resorcinol, Catechol..., J. Phys. Chem. B. 105 (2001) 7145–7154. doi:10.1021/jp0105084.

[46] E.D. Goddard, J.A. Ackilli, Monolayer properties of fatty acids, J. Colloid Sci. 18 (1963) 585–595. doi:10.1016/0095-8522(63)90050-3.

[47] A.F.D. De Namor, J.S. Velarde, R.G. Hutcherson, E. Piro, E.E. Castellano, X-Ray diffraction studies and solution thermodynamics of 5,7,17,23-para-tert-butyl-25,26,27,28-tetra(diethylamine)ethoxy- calix(4)arene, J. Chem. Soc. Faraday Trans. 94 (1998) 1257–1261. doi:10.1039/A708720I.

[48] P.A. Borea, K. Varani, S. Gessi, P. Gilli, A. Dalpiaz, Receptor binding thermodynamics as a tool for linking drug efficacy and affinity, Farm. 53 (1998) 249–254. doi:10.1016/S0014-827X(98)00017-2.

[49] Á. Juhász, M. Luty-Błocho, M. Wojnicki, G.K. Tóth, E. Csapó, General method for kinetic and thermodynamic evaluation of a receptor model peptide-drug molecule interaction studied by surface plasmon resonance, Microchem. J. 147 (2019) 311–318. doi:10.1016/j.microc.2019.03.048.

[50] F. Fathi, J. Ezzati Nazhad Dolatanbadi, M.R. Rashidi, Y. Omidi, Kinetic studies of bovine serum albumin interaction with PG and TBHQ using surface plasmon resonance, Int. J. Biol. Macromol. 91 (2016) 1045–1050. doi:10.1016/j.ijbiomac.2016.06.054.

[51] N.J. de Mol, M.J.E. Fischer, Chapter 5 - Kinetic and Thermodynamic Analysis of Ligand-Receptor Interactions: SPR Applications in Drug Development, in: R.B.M. Schasfoort, A.J. Tudos (Eds.), Handb. Surf. Plasmon Reson., 1st ed., 2008: pp. 123–172. doi:doi:10.1039/9781847558220-00123.

[52] H.M.C. de Paula, Y.L. Coelho, A.J.P. Agudelo, J. de P. Rezende, G.M.D. Ferreira, G.M.D. Ferreira, A.C. dos S. Pires, L.H.M. da Silva, Kinetics and thermodynamics of bovine serum albumin interactions with Congo red dye, Colloids Surfaces B Biointerfaces. 159 (2017) 737–742. doi:10.1016/j.colsurfb.2017.08.036.

[53] E.A. Hudson, H.M.C. de Paula, G.M.D. Ferreira, G.M.D. Ferreira, M. do C. Hespanhol, L.H.M. da Silva, A.C. dos S. Pires, Thermodynamic and kinetic analyses of curcumin and bovine serum albumin binding, Food Chem. 242 (2018) 505–512. doi:http://dx.doi.org/10.1016/j.foodchem.2017.09.092.

[54] M.K. Wild, M.C. Huang, U. Schulze-Horsel, P.A. Van der Merwe, D. Vestweber, Affinity, Kinetics, and Thermodynamics of E-selectin Binding to E-selectin Ligand-1, J. Biol. Chem. 276 (2001) 31602–31612. doi:10.1074/jbc.M104844200.

[55] T.S.G. Olsson, M.A. Williams, W.R. Pitt, J.E. Ladbury, The Thermodynamics of Protein – Ligand Interaction and Solvation : Insights for Ligand Design, J. Mol. Biol. 384 (2008) 1002–1017. doi:10.1016/j.jmb.2008.09.073.

[56] J.C. Martinez, J. Murciano-calles, E.S. Cobos, M. Iglesias-bexiga, I. Luque, J. Ruiz-sanz, Isothermal Titration Calorimetry : Thermodynamic Analysis of the Binding Thermograms of Molecular Recognition Events by Using Equilibrium Models, in: Appl. Calorim. a Wide Context – Differ. Scanning Calorimetry, Isothermal Titration Calorim. Microcalorim., 2013: pp. 73–104. doi:http://dx.doi.org/10.5772/53311.

CAPÍTULO 3: ENERGETIC CHARACTERIZATION OF SUPRAMOLECULAR STRUCTURE FORMATION BETWEEN LACTOFERRIN AND CARBOXYMETHYLCELLULOSE

Abstract

The characterization of interactions between proteins and polysaccharides is fundamental to understand the molecular recognition processes that take place in supramolecular systems. In this study, the kinetics and thermodynamics of the formation of soluble complexes between bovine lactoferrin (BLF) and carboxymethylcellulose (CMC) have been investigated by surface plasmon resonance (SPR) and fluorescence spectroscopy (FS). SPR measurements indicated that at temperatures ≤289.2 K, activated complex formation is dominated by the energy released from specific interactions between the protein and polysaccharide ($E_a^{\ddagger}$ and $E_d^{\ddagger} < 0$). In both techniques, the binding constant was as high as 10^6 mol^{-1} L and negative ΔG^o values were determined (-38.18 ≥ ΔG_{FS}^o ≥ -43.44 kJ mol^{-1} and -34.1 ≥ ΔG_{SPR}^o ≥ -37.4 kJ mol^{-1}). However, although the SPR data demonstrated that the formation of the BLF-CMC complexes was entropically driven (57 ≤ $T\Delta S_{SPR}^o$ ≤ 60 kJ mol^{-1}) and enthalpically unfavorable (ΔH_{SPR}^o = 23 kJ mol^{-1}), the fluorescence assays returned exothermic ΔH_{FS}^o values (-96 and -31 kJ mol^{-1}) up to 293.2 K and endothermic (39, 111, and 187 kJ mol^{-1}) at temperatures ≥298.2 K, whilst the $T\Delta S_{FS}^o$ values ranged from -58 to 230 kJ mol^{-1}. This study provides useful information on the formation of BLF-CMC soluble complexes, which could facilitate their application in functional ingredient encapsulation in the food, nutraceutical, and pharmaceutical industries.

Keywords: Activated complex, kinetics, thermodynamic, carboxymethylcellulose, supramolecular structures, lactoferrin.

3.1 Introduction

The protein-polysaccharide interaction is a fundamental physico-chemical phenomenon that is relevant to numerous biological processes such as protein transcription, antigen-antibody reactions, and enzymatic channeling [1]. In addition, the formation of supramolecular structures containing these biomolecules is very important for industrial applications such as encapsulation processes [2–4], the design of multi-layer structures [5], formation and stabilization of food emulsions [6], formation of new food gels [7] and the recovery of proteins from industrial by-products [7,8]. Therefore, proper understanding of the interactions between proteins and polysaccharides is vital for the design and development of new functional systems and has become a topic of continuous investigation [9–11].

Depending on the charge density, molecular weight, and chemical nature of the biopolymers and the proportion between the macromolecules, as well as the experimental conditions of the investigation or application, such as the pH and ionic strength, the association between proteins and polysaccharides may result in the formation of either a soluble complex or an insoluble microaggregate (coacervate or precipitate) [12–14]. The formation of soluble complexes between proteins and polysaccharides has a number of potentially useful applications in foods, pharmaceuticals, and personal care products [15]. Thus, over the past years, lactoferrin-polysaccharide complex formation has been attracting considerable attention mainly due to the micro- and nano-encapsulation properties of these materials [16–18].

Lactoferrin is an iron-binding protein present in many mammalian biological fluids, which plays an important role in the defense mechanism of the organism due its antioxidant, antimicrobial, and anti-inflammatory properties. The human and bovine lactoferrin structures are similar and comprise 691 and 681 amino acid residues, of which 10 and 13, respectively, are tryptophan (Trp) residues. The tridimensional structure comprises two lobes (N and C) with two domains each (N1, N2, C1, and C2), which form a cleft where the ferric ion (Fe^{3+}) is strongly bonded ($K_b \sim 10^{20}$) [19,20]. In addition to these structural features, this protein has a relatively high isoelectric point (pH 8–9), indicating that it has a positive charge across a wide range of pH conditions [21]. Consequently, bovine lactoferrin (BLF) can form soluble complexes with negatively charged polysaccharides, as is the case with carboxymethylcellulose (CMC).

CMC is a polysaccharide derived from cellulose, comprising linear β-(1,4)-linked d-glucopyranose chains (Fig. 3.1) [22]. CMC molecules containing carboxylate groups are

negatively charged, thereby enabling interaction with proteins to form complexes that have different physicochemical and functional properties to those of the single macromolecules [23,24]. Both CMC and BLF are environmentally friendly, nontoxic, and abundant resources and are therefore widely used in the food, pharmaceutical, and cosmetic industries [25–28]. The formation of complexes or conjugates can enhance the BLF stability at high temperatures, high ionic strengths, and extreme pH conditions [29,30]. Moreover, it can be used to design colloidal delivery systems for the encapsulation, protection, and controlled release of functional chemical products [17,31].

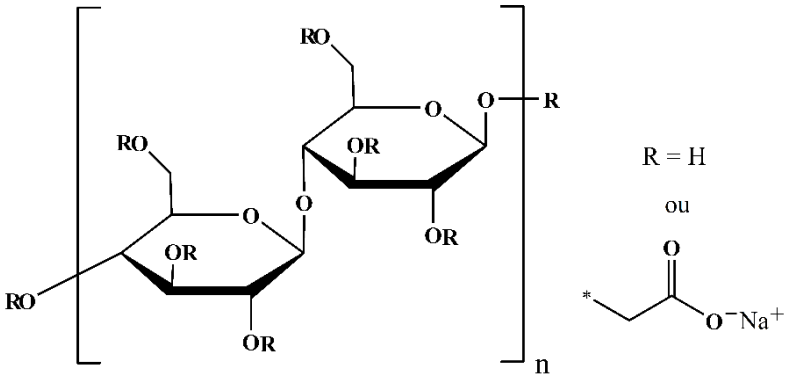

Fig. 3.1. Chemical structure of carboxymethylcellulose.

Owing to the biological significance of BLF-polysaccharide interactions and the industrial potential of such systems, many studies focusing on these interactions have been reported in the literature. However, a critical analysis of articles and reviews reveals that some fundamental aspects, such as the kinetics and thermodynamics of interaction between these biopolymers are yet to be fully elucidated [17,18,30,32,33].

In this work, the kinetics and thermodynamics of interaction between these two important biopolymers were investigated at pH 4 by fluorescence spectroscopy (FS) and surface plasmon resonance (SPR) to gain further insight into the formation processes of these BLF-CMC soluble complexes. This study provides a good understanding of the interactions between BLF and CMC as well as useful information for the research and development of new supramolecular systems with strategic applications in the various fields of science.

3.2 Material and Methods

3.2.1 Materials

CMC (>99 % wt), BLF (>99 % wt), sodium acetate (CH_3COONa; analytical grade), and acetic acid (CH_3CO_2H; analytical grade) were purchased from Sigma-Aldrich (St. Louis, MO, USA). Research-grade CM5 sensor chips and the coupling reagents (N-ethyl-N′,N′-dimethylaminopropylcarbodiimide (EDC), N-hydroxysuccinimide (NHS), and ethanolamine hydrochloride (1 M, pH 8.5) were purchased from GE Healthcare (Pittsburgh, PA, USA).

3.2.2 BLF-CMC interactions investigated by SPR

The kinetic and thermodynamic parameters for the interactions between CMC and BLF were obtained by SPR using a Biacore X100 instrument (GE Healthcare, Pittsburgh, PA, USA). Prior to use, BLF was immobilized (3864 RU) on a CM5 sensor chip, using a Biacore amine coupling kit according to the manufacturer's instructions. Briefly, the CM5 chips were activated for 7 min with EDC/NHS, after which the excessive activated carboxyl groups were blocked with ethanolamine for a further 7 min. BLF was then immobilized on the chip (15 μg mL^{-1}) in 0.01 mol L^{-1} sodium acetate (pH 4). BLF immobilization was performed at low levels (3864 RU) to reduce any potential mass transport and crowding phenomena. In experiments with immobilized BLF, a one flow cell was used as a reference surface; this surface was prepared as described above, but without BLF immobilization. The BLF-CMC interaction experiments were carried out at pH 4 and temperatures in the range 285.2–301.2 K. CMC solutions at the working concentration range 3×10^{-6}–3.4×10^{-6} mol L^{-1} were prepared in buffer at pH 4. For each binding experiment, CMC solutions at a determined concentration were injected in the flowing system to increase their concentration over both the sample (immobilized BLF) and reference (without BLF) surfaces, to correct for systematic noise and instrument drift. Prior to each CMC binding cycle, a buffer at pH 4 was injected in order to obtain the baseline.

3.2.3 BLF-CMC interactions investigated by FS

All the fluorescence spectra were measured using a Cary Eclipse Fluorescence Spectrophotometer (Agilent Technologies, Santa Clara, USA) equipped with a thermostat bath, using quartz cells having a 1-cm path length. The temperature was controlled at 288.2, 293.2,

298.2, 303.2, and 308.2 K. The BLF Trp residues were excited at 295 nm using an excitation slit of 2.5 nm, emission slit of 5.0 nm, and a photomultiplier tube (PMT) voltage of 750 V, at a scan rate of 600 nm/min, to obtain emission spectra in the range 296–500 nm. The fluorescence spectra were recorded at pH 4, using a fixed BLF concentration (1.97×10^{-5} mol L^{-1}) in the presence of CMC of varied concentrations in the range 0–1.7×10^{-4} mol L^{-1}.

Since CMC has absorption at wavelengths near the wavelengths of excitation and emission used in this study, all of the fluorescence intensities were corrected according to Eq. 1 [34]:

$$F_{obs} = F_{corr} \cdot 10^{-\frac{A_{ex} \cdot d_{ex}}{2} - \frac{A_{em} \cdot d_{em}}{2}} \quad (1)$$

where F_{obs} is the measured fluorescence by spectrofluorometer, F_{corr} is fluorescence intensity after correction of inner-filter effect, A_{ex} and A_{em} are the measured change in absorbance value at the excitation and emission wavelength, respectively, caused by CMC addition (in a 1 cm pathlength cuvette) and d_{ex} and d_{em} are the cuvette pathlength in the excitation and emission direction (in cm), respectively.

3.3 Results and Discussion

3.3.1 Kinetics of BLF-CMC complex formation determined by SPR

In general, protein-polysaccharide interactions yield insoluble molecular aggregates, such as coacervates and conjugates, depending on thermodynamic conditions including the pH, concentration, and ionic strength [14,31,35]. However, it is possible to obtain stable, soluble protein-polysaccharide complexes by modulating these thermodynamic conditions, thereby enabling the determination of the kinetic and thermodynamic parameters of these complex formation processes. A few studies on thermodynamic binding between proteins and polysaccharides in solution have been performed using different techniques, e.g., isothermal titration calorimetry and FS [36,37]. However, no kinetic data on such interactions are available to date. SPR is a real-time technique that allows the examination of the intermolecular interactions between biomolecules. It provides kinetic parameters for the association of free biomolecules and dissociation of thermodynamic stable complexes by processing the sensorgram data, where the resonance units (RU) are expressed as a function of time. Fig. 3.2

illustrates the sensorgrams for BLF-CMC interaction at 298.2 K and pH 4. Similar sensorgrams were obtained for the other five different temperatures (Fig. S.B.1).

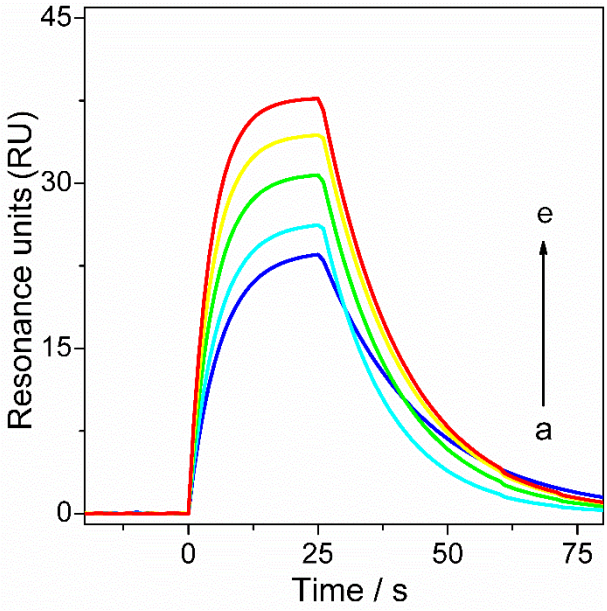

Fig. 3.2. Sensorgrams for BLF interacting with CMC at different concentrations (a–e: 3×10^{-6}–3.4×10^{-6} mol L^{-1}), flowing over a CM5 low-density protein-immobilized sensor-chip surface (3864 RU) at pH 4 and 298.2 K.

The sensorgrams reveal changes in the RU values over time and can be related to the association between the free BLF and CMC molecules to form the BLF-CMC complex as well as to the dissociation of this complex. This is represented by the chemical equilibrium equation indicated by Eq. 2:

$$BLF + CMC \rightleftharpoons BLF - CMC \tag{2}$$

The kinetic parameters were obtained by globally fitting (Eqs. 3 and 4) the RU data *versus* time to a 1:1 binding model:

$$RU(t) = RU(t_m)\, e^{-k_d(t-t_m)} \tag{3}$$

where k_d is the dissociation rate constant and t_m is the time at the beginning of the descending phase, i.e., when only the dissociation process occurs.

$$RU(t) = RU_{max}(t_\infty)[1 - e^{-k_{obs}(t)}] \quad (4)$$

where k_{obs} is the observed constant and $[RU_{\max}(t_\infty)]$ is the SPR response at BLF saturation by CMC. The value of k_{obs} was used to determine the association rate constant (k_a) value from the slope of the k_{obs} *versus* [CMC] curve (Fig. S.B.2).

The k_a and k_d values for the BLF-CMC complexes at pH 4 and different temperatures are presented in Table 3.1.

Table 3.1. Rate constants for the association (k_a) of the free BLF and CMC biomolecules and the dissociation (k_d) of the BLF-CMC stable complex at pH 4 and different temperatures.

T	k_a	k_d
K	10^5 L mol^{-1} s^{-1}	10^{-2} s^{-1}
285.2	1.4 ± 0.1	7.7 ± 0.1
289.2	1.20 ± 0.05	5.6 ± 0.1
293.2	1.2 ± 0.1	4.9 ± 0.2
297.2	1.6 ± 0.1	5.9 ± 0.2
298.2	1.80 ± 0.08	6.4 ± 0.1
301.2	2.8 ± 0.1	9.3 ± 0.3

Considering that k_a represents the number of BLF-CMC complexes formed per second and k_d denotes the fraction of complexes that dissociate per second, the high k_a values (in the order of 10^5 L mol^{-1} s^{-1}) and low k_d values (~10^{-2} s^{-1}) demonstrated that probably the complexes formed between BLF and CMC occurred without intense conformational changes in the biopolymer chemical structure, since smaller k_a and higher k_d values are expected in the binding process involving molecular dynamics with strong conformational changes [38]. Thus, it is likely that CMC interacts on the surface sites of BLF, inducing small changes in the protein and/or polysaccharide conformation.

The k_a values determined in our study were of the same magnitude as those obtained for the interaction between antigen/antibody complexes (mAb/IgG pAb) at 298.2 K (1.13×10^5 L mol^{-1} s^{-1}) [39] , and 3.8 times higher than those reported for actin-aplyronine A complexes with tubulin heterodimers (4.78×10^4 L mol^{-1} s^{-1}) [40]. On the other hand, because antigen/antibody complexes are formed under very specific conditions with specific interactions, thus, in this case, the k_d values were significantly lower (2.23×10^{-4} s^{-1}). For

heterodimer formation, the k_d values were of the same order (8.82×10^{-2} s^{-1}) as those recorded in this study.

The study of the temperature dependence of $ln\ k_a$ and $ln\ k_d$ yielded important energetic parameters related to the formation of an activated BLF-CMC complex from the association of free BLF and CMC and the dissociation of the BLF-CMC thermodynamic stable complex, respectively. The plots of $ln\ k_a$ or $ln\ k_d$ *versus* 1/T (Fig. 3.3) afforded the activation energies ($E_x^{\ddagger}$) for the association ($x = a$) or dissociation ($x = d$) processes (Eq. 5).

$$E_x^{\ddagger}(T) = -R\left(\frac{d \ln k_x}{d\,T}\right) \tag{5}$$

where k_x is the association or dissociation rate constant (L mol^{-1} s^{-1} or s^{-1}, respectively); $E_x^{\ddagger}$ is the activation energy (kJ mol^{-1}), and R is the universal gas constant.

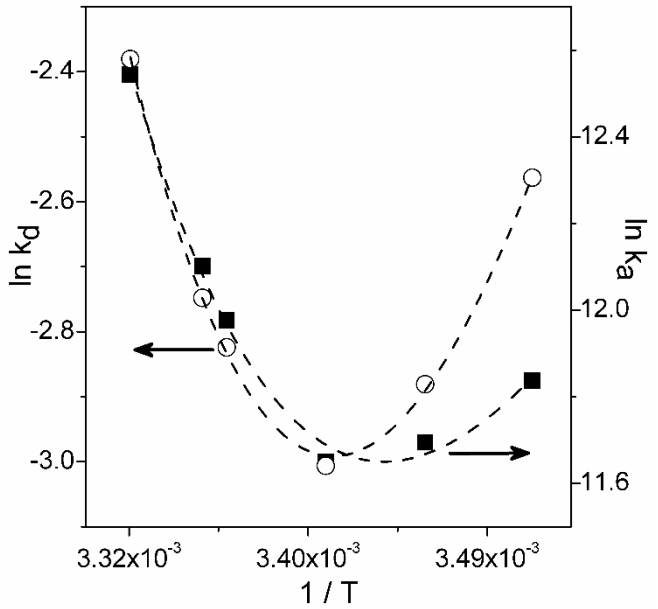

Fig. 3.3. Arrhenius plots: $ln\ k_a$ (■) and $ln\ k_d$ (○) as function of the reciprocal temperature associated with BLF-CMC activated complex formation at pH 4.

The Arrhenius plots displayed a second-order polynomial profile for the dependence of $ln\ k_a$ and $ln\ k_d$ with $1/T$, which suggests a multi-site- and multi-step-induced fit process [41]. The $E_x^{\ddagger}$ values for each temperature are listed in Table 3.2.

Table 3.2. Energetic parameters for the formation of BLF-CMC activated complexes from the: association of free BLF and CMC biomolecules (a) and dissociation of the BLF-CMC thermodynamic stable complexes (d), at pH 4.

T	Association phase (a)				Dissociation phase (d)			
	$E_a^{\ddagger}$	$\Delta H_a^{\ddagger}$	$\Delta G_a^{\ddagger}$	$T\Delta S_a^{\ddagger}$	$E_d^{\ddagger}$	$\Delta H_d^{\ddagger}$	$\Delta G_d^{\ddagger}$	$T\Delta S_d^{\ddagger}$
K	kJ mol^{-1}							
285.2	-42.1 ± 0.5	-44.4 ± 0.5	41.7 ± 0.2	-86.1 ± 0.5	-70.2 ± 0.7	-72.5 ± 0.7	75.80 ± 0.03	-148.3 ± 0.7
289.2	-14.9 ± 0.8	-17.3 ± 0.8	42.6 ± 0.1	-59.9 ± 0.8	-37.5 ± 0.9	-39.9 ± 0.9	77.69 ± 0.04	-117 ± 0.9
293.2	25 ± 1	22 ± 1	43.4 ± 0.2	-21 ± 1	4.0 ± 0.1	1.0 ± 0.1	79.1 ± 0.1	-78.0 ± 0.1
297.2	78 ± 2	75 ± 2	43.2 ± 0.2	32 ± 2	56 ± 1	53 ± 1	79.74 ± 0.08	-27 ± 1
298.2	93 ± 2	90 ± 2	43 ± 1	47 ± 2	70 ± 2	68 ± 2	79.83 ± 0.04	-12 ± 2
301.2	142 ± 2	140 ± 2	42 ± 2	98 ± 3	116 ± 2	114 ± 2	79.74 ± 0.08	34 ± 2

The $E_a^{\ddagger}$ and $E_d^{\ddagger}$ values increased exponentially with temperature (Fig. S.B.3). At all the studied temperatures, the $E_a^{\ddagger}$ values were higher than the $E_d^{\ddagger}$ values, indicating that to form the activated complex from the free BLF and CMC molecules more energy is required to overcome the potential energy barrier required to form the BLF-CMC activated complex.

The negative $E_a^{\ddagger}$ and $E_d^{\ddagger}$ values observed at low temperatures could be explained on the basis that $E_x^{\ddagger}$ (x = a or d) can be divided in three submolecular processes, as indicated by Eq. 6:

$$E_x^{\ddagger} = E_{des}^{\ddagger} + E_{int}^{\ddagger} + E_{conf}^{\ddagger} \quad (6)$$

where $E_{des}^{\ddagger}$ is the energy absorbed during the transfer of water molecules from the ligand (protein or polysaccharide) solvation shell to the bulk system, $E_{conf}^{\ddagger}$ is the energy absorbed when the biopolymer conformational changes are induced by the interactions, and $E_{int}^{\ddagger}$ is the energy released due to the protein-polysaccharide interactions.

At temperatures <289.2 K, $E_{des}^{\ddagger}$ and $E_{conf}^{\ddagger}$ are lower than the $E_{int}^{\ddagger}$ modulus. At this temperature range, there is insufficient average molecular kinetic energy (<E_k>) to cause a change in the H-bonding of the water molecules and thus, the 3D water structure in the solvation shell of the biomolecules is similar to that of the bulk of the system. In addition, the potential rotational barrier within the biopolymer structure is high enough to avoid conformational changes induced by molecular collision or intermolecular BLF-CMC interaction. Hence, $E_x^{\ddagger}$ is <0 because it is dominated by the energy released from specific interactions between the protein and polysaccharide. However, with increasing temperature, $E_x^{\ddagger}$ became positive because the energy absorbed to release the biopolymer solvation shell and cause macromolecule conformational changes contributed to the $E_x^{\ddagger}$. Moreover, at higher temperatures there are more energetic and 3D structural differences between the water molecules at the solvation shell and those in the bulk of the system. Additionally, <E_k> is high enough to overcome the rotational potential energy barrier of the biopolymer interacting sites through energy transfer by molecular collisions.

We next investigated the relative contributions of the intermolecular interactions and configurational system changes to BLF-CMC activated complex formation from the association and dissociation phases. Thus, the Gibbs free energy change of activation

($\Delta G_x^{\ddagger}$), enthalpy change of activation ($\Delta H_x^{\ddagger}$), and entropy change of activation ($\Delta S_x^{\ddagger}$) for both phases were determined from Eqs. 7, 8, and 9, respectively (Table 3.2).

$$\Delta G_x^{\ddagger} = -RTln\left(\frac{k_x h}{K_B T}\right) \tag{7}$$

$$\Delta H_x^{\ddagger} = E_x^{\ddagger} - RT \tag{8}$$

$$T\Delta S_x^{\ddagger} = \Delta H_x^{\ddagger} - \Delta G_x^{\ddagger} \tag{9}$$

where K_B and h are the Boltzmann's and Planck's constants, respectively.

The $\Delta G_x^{\ddagger}$ values were positive for the association and dissociation phases at all temperatures. However, when compared to the dependence of $E_x^{\ddagger}$ with temperature, the $\Delta G_x^{\ddagger}$ values were near-constant with temperature. In general, when the activation Gibbs free energy change for the protein-ligand binding processes is poorly affected by temperature, iso-kinetic compensation (IKC) is assumed. In this phenomenon, large changes in the activation entropic term are accompanied by a proportional change in the activation enthalpic component, resulting in a small variation in the overall free energy. Fig. 3.4 illustrates the linear relationship between the $\Delta H_x^{\ddagger}$ and $T\Delta S_x^{\ddagger}$ values obtained in this study, with slopes of 1.021 ± 0.008 in the association ($x = a$) and 1.006 ± 0.005 in the dissociation ($x = d$) processes.

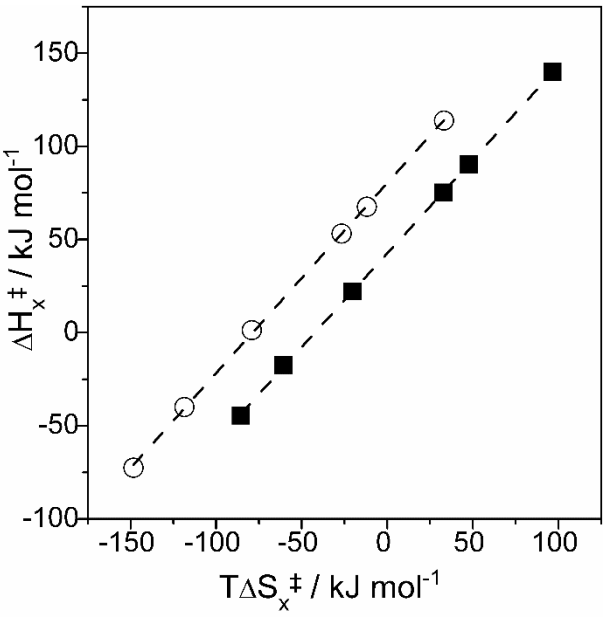

Fig. 3.4. Iso-kinetic compensation for the BLF-CMC binding process from the association (■) and dissociation (○) phases.

The observed IKC for BLF-CMC binding supports the molecular explanation on the temperature dependence of $E_x^{\ddagger}$. The interaction of the free BLF and CMC biomolecules results in solvent reorganization, caused by the disruption of water molecules solvating the macromolecules and the formation of water-water interactions on the bulk system [42]. This solvent reorganization promotes a proportional increase in the activation enthalpy and entropy of the system. Another source of IKC is the decrease in activation enthalpy caused by the BLF and CMC conformational restriction of the bound states, where the energy of the BLF-CMC bound ligand population is narrowed or restricted, thereby diminishing the conformational entropy. This results in a decrease in the activation entropy that is proportional to the activation enthalpy reduction after binding.

This molecular explanation for IKC contribution can be applied to both the association of free BLF and CMC biomolecules and the dissociation of the thermodynamically stable BLF-CMC complex to form the activated complex.

3.3.1.1 Thermodynamics of BLF-CMC complex formation process

The thermodynamic parameters of complex formation, such as the standard Gibbs free energy change (ΔG^o), standard enthalpy change (ΔH^o), and standard entropy change

(ΔS^o), are useful to understand the main forces involved in the process of complex formation between proteins and different molecules [43]. Thus, these parameters were determined to provide comprehensive insight into the stability and driven forces of the BLF-CMC complex.

To calculate the binding constant (K_b^{SPR}) for the stable BLF-CMC complex using the SPR kinetic data, we used the well-established relationship $K_b^{SPR} = k_a/k_d$ at each temperature. Then, we calculated the ΔH^o values with the van't Hoff approach ($ln\ K_b^{SPR}$ *versus* 1/T, Fig. S.B.4 and Eq. 10).

$$ln\left(\frac{K_b(T_2)}{K_b(T_1)}\right) = -\frac{\Delta H^0}{R}\left(\frac{1}{T_2} - \frac{1}{T_1}\right) \quad (10)$$

The ΔG^o and $T\Delta S^o$ values were calculated from Eqs. 11 and 12, respectively:

$$\Delta G^0 = -RTlnK_b \quad (11)$$

$$T\Delta S^0 = \Delta H^0 - \Delta G^0 \quad (12)$$

The thermodynamic parameters of BLF-CMC complex formation determined by SPR at pH 4 are presented in Table 3.3.

Table 3.3. Thermodynamic parameters for the formation of BLF-CMC complexes at different temperatures (T) and pH 4 obtained by surface plasmon resonance (SPR) experiments.

T	K_b^{SPR}	ΔH^o_{SPR}	ΔG^o_{SPR}	$T\Delta S^o_{SPR}$
K	10^6 mol^{-1} L		kJ mol^{-1}	
285.2	1.8 ± 0.2	23 ± 1	-34.1 ± 0.2	57 ± 1
289.2	2.1 ± 0.1		-35.1 ± 0.1	58 ± 1
293.2	2.3 ± 0.2		-35.7 ± 0.2	59 ± 1
297.2	2.7 ± 0.2		-36.6 ± 0.2	60 ± 1
298.2	2.8 ± 0.1		-37 ± 1	60 ± 1
301.2	3.0 ± 0.2		-37.4 ± 0.1	60 ± 1

The K_b^{SPR} values were of the order 10^6 mol^{-1} L and increased with increasing temperature. This demonstrated that the equilibrium BLF + CMC ⇌ BLF-CMC favored complex formation and that BLF-CMC complex formation occurred via energy absorption. The ΔG_{SPR}^o values were negative and became more negative with increasing temperature, confirming that the BLF-CMC complexes are more stable at higher temperatures.

To determine the enthalpic and entropic contributions for the negative ΔG_{SPR}^o, ΔH_{SPR}^o and $T\Delta S_{SPR}^o$ values were also calculated (Table 3.3). The positive ΔH_{SPR}^o and $T\Delta S_{SPR}^o$ values indicated that the thermodynamic process of BLF-CMC complex formation was entropically driven and enthalpically unfavorable. This supported the hypothesis of the important role of the release of water molecules and counter-ions from the solvation shell of both biomolecules to the bulk solution for complex synthesis.

To understand the relatively small contribution of the electrostatic interactions between the positively-charged BLF and negatively-charged CMC to the ΔH_{SPR}^o value, i.e., electrostatic interaction should produce negative ΔH_{SPR}^o values, it is worth noting that this parameter encompasses four molecular processes (Eq. 13):

$$\Delta H^0 = \Delta H^0_{desol} + \Delta H^0_{BLF-CMC} + \Delta H^0_{H_2O-H_2O} + \Delta H^0_{conf} \quad (13)$$

where ΔH^0_{desol} is the positive enthalpic change due to the breakage of the water-water interactions in the solvation shell of the BLF and CMC biomolecules, $\Delta H^0_{BLF-CMC}$ is the negative enthalpic change due to the interaction between BLF and CMC, $\Delta H^0_{H_2O-H_2O}$ is the negative enthalpic change due to the interaction between the water molecules in the bulk solution, and ΔH^0_{conf} is the positive enthalpic change associated with the protein and CMC conformational changes upon complex formation.

The positive ΔH_{SPR}^o values suggested that a higher amount of energy was required to desolvate the BLF and CMC molecules and change the ligand conformation than the energy released in the BLF-CMC and water-water interactions in the bulk.

3.3.2 Characterization of BLF-CMC complex formation by FS

Although SPR is a very sensitive technique to determine the kinetic and thermodynamic binding parameters, it is limited to the analysis of anchored proteins in a

solid substrate. On the other hand, the thermodynamic binding parameters of biomolecules interacting in solution can be acquired by FS [44]. BLF contains 13 Trp residues that emit fluorescence when excited at 295 nm. However, the interaction between different molecules such as polysaccharides with proteins near these residues (~5 Å) often quench the protein intrinsic fluorescence [45], thereby allowing the use of FS for measuring the interactions between BLF and various ligands. The fluorescence spectra of BLF in the presence of increasing concentrations of CMC at 298.2 K and pH 4 are presented in Fig. 3.5.

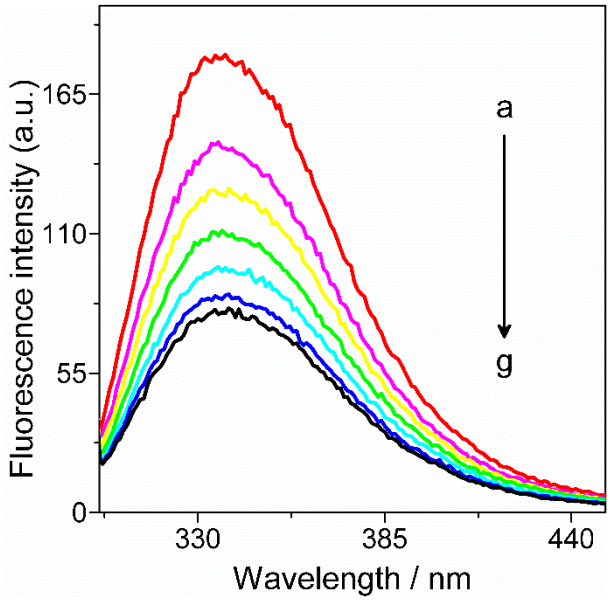

Fig. 3.5. Fluorescence spectra of lactoferrin ([BLF] = 1.97 x 10^{-5} mol L^{-1}) with increasing concentrations of carboxymethylcellulose (a–g: 0 –1.7 x 10^{-4} mol L^{-1}) at 298.2 K and pH 4.

BLF fluorescence quenching increased with increasing CMC concentration, without displacement in the maximum fluorescence emission wavelength (λ_{max}). This decrease in the fluorescence intensity of the fluorophore can occur by different mechanisms, classified as dynamic or static. Dynamic quenching refers to a process resulting from collisions between the quencher and fluorophore during the excited state, whilst static quenching refers to fluorophore-quencher complex formation at the ground state [46]. To determine the mechanism responsible for BLF fluorescence quenching by CMC, we used the Stern-Volmer equation (Eq. 14):

$$\frac{F_0}{F} = 1 + k_q \tau_0 [\mathrm{CMC}] \quad (14)$$

where F and F_o are the fluorescence intensities of BLF in the presence and absence of CMC, respectively, [CMC] is the concentration of CMC, k_q is the bimolecular quenching rate constant of the protein fluorescence, and τ_0 (1.06×10^{-9} s) is the lifetime of the fluorophore (in this case, excited Trp residues in BLF) in the absence of CMC [47].

The k_q values were provided by the plot of F_o/F *versus* [CMC] (Fig. S.B.5). The k_q values ranged from $6.8 \pm 0.1 \times 10^{12}$ to $11.4 \pm 0.6 \times 10^{12}$ L mol^{-1} s^{-1} (Table 3.4), which are much higher than the maximum rate constant for dynamic quenching (2×10^{10} L mol^{-1} s^{-1}). This indicated that the quenching of BLF fluorescence was induced by complex formation between BLF and CMC [48]. When considering static quenching interactions, assuming that there are similar and independent binding sites in the BLF, the binding constant (K_b^{FS}) and stoichiometry number of complex formation (n) can be determined according to the double-logarithm regression model (Eq. 15) [49].

$$log \frac{F_0 - F}{F} = log K_b^{FS} + n\, log[CMC] \quad (15)$$

where F_o and F are the fluorescence intensities of BLF in the absence and presence of CMC, respectively; n is the stoichiometry number; K_b^{FS} is the binding constant; and [CMC] is the CMC concentration. The n and K_b^{FS} values were obtained from the slope and intercept, respectively, of the plot of $log\, F_o - F/F$ *versus* $log[CMC]$ (Fig. S.B.6). The $K_b^{FS}$and n values are listed in Table 3.4.

Table 3.4. Bimolecular quenching rate constant (k_q), binding constants (K_b^{FS}) and stoichiometry numbers (n) of complex formation between BLF and CMC at different temperatures and pH 4.

T	k_q	K_b^{FS}	n	r^2
K	10^{12} L mol^{-1}s^{-1}	10^6 L mol^{-1}		
288.2	10.3 ± 0.4	8.40 ± 0.01	1.80 ±0.04	0.997
293.2	6.8 ± 0.1	5.47 ± 0.02	1.39 ± 0.05	0.992
298.2	9.1 ± 0.5	5.32 ± 0.02	1.77 ± 0.07	0.991
303.2	10.9 ± 0.4	9.19 ± 0.01	1.80 ± 0.04	0.997
308.2	11.4 ± 0.6	23.28 ± 0.01	1.91 ± 0.05	0.997

The K_b^{FS} values were in the same order as that of the values obtained by SPR (10^6 L mol^{-1}). For the FS experiment, the average stoichiometry number was 1.77, indicating that there is a distribution of CMC monomers around one Trp residue, producing an average CMC monomer density of 1.77. This result is reasonable because the calculations of K_b and n were performed by considering the concentration of the monomers present in the CMC macromolecule. Notably the average n value obtained by FS is not the same as that obtained by the SPR technique. In the SPR assays, n refers to the number of CMC macromolecules bound to one BLF biomolecule, whilst in the FS assays n is the average number of CMC monomers bound to the Trp surroundings.

The thermodynamic parameters of complex formation were also determined by fluorescence (ΔH_{FS}^o, $\Delta G_{FS,}^o$ and $T\Delta S_{FS}^o$) using the previously described equations (Eqs. 9–11). The van't Hoff plot is presented in Fig. 3.6, while the standard thermodynamic parameters for BLF-CMC complex formation determined by fluorescence are listed in Table 3.5.

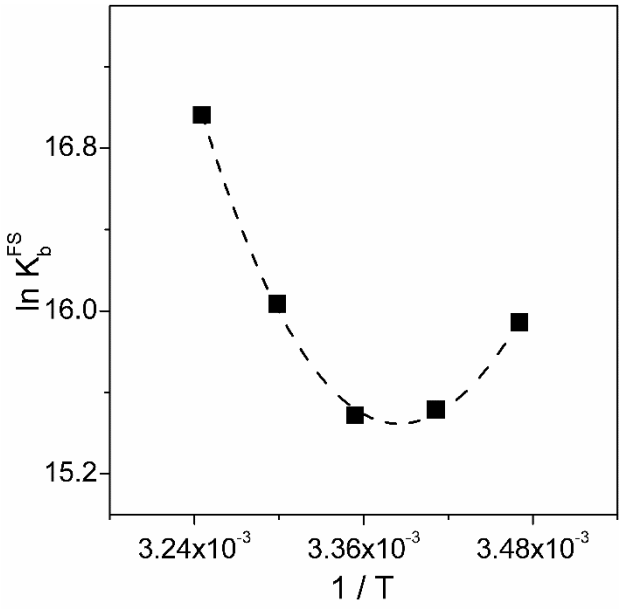

Fig. 3.6. Van't Hoff plot (ln K_b^{SPR} as a function of $1/T$) for the interaction between BLF and CMC studied by FS at pH 4.

Table 3.5. Standard enthalpy change (ΔH_{FS}^{o}), standard Gibbs free energy change (ΔG_{FS}^{o}), and standard entropy change ($T\Delta S_{FS}^{o}$) obtained by fluorescence for complex formation between BLF and CMC at pH 4.

T	ΔH_{FS}^{o}	ΔG_{FS}^{o}	$T\Delta S_{FS}^{o}$
K		kJ mol^{-1}	
288.2	-96 ± 1	-38.18 ± 0.00	-58 ± 1
293.2	-31 ± 1	-37.79 ± 0.01	7 ± 1
298.2	39 ± 1	-38.37 ± 0.01	77 ± 1
303.2	111 ± 2	-40.39 ± 0.00	151 ± 2
308.2	187 ± 2	-43.44 ± 0.00	230 ± 2

The ΔG_{FS}^{o} values were all negative, indicating that the BLF-CMC complex is stable at all the studied temperatures. The stabilities of the BLF-CMC complexes determined by FS were ~5 kJ mol^{-1} more intense than those determined by the SPR technique.

The ΔH_{FS}^{o} values increased linearly with temperature (Fig. S.B.7) and were exothermic up to a temperature of 293.2 K and endothermic at temperatures ≥298.2 K. The relationship between ΔH_{FS}^{o} and T allows the determination of ΔCp_{FS}^{0} ($\Delta Cp_{FS}^{0} = \delta H_{FS}^{0}/\delta T$). For the BLF-CMC complex formation process, ΔCp_{FS}^{0} = 14.14 ± 0.04 kJ mol^{-1} K^{-1}. This positive ΔCp_{FS}^{0} value reveals that despite any conformational changes of the interacting biopolymers, which occur by the breaking of the intramolecular interactions, the formation of new intermolecular interactions between BLF and CMC is sufficient to promote an increase in the potential energy component of the system [50].

The values of the entropic term obtained by FS were very different from those determined by the SPR experiments. While the $T\Delta S_{FS}^{o}$ values increased linearly with temperature (-58 ± 1 to 230 ± 2 kJ mol^{-1}) in the former technique, the $T\Delta S_{SPR}^{o}$ values presented little change (~60 kJ mol^{-1}). This difference between the $T\Delta S^{o}$ values obtained by both techniques occurs because SPR considers all the interacting sites of both the CMC and BLF biomolecules. On the other hand, FS only considers the interactions occurring between the sites of CMC and the BLF Trp residues.

As is observed in other processes of interaction between proteins and ligands [51], the fluorescence results in this study exhibited an enthalpy-entropy compensation phenomenon (Fig. 3.7).

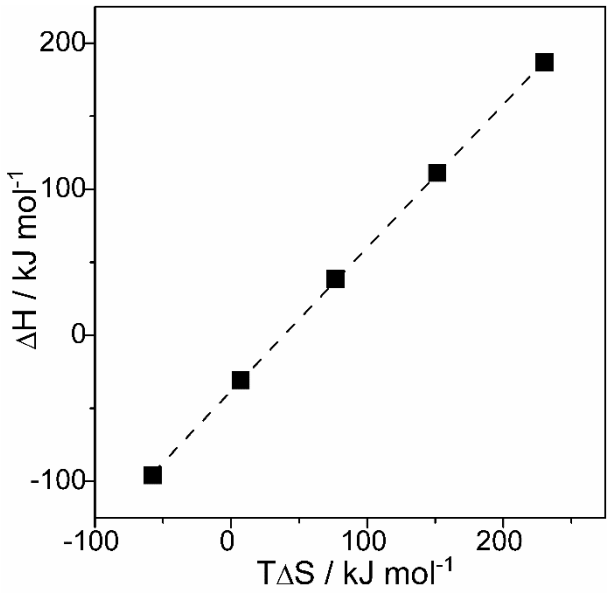

Fig. 3.7. Enthalpy-entropy compensation for the BLF-CMC binding process examined by the fluorescence technique.

Notably, at first glance, the single line in Fig. 3.7 very well fits all the data ($r^2 \cong 0.999$). A proper explanation can be given for this phenomenon: The enthalpy-entropy compensation in protein-ligand binding may be rooted in the formation and disruption of the weak noncovalent interactions. Multiple factors seem to influence this compensation behavior, including the structural and thermodynamic properties of the solvent (hydrophobic effect, solvation, desolvation, and local water structure), flexibility of the binding sites or regions surrounding the localized site, molecular structure of the ligand, and the changes in intermolecular forces during the binding process [52,53].

For instance, BLF-CMC complex formation resulting from favorable noncovalent interactions between the macromolecules can lead to a negative enthalpy change; however, this can be accompanied by a negative entropy change due to the restricted mobility of the interacting partners, resulting in a small variation in ΔG^o. On the other hand, free ligand desolvation is usually accompanied by a gain in entropy and an enthalpic penalty (positive enthalpy change). In addition, the interaction of the ligand with BLF can induce a conformational change at the binding site of the protein. This results in an entropy gain due to the increase in the conformational freedom degrees of the protein segments and a concomitant increase in ΔH^o due to the break of intramolecular interactions among the protein amino acids, so that ΔG^o becomes near-constant.

3.4 Conclusions

The interaction between lactoferrin and CMC was investigated by SPR and FS techniques. The afforded results revealed that CMC can bind to BLF with high affinity (10^6 mol^{-1} L), forming more stable complexes at higher temperatures. Intriguingly, although electrostatic interactions contributed to the BLF-CMC binding, non-polyelectrolytic forces dominated the binding process. The SPR measurements provided kinetic parameters related to the formation of an BLF-CMC activated complex from the association of free BLF and CMC or dissociation of the BLF-CMC stable complexes. BLF-CMC activated complex formation at temperatures ≤289.2 K is dominated by the energy released from specific interactions between the protein and polysaccharide. However, with increasing temperature, the energy absorbed due to the release of the biopolymer solvation shell as well as its conformational changes also began to contribute to the activation energy. This work presents a detailed kinetic and thermodynamic study of the BLF-CMC interactions, thereby providing important information for the successful technological application of such systems in different formulations.

References

[1] S.L. Turgeon, C. Schmitt, C. Sanchez, Protein–polysaccharide complexes and coacervates, Curr. Opin. Colloid Interface Sci. 12 (2007) 166–178. doi:10.1016/j.cocis.2007.07.007.

[2] F. Xing, G. Cheng, B. Yang, L. Ma, Nanoencapsulation of capsaicin by complex coacervation of gelatin, acacia, and tannins, J. Appl. Polym. Sci. 96 (2005) 2225–2229. doi:10.1002/app.21698.

[3] C.P. Champagne, P. Fustier, Microencapsulation for the improved delivery of bioactive compounds into foods, Curr. Opin. Biotechnol. 18 (2007) 184–190. doi:10.1016/j.copbio.2007.03.001.

[4] N. Devi, M. Sarmah, B. Khatun, T.K. Maji, Encapsulation of active ingredients in polysaccharide – protein complex coacervates, Adv. Colloid Interface Sci. 239 (2017) 136–145. doi:10.1016/j.cis.2016.05.009.

[5] T.R. Noel, A. Krzeminski, J. Moffat, R. Parker, N. Wellner, S.G. Ring, The deposition and stability of pectin/protein and pectin/poly-l-lysine/protein multilayers, Carbohydr. Polym. 70 (2007) 393–405. doi:10.1016/j.carbpol.2007.04.018.

[6] E. Dickinson, Colloid science of mixed ingredients, Soft Matter. 2 (2006) 642–652. doi:10.1039/b605670a.

[7] M. Vikelouda, V. Kiosseoglou, The use of carboxymethylcellulose to recover potato proteins and control their functional properties, Food Hydrocoll. 18 (2004) 21–27. doi:10.1016/S0268-005X(03)00038-9.

[8] K. Damianou, V. Kiosseoglou, Stability of emulsions containing a whey protein concentrate obtained from milk serum through carboxymethylcellulose complexation, Food Hydrocoll. 20 (2006) 793–799. doi:10.1016/j.foodhyd.2005.07.011.

[9] M. Corredig, N. Sharafbafi, E. Kristo, Polysaccharide-protein interactions in dairy matrices, control and design of structures, Food Hydrocoll. 25 (2011) 1833–1841. doi:10.1016/j.foodhyd.2011.05.014.

[10] C. Schmitt, C. Sanchez, S. Desobry-banon, J. Hardy, Structure and Technofunctional Properties of Protein- Polysaccharide Complexes : A Review, Crit. Rev. Food Sci. Nutr. 38 (1998) 689–753. doi:10.1080/10408699891274354.

[11] O.G. Jones, D.J. McClements, Functional biopolymer particles: Design, fabrication, and applications, Compr Rev Food Sci Food Saf. 9 (2010) 374–397. doi:10.1111/j.1541-4337.2010.00118.x.

[12] V.B.Tolstoguzov, Functional properties of food proteins and role of protein-polysaccharide interaction, Food Hydrocoll. 4 (1991) 429–468. doi:10.1016/S0268-005X(09)80196-3.

[13] V.Y. Grinberg, V.B. Tolstoguzov, Thermodynamic incompatibility of proteins and polysaccharides in solutions, Food Hydrocoll. 11 (1997) 145–158.

doi:10.1016/S0268-005X(97)80022-7.

[14] F. Comert, A.J. Malanowski, F. Azarikia, P.L. Dubin, Coacervation and precipitation in polysaccharide-protein systems, Soft Matter. 12 (2016) 4154–4161. doi:10.1039/c6sm00044d.

[15] T. Wagoner, B. Vardhanabhuti, E.A. Foegeding, Designing Whey Protein–Polysaccharide Particles for Colloidal Stability, Annu Rev Food Sci Technol. 7 (2016) 93–116. doi:10.1146/annurev-food-041715-033315.

[16] Y.D. Livney, Milk proteins as vehicles for bioactives, Curr. Opin. Colloid Interface Sci. 15 (2010) 73–83. doi:10.1016/j.cocis.2009.11.002.

[17] F. Liu, S. Zhang, J. Li, D.J. McClements, X. Liu, Recent development of lactoferrin-based vehicles for the delivery of bioactive compounds: Complexes, emulsions, and nanoparticles, Trends Food Sci. Technol. 79 (2018) 1–43. doi:10.1016/J.TIFS.2018.06.013.

[18] I. Peinado, U. Lesmes, A. Andrés, J.D. McClements, Fabrication and morphological characterization of biopolymer particles formed by electrostatic complexation of heat treated lactoferrin and anionic polysaccharides, Langmuir. 26 (2010) 9827–9834. doi:10.1021/la1001013.

[19] J.M. Steijns, A.C.M. van Hooijdonk, Occurrence, structure, biochemical properties and technological characteristics of lactoferrin, Br. J. Nutr. 84 (2000) 281–336. doi:10.1017/S0007114500002191.

[20] E.N. Baker, H.M. Baker, Molecular structure, binding properties and dynamics of lactoferrin, Cell. Mol. Life Sci. 62 (2005) 2531–2539. doi:10.1007/s00018-005-5368-9.

[21] H. Bokkhim, N. Bansal, L. Grndahl, B. Bhandari, Physico-chemical properties of different forms of bovine lactoferrin, Food Chem. 141 (2013) 3007–3013. doi:10.1016/j.foodchem.2013.05.139.

[22] K. Kamide, 2 - Characterization of Molecular Structure of Cellulose Derivatives, in: Cellul. Cellul. Deriv. Mol. Charact. Its Appl., 2005: p. 652. doi:10.1016/B978-0-444-82254-3.50004-7.

[23] K. Kamide, 3 - Molecular Properties of Cellulose and Cellulose Derivatives, in: Cellul. Cellul. Deriv. Mol. Charact. Its Appl., 2005: p. 652. doi:10.1016/B978-044482254-3/50005-9.

[24] H. Zaleska, P. Tomasik, C.Y. Lii, Formation of carboxymethyl cellulose-casein complexes by electrosynthesis, Food Hydrocoll. 16 (2002) 215–224. doi:10.1016/S0268-005X(01)00085-6.

[25] H. Kono, Characterization and properties of carboxymethyl cellulose hydrogels crosslinked by polyethylene glycol, Carbohydr. Polym. 106 (2014) 84–93. doi:10.1016/j.carbpol.2014.02.020.

[26] E. Arinaitwe, M. Pawlik, Dilute solution properties of carboxymethyl celluloses of various molecular weights and degrees of substitution, Carbohydr. Polym. 99 (2014) 423–431. doi:10.1016/j.carbpol.2013.08.030.

[27] C. Conesa, M. Calvo, L. Sánchez, Recombinant human lactoferrin: A valuable protein for pharmaceutical products and functional foods, Biotechnol. Adv. 28 (2010) 831–838. doi:10.1016/j.biotechadv.2010.07.002.

[28] H. Wakabayashi, K. Yamauchi, M. Takase, Lactoferrin research, technology and applications, Int. Dairy J. 16 (2006) 1241–1251. doi:10.1016/j.idairyj.2006.06.013.

[29] F. Liu, D. Wang, C. Ma, Y. Gao, Conjugation of polyphenols prevents lactoferrin from thermal aggregation at neutral pH, Food Hydrocoll. 58 (2016) 49–59. doi:10.1016/j.foodhyd.2016.02.011.

[30] C. Bengoechea, O.G. Jones, A. Guerrero, D.J. McClements, Formation and characterization of lactoferrin/pectin electrostatic complexes: Impact of composition, pH and thermal treatment, Food Hydrocoll. 25 (2011) 1227–1232.

doi:doi:10.1016/j.foodhyd.2010.11.010.

[31] E. Duhoranimana, J. Yu, O. Mukeshimana, I. Habinshuti, E. Karangwa, X. Xu, B. Muhoza, S. Xia, X. Zhang, Thermodynamic characterization of Gelatin–Sodium carboxymethyl cellulose complex coacervation encapsulating Conjugated Linoleic Acid (CLA), Food Hydrocoll. 80 (2018) 149–159. doi:10.1016/j.foodhyd.2018.02.011.

[32] H. Bokkhim, N. Bansal, L. Grøndahl, B. Bhandari, Interactions between different forms of bovine lactoferrin and sodium alginate affect the properties of their mixtures, Food Hydrocoll. 48 (2015) 38–46. doi:10.1016/j.foodhyd.2014.12.036.

[33] B. Wang, E. Blanch, C.J. Barrow, B. Adhikari, Preparation and study of digestion behavior of lactoferrin-sodium alginate complex coacervates, J Funct Foods. 37 (2017) 97–106. doi:10.1016/j.jff.2017.07.044.

[34] J.R. Lakowicz, Principles of Fluorescence Spectroscopy, Trird edit, Maryland, USA, 2006. doi:10.1007/978-0-387-46312-4.

[35] Z. Li, Y. Wang, Y. Pei, W. Xiong, W. Xu, B. Li, J. Li, Effect of substitution degree on carboxymethylcellulose interaction with lysozyme, Food Hydrocoll. 62 (2017) 222–229. doi:10.1016/j.foodhyd.2016.07.020.

[36] A.A. Perez, C.R. Carrara, C.C. Sánchez, L.G. Santiago, J.M.R. Patino, Interfacial dynamic properties of whey protein concentrate/polysaccharide mixtures at neutral pH, Food Hydrocoll. 23 (2009) 1253–1262. doi:10.1016/j.foodhyd.2008.08.013.

[37] S. Wu, M. Lai, J. Luo, J. Pan, L.M. Zhang, L. Yang, Interactions between α-amylase and an acidic branched polysaccharide from green tea, Int. J. Biol. Macromol. 94 (2017) 669–678. doi:10.1016/j.ijbiomac.2016.09.036.

[38] I.H. Moal, P.A. Bates, Kinetic rate constant prediction supports the conformational selection mechanism of protein binding, PLoS Comput Biol. 8 (2012) 1–13. doi:10.1371/journal.pcbi.1002351.

[39] A.W. Drake, M.L. Tang, G.A. Papalia, G. Landes, M. Haak-Frendscho, S.L. Klakamp, Biacore surface matrix effects on the binding kinetics and affinity of an antigen/antibody complex, Anal. Biochem. 429 (2012) 58–69. doi:10.1016/j.ab.2012.06.024.

[40] Y. Hirayama, K. Yamagishi, T. Suzuki, H. Kawagishi, M. Kita, H. Kigoshi, Analysis of the aplyronine A-induced protein-protein interaction between actin and tubulin by surface plasmon resonance, Bioorg. Med. Chem. 24 (2016) 2809–2814. doi:10.1016/j.bmc.2016.04.049.

[41] W. Wang, C.J. Roberts, Non-Arrhenius Protein Aggregation, AAPS J. 15 (2013) 840–851. doi:10.1208/s12248-013-9485-3.

[42] L. Liu, Q.X. Guo, Isokinetic relationship, isoequilibrium relationship, and enthalpy-entropy compensation, Chem. Rev. 101 (2001) 673–695. doi:10.1021/cr990416z.

[43] C.A. Lelis, E.A. Hudson, G.M.D. Ferreira, G.M.D. Ferreira, L.H.M. da Silva, M. do C.H. da Silva, M.S. Pinto, A.C. dos S. Pires, Binding thermodynamics of synthetic dye Allura Red with bovine serum albumin, Food Chem. 217 (2017) 52–58. doi:10.1016/j.foodchem.2016.08.080.

[44] P. Brown, C. Royer, Fluorescence spectroscopy as a tool to investigate protein interactions, Curr. Opin. Biotechnol. 8 (1997) 45–49. doi:10.1016/S0958-1669(97)80156-5.

[45] V.D. Suryawanshi, L.S. Walekar, A.H. Gore, P. V Anbhule, G.B. Kolekar, Spectroscopic analysis on the binding interaction of biologically active pyrimidine derivative with bovine serum albumin, J. Pharm. Anal. 6 (2016) 56–63. doi:10.1016/j.jpha.2015.07.001.

[46] N. Shahabadi, M. Maghsudi, Z. Kiani, M. Pourfoulad, Multispectroscopic studies on the interaction of 2-tert-butylhydroquinone (TBHQ), a food additive, with bovine serum albumin, Food Chem. 124 (2011) 1063–1068. doi:10.1016/j.foodchem.2010.07.079.

[47] P.L. Xavier, K. Chaudhari, P.K. Verma, S.K. Pal, T. Pradeep, Luminescent quantum clusters of gold in transferrin family protein, lactoferrin exhibiting FRET, Nanoscale. 2 (2010) 2769–2776. doi:10.1039/c0nr00377h.

[48] E.A. Hudson, H.M.C. de Paula, G.M.D. Ferreira, G.M.D. Ferreira, M. do C. Hespanhol, L.H.M. da Silva, A.C. dos S. Pires, Thermodynamic and kinetic analyses of curcumin and bovine serum albumin binding, Food Chem. 242 (2018) 505–512. doi:http://dx.doi.org/10.1016/j.foodchem.2017.09.092.

[49] C.A. Lelis, G.M.D. Ferreira, G.M.D. Ferreira, M. do C. Hespanhol, M.S. Pinto, L.H.M. da Silva, A.C. dos S. Pires, Determination of driving forces for bovine serum albumin-Ponceau4R binding using surface plasmon resonance and fluorescence spectroscopy: A comparative study, Food Hydrocoll. 70 (2017) 29–35. doi:http://dx.doi.org/10.1016/j.foodhyd.2017.03.027.

[50] J. Gómez, E. Freire, Thermodynamic Mapping of the Inhibitor Site of the Aspartic Protease Endothiapepsin, J. Mol. Biol. 252 (1995) 337–350. doi:10.1006/jmbi.1995.0501.

[51] J.A. Molina-Bolívar, C.C. Ruiz, F. Galisteo-González, M.M. O'Donnell, A. Parra, Energetics of albumin-disuccinylmaslinic acid binding determined by fluorescence spectroscopy, Fluid Phase Equilib. 400 (2015) 43–52. doi:10.1016/j.fluid.2015.05.011.

[52] J.D. Chodera, D.L. Mobley, Entropy-enthalpy compensation: Role and ramifications in biomolecular ligand recognition and design, Annu Rev Biophys. 42 (2013) 121–142. doi:10.1146/annurev-biophys-083012-130318.

[53] J.M. Fox, M. Zhao, M.J. Fink, K. Kang, G.M. Whitesides, The Molecular Origin of Enthalpy/Entropy Compensation in Biomolecular Recognition, Annu. Rev. Biophys. 47 (2018) 223–250. doi:10.1146/annurev-biophys-070816-033743.

CAPÍTULO 4: COMPLEXATION BETWEEN LACTOFERRIN AND κ-CARRAGEENAN: MOLECULAR INSIGHTS OBTAINED BY SURFACE PLASMON RESONANCE AND FLUORESCENCE SPECTROSCOPY

Abstract

Protein-polysaccharide complexes play important roles in both living structures and technological processes. To understand how bovine lactoferrin (BLF) and κ-carrageenan (κCG) interact to form bionanostructures, the energetic and dynamic characterization is essential. Therefore, the thermodynamic and kinetic parameters were determined using fluorescence spectroscopy (FS) and surface plasmon resonance (SPR). The formation of the 1:1 BLF-κCG complex is favored in the thermodynamic equilibrium ($-23.1 \leq \Delta G^{o}_{FS} \leq -24.5$ kJ mol^{-1} and $-27.2 \leq \Delta G^{o}_{SPR} \leq -24.3$ kJ mol^{-1}) and was enthalpy-driven ($\Delta H^{o}_{FS} = -8.07$ kJ mol^{-1} and $\Delta H^{o}_{SPR} = -81$ kJ mol^{-1}). The comparison between SPR and FS results showed that the BLF-κCG interaction occur in multiple sites of BLF. Kinetic parameters obtained by SPR showed that the interaction occurs through the transition complex formation ($[\mathrm{BLF} - \kappa\mathrm{CG}]^{\ddagger}$), and that this process is faster from the association of the free molecules ($50.4 \leq \Delta G^{\ddagger}_{a} \leq 57.37$ kJ mol^{-1}) than from dissociation of the thermodynamic stable complex ($77.61 \leq \Delta G^{\ddagger}_{d} \leq 81.62$ kJ mol^{-1}). Besides that, for all temperatures, the energetic barrier was higher for dissociation processes ($E^{\ddagger}_{d} = 96.08$ and $\Delta H^{\ddagger}_{d} = 93.6$ kJ mol^{-1} at 298.2 K) then for the association step ($E^{\ddagger}_{a} = 42.17$ and $\Delta H^{\ddagger}_{a} = 39.69$ kJ mol^{-1} at 298.2 K). The change in the ionic strength altered the manner in which BLF and κCG interacts, making the binding a one-step process instead of multi-step. This work provides fundamental information for optimizing the use of BLF-κCG supramolecular complex in different applications, such as in the food, cosmetic, and pharmaceutical formulations.

Keywords: kinetics, thermodynamic, transition complex, supramolecular structures, lactoferrin.

4.1 Introduction

The interaction between proteins and polysaccharides has been widely studied in the recent years for its applications in food, pharmaceutical, cosmetic and textile industries [1,2]. Several papers report the use of these complexes in drug-delivery systems and for the production of food with better nutritional benefits [3–6]. However, for discovering new nutraceutical properties and uses for these complexes, understanding how the interaction between these biopolymers occurs is also important, since these macromolecules are essential components in biological systems and play an important role in various biochemical processes that enable life [7,8].

The mix of a protein with a polysaccharide in aqueous solution can lead to different complexes formation (water soluble, water insoluble or coacervate), depending on polymer-polymer and solvent-polymer interactions. Therefore, environmental parameters of a system, such as pH, ionic strength, the protein to polysaccharide ratio play important roles in interaction between these species [9,10].

One of the promising polysaccharides to form functional complexes with proteins is κ-carrageenan (κCG). It is an important polysaccharide with a wide range of food applications for its gelling, thickening, and emulsifying properties [11–13]. Moreover, due to its properties such as compatibility, degradability, solubility, and nontoxicity, the use this polymer for encapsulation of nutraceutical molecules is gaining increasing attention [14–17]. This polysaccharide consists of an biopolymer extracted from the cell wall of red algae, which is composed by alternating units of (1–3)- α-D-galactose-4-sulphate and (1–4)-β-3,6-anydro-D-galactose (Fig. 4.1) [18,19]. Although there is a large number of studies concerning interaction of various proteins with kCG, for example, serum albumin [20,21]; casein [22–24]; beta lactoglobulin [25,26]; lysozyme [27,28], as far as we know there is no study on the interaction of bovine lactoferrin (BLF) with this polysaccharide.

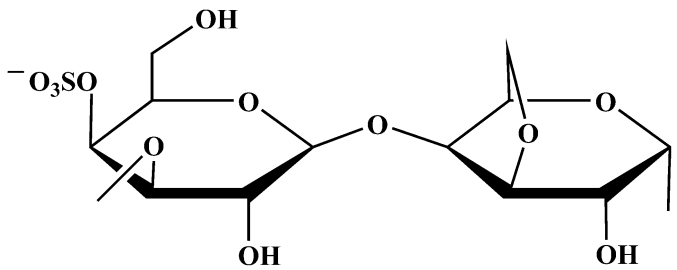

Fig. 4.1. Chemical structure of κ-carrageenan.

BLF is a cationic protein with a pI≈8.7, molecular mass of about 80 kDa and approximately 700 amino acid residues. The tertiary structure of lactoferrin provides two homologous globular lobes (N and C). Each lobe is able to bind to a Fe^{+2} or Fe^{+3} atom [29]. BLF play an active role in a wide spectrum of biological functions. Its protective effects range from of organism immuno-regulatory, anti-microbial, anti-viral, anti-fungal, anti-tumor, and anti-inflammatory properties [30]. In addition, their intrinsic health benefits also aid to develop nutraceutical foods [31]. This wide range of activities is made possible by the capacity of BLF to bind iron, as well as, interactions with other components such as polysaccharides.

It is already known that BLF can interact with some polysaccharides to form complexes that have physicochemical and functional properties different of isolated molecules that, when incorporated in a product, can improve its techno-functional properties [32]. Thus, the inexistence of data about the BLF-κCG system and the great application potential of this complexes motivated us to embark on a systematic investigation. However, to a better understanding and application of this system it is a complete thermodynamic and kinetic study is required. Therefore, the present paper investigated the energetic (binding constant (K_b), standard Gibbs free energy change (ΔG^o), standard enthalpy change (ΔH^o), and standard entropy change (ΔS^o) and dynamic (association (k_a) and dissociation (k_d) kinetic rate constants, activation energy ($E^{\ddagger}$), variations in Gibbs free energy ($\Delta G^{\ddagger}$), and enthalpy ($\Delta H^{\ddagger}$) and entropy ($T\Delta S^{\ddagger}$) of activation) of complex formation between κ-carrageenan and bovine lactoferrin, in the absence and presence of KCl, using fluorescence spectroscopy (FS) and surface plasmon resonance (SPR).

4.2 Material and Methods

4.2.1 Materials

κCG (quality level 100), BLF (>99 % wt), sodium acetate (CH_3COONa; analytical grade), acetic acid (CH_3CO_2H; analytical grade), and potassium chloride (>99 % wt) were purchased from Sigma-Aldrich (St. Louis, MO, USA). Research-grade CM5 sensor chips and the coupling reagents (N-ethyl-N′, N′-dimethylaminopropylcarbodiimide (EDC), N-hydroxysuccinimide (NHS), and ethanolamine hydrochloride (1 M, pH 8.5) were purchased from GE Healthcare (Pittsburgh, PA, USA).

4.2.2 FS analysis

The fluorescence experiments were performed in a Cary Eclipse Fluorescence Spectrophotometer (Agilent Technologies, Santa Clara, USA) with quartz cells having a 1-cm path length, and equipped with a thermostat bath, which allowed the experiments to be performed at 288.2, 293.2, 298.2, 303.2, and 313.2 K. The emission spectra were obtained in the wavelength range of 296–500 nm, through the excitation of the BLF Trp residues at 295 nm, using an excitation slit of 2.5 nm, emission slit of 5.0 nm, and a photomultiplier tube (PMT) voltage of 750 V, at a scan rate of 600 nm/min. All solutions were prepared using an acetate buffer (pH 4), and the fluorescence spectra were recorded, using a fixed BLF concentration (19.5 μM) in the presence of different κCG concentrations (0-56.8 μM).

4.2.3 SPR analysis

The SPR experiments were performed using a Biacore X100 instrument (GE Healthcare, Pittsburgh, PA, USA), which allowed the determination of the kinetics and thermodynamics of the BLF-κCG interaction. For the BLF immobilization, first the CM5 chips were activated for 7 min with EDC/NHS and, posteriorly, the excessive activated carboxyl groups were blocked with ethanolamine for another 7 min. After that, BLF was immobilized on the chip (15 μg mL^{-1}) in 0.01 mol L^{-1} sodium acetate (pH 4), at low levels (3864 RU) to reduce any potential mass transport and crowding phenomena. To correct for systematic noise and Biacore drift, a flow cell was prepared as described above but without the protein immobilization and used as a reference surface. The κCG solutions (28-52 μM) were prepared in acetate buffer (pH 4), in the absence and presence of KCl (100 mM), and the experiments were carried out at temperatures ranging from 285.2 to 301.2 K. For each binding experiment, κCG solutions, at a determined concentration, were injected in the flowing system to increase their concentration over the sample and reference surfaces. The buffer at pH 4 was injected before each BLF-κCG binding cycle to obtain the baseline.

4.3 Results and Discussion

4.3.1 BLF and κCG interaction study by fluorescence spectroscopy

A commonly used technique for studying the formation of protein based complexes is the fluorescence spectroscopy that allows, through the fluorescence quenching phenomenon, the determination of the binding constant (K_b) and, indirectly, the thermodynamic parameters (standard Gibbs free energy change (ΔG^o), standard enthalpy change (ΔH^o), and standard entropy change (ΔS^o) [33].

The tryptophan (Trp) residues are the mainly fluorophores in proteins and if a molecule binds near (around 5 Å) one of these residues, a change in the intrinsic fluorescence is observed [34]. In this way, as shown in Fig. 4.2, to better understand how κCG affects the Trp environment in the native BLF at pH 4, the intrinsic fluorescence of this protein, upon excitation at 295 nm, at increasing κCG concentrations was studied.

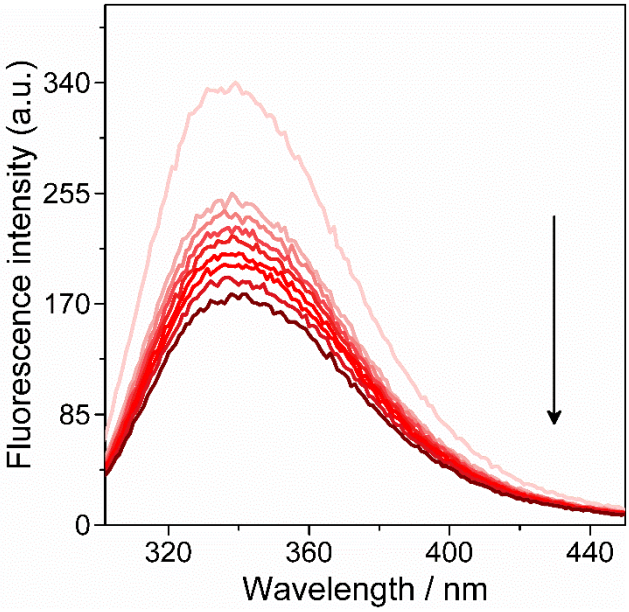

Fig. 4.2. Steady-state fluorescence emission spectra of native BLF (19.5 μM), in buffer pH 4 at 298.2 K, in the presence of different κCG concentrations (0-56.8 μM).

The fluorescence intensity of native BLF at 336 nm decreased with the increase of κCG concentration. There was no shift in the maximum emission wavelength, which means that the interaction did not modify the Trp microenvironment. Since most of the Trp residues are buried in hydrophobic cavities of the protein, this result indicates that

the interaction did not cause a conformational change in the tertiary structure of native BLF [35].

The decrease in the fluorescence intensity can be caused by different processes (molecular rearrangement, energy transfer, ground state complex formation and collisional quenching) [36], the most common being static and dynamic quenching and, for each one, there are various models used in the treatment of the data to study the protein-polysaccharide interaction [37]. The Stern-Volmer model (Eq. 1) was used to determine whether the mechanism was static or dynamic.

$$\frac{F_0}{F} = 1 + K_{SV}[\kappa CG\,] = 1 + k_q \tau_0 [\kappa CG\,] \qquad (1)$$

where F_0 and F are the fluorescence intensity of fluorophore (BLF) in the absence and presence of the quencher (κCG), K_{SV} is the Stern-Volmer quenching constant and [κCG] is the quencher concentration. k_q is the bimolecular quenching rate constant and τ_0 is the average protein fluorescence lifetime in the absence of quencher (1.06 ns) [38].

The Stern-Volmer plot for the quenching of native BLF by κCG at 298.2 K were displayed in Fig. 4.3a, and K_{SV} and $k_q$parameters estimated from the slope of this curve are presented in Table 4.1. Similar profiles were obtained for the temperatures 288.2 K; 293.2 K; 303.2 K and 313.2 K (Fig. S.C.1a).

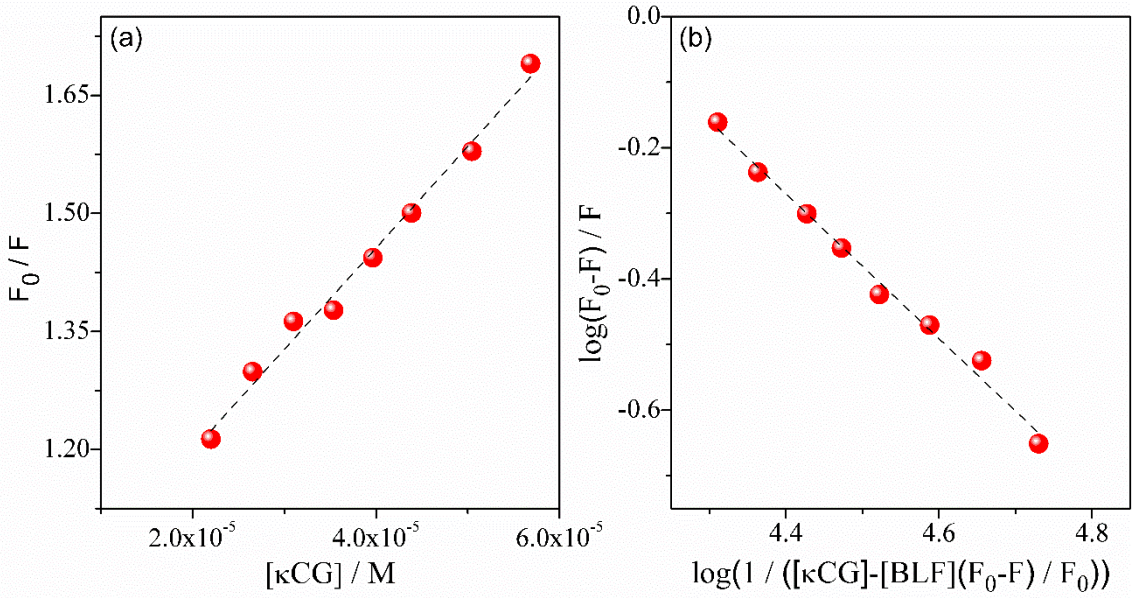

Fig. 4.3. Plots for determination of the interaction parameters between native BLF and κCG, according to (a) Stern-Volmer and (b) modified double logarithm models, obtained at 298.2 K and pH 4.

Table 4.1. Stern-Volmer constant (K_{SV}), bimolecular quenching rate constant (k_q), binding constant (K_b^{FS}), stoichiometry (n), of BLF-κCG complex formation, at different temperatures (T) and pH 4.

T	K_{SV}	k_q	K_b^{FS}	n
K	10^4 M^{-1}	10^{13} $M^{-1}s^{-1}$	10^4 M^{-1}	
288.2	1.36 ± 0.04	1.28 ± 0.04	1.54 ± 0.05	1.13 ± 0.05
293.2	1.31 ± 0.07	1.24 ± 0.06	1.48 ± 0.05	1.36 ± 0.06
298.2	1.29 ± 0.06	1.22 ± 0.05	1.43 ± 0.05	1.10 ± 0.04
303.2	1.23 ± 0.05	1.16 ± 0.04	1.35 ± 0.04	0.87 ± 0.03
313.2	1.11 ± 0.06	1.05 ± 0.05	1.21 ± 0.06	0.99 ± 0.05

The K_{SV} values decrease with increasing temperature and the k_q values (1.28 x 10^{-13}-1.05 x 10^{-13} $M^{-1}s^{-1}$) were higher than the maximum value for the diffusion-limited collisional quenching (2.0 x 10^{10} M^{-1} s^{-1}), indicating that the mechanism responsible for the fluorescence quenching of BLF by κCG is static, as a consequence of an association in the ground-state between the protein and the polysaccharide [34]. Therefore, the binding constant (K_b) and the number of ligand molecules in the binding site of protein (n) was determined from the intercept and slope of the modified double logarithm model curve (Eq. 2) [39], shown in Fig. 4.3b for 298.2 K. For the other temperatures, the curves are shown in Fig. S.C.1b.

$$log\frac{(F_0 - F)}{F} = n\,logK_b + n\,log\left([\kappa CG] - \frac{[BLF](F_0 - F)}{F_0}\right) \quad (2)$$

where n is the number of ligand molecules in the binding site of protein and [κCG] is the total ligand concentration. The obtained K_b and n values are shown in Table 4.1.

The K_b^{FS} values obtained have an order of magnitude of 10^4 M^{-1} and decreasing with increasing temperature, showing that the complex formation was an exothermic process, which is common for various protein-based systems [40]. Besides that, for all temperatures, n was approximately 1, suggesting that the stoichiometry for the binding site is 1:1.

The interaction between proteins and polysaccharides usually involves hydrogen bonds, hydrophobic forces, electrostatic interactions and van der Waals forces [41]. From the sign, as well as, the magnitude of the thermodynamic parameters, it is possible to

suggest what is the intermolecular interaction responsible for the binding and, thus, understand the mechanism involved. From the K_b^{FS}values obtained, the standard Gibbs free energy change ($\Delta G°$) was calculated using Eq. 3.

$$\Delta G° = -RTlnK_b \quad (3)$$

where $\Delta G°$ is the standard Gibbs free energy change, R is the universal gas constant (8,314 J/mol K) and T is the temperature in kelvin. The standard enthalpy change ($\Delta H°$) was calculated from the van't Hoff equation (Eq. 4), using the slope of the $ln\ K_b^{FS}\ versus\ 1/T$ plot (Fig. 4.4).

$$ln\left(\frac{K_b(T_2)}{K_b(T_1)}\right) = -\frac{\Delta H^0}{R}\left(\frac{1}{T_2} - \frac{1}{T_1}\right) \quad (4)$$

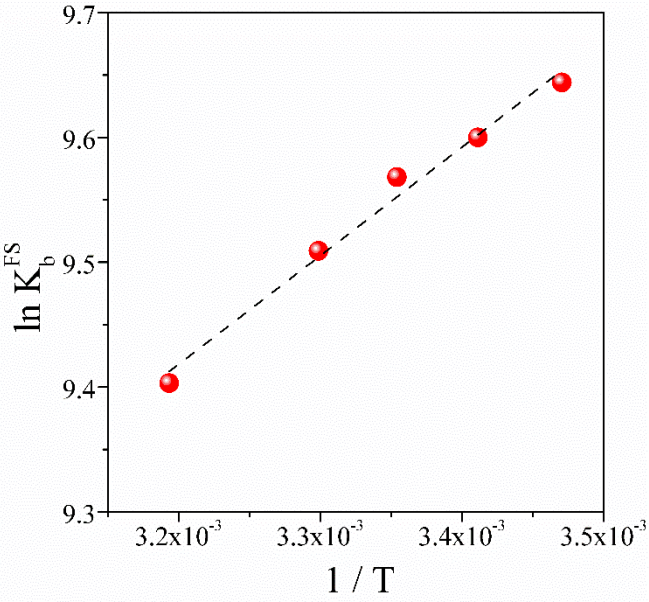

Fig. 4.4. Van't Hoff plot for the dependence of K_b^{FS} with the temperature for the interaction between BLF and κCG.

With the obtained $\Delta H°$ and $\Delta G°$ values, the standard entropy change ($\Delta S°$) was calculated using the fundamental Gibbs equation (Eq. 5). The thermodynamic parameters for the formation of the complex, in all studied temperatures, are shown in Table 4.2.

$$\Delta G° = \Delta H° - T\Delta S° \quad (5)$$

Table 4.2. Thermodynamic parameters (ΔG^o_{FS}, ΔH^o_{FS}, and $T\Delta S^o_{FS}$) for the formation of BLF-κCG complex, at different temperatures (T) and pH 4. Data obtained from fluorescence measurements.

T	ΔG^o_{FS}	ΔH^o_{FS}	$T\Delta S^o_{FS}$
K		kJ mol^{-1}	
288.2	-23.10 ± 0.08		15.03 ± 0.09
293.2	-23.40 ± 0.08		15.32 ± 0.08
298.2	-23.72 ± 0.08	-8.07 ± 0.01	15.64 ± 0.08
303.2	-23.97 ± 0.07		15.89 ± 0.07
313.2	-24.5 ± 0.1		16.4 ± 0.1

ΔG^o_{FS} values were negatives and decreased with increasing temperature, indicating that in the system, the amount of the complex is predominant in relation to the free molecules and the BLF-κCG complexes became more stable at higher temperatures. These values result from the contribution of different processes occurring in the system and, to better understand them, the analysis of the enthalpic and entropic terms is necessary.

Despite the occurrence of electrostatic repulsion between BLF and κCG, due to the positive charge on both macromolecules at pH 4, the ΔH^o_{FS} value was negative. The obtained negative ΔH^o_{FS} value suggests that the energy content released due to the formation of new intermolecular interactions between BLF and kCG outweighs the energetic cost resulted from desolvating and, especially, releasing the counterions from the electric double layer of the interacting molecules. On the other hand, the $T\Delta S^o_{FS}$ values were positive. The entropy gain due to desolvation of BLF and κCG free molecules and release of counterions from the electric double layer contributes more to the system entropic increase than the configurational entropy reduction caused by formation of the BLF-κCG complex. Considering that $\Delta H^o_{FS} < 0$ and $T\Delta S^o_{FS} > 0$, it can be suggested that the BLF-κCG complex formation is mainly driven by attractive forces (van der Waals forces and hydrogen bonds) that overcome electrostatic repulsion between macromolecules.

4.3.2 Kinetics and thermodynamics of BLF-κCG complex formation determinated by surface plasmon resonance

4.3.2.1 Kinetic study

Although the thermodynamic parameters provide important information about the energetics involved in the formation of protein-polysaccharide complexes, the kinetic study is indispensable for comprehending the molecular dynamics that occur during the interaction between these species. In contrast to thermodynamic parameters obtained by equilibrium data, nonequilibrium kinetics parameters give information not restricted to only bound and unbound states [42,43].

Surface plasmon resonance (SPR)-based biosensors are commonly employed to determine interaction kinetics between macromolecules [44–46]. This optical approach measures the refractive index change near a sensor surface (≈ 100 nm) to which a ligand (BLF) is immobilized. When an analyte molecule (κCG) bind to immobilized ligand, it results in a refractive index alteration that can be measured in real time. The results are then plotted as sensorgrams (resonance units (RU) *versus* time curves), as shown in Fig. 4.5 for BLF-κCG interaction at 298.2 K and pH 4.

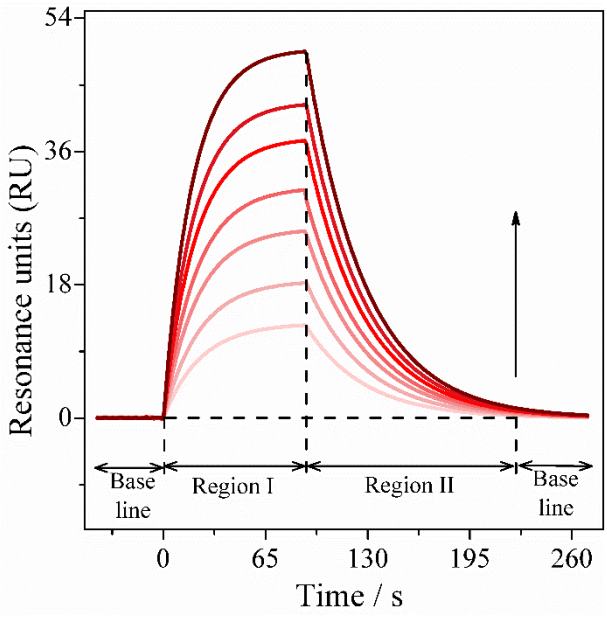

Fig. 4.5. Sensorgrams (RU *versus* time) for interaction between BLF and κCG formed by flowing 28–52 μM κCG solutions over a CM5 low-density BLF immobilized sensor-chip surface (3864 RU) at 298.2 K. The arrows indicate increasing κCG concentration, at pH 4. The sensorgrams obtained for other temperatures are showed in Fig. S.C.2.

SPR data demonstrated that, even though the BLF is attached to the chip's surface, it continues to form thermodynamically stable complexes with κCG. In the sensorgrams there are two distinct regions: I) an ascendant curve corresponds to the association phase and II) a descendant curve, which called and dissociation phase. In the time interval corresponding to region I (0–90 s), events of free BLF and κCG molecules association, and dissociation of BLF-κCG thermodynamically stable complexes occur simultaneously, being the first process predominant at begging of the ascendant curve. While in the region II (90–224 s), only the complexes dissociation is predominant.

In order to determine the kinetic parameters of BLF-κCG complex formation, namely the association (k_a) and dissociation (k_d) rate constants, the data of regions I and II of the sensorgrams were globally fitted to a 1:1 binding model (Eqs. 6 and 7), and the values obtained are presented in Table 4.3.

$$RU(t) = RU(t_m)\, e^{-k_d(t-t_m)} \tag{6}$$

$$RU(t) = RU_{max}(t_\infty)[1 - e^{-k_{obs}(t)}] \tag{7}$$

where $RU(t)$ is the SPR response at time t; $RU(t_m)$ is the SPR signal where the descendent exponential curve of the sensorgram starts; k_{obs} is the observed constant and $[RU_{\max}(t_\infty)]$ denotes the resonance units obtained at an infinite time (t_∞).

Since $k_{obs} = k_a$ [κCG] + k_d , the k_a values can be determinated through the slope of the k_{obs} *versus* [κCG] curves (Fig. S.C.3).

Table 4.3. Kinetic rate constants for the association (k_a) of free BLF and κCG molecules and for dissociation (k_d) of the BLF-κCG thermodynamic stable complexes, at different temperatures and pH 4.

T	k_a	k_d
K	10^3 M^{-1} s^{-1}	10^{-2} s^{-1}
285.2	3.52 ± 0.04	0.036 ± 0.000
289.2	1.07 ± 0.03	0.022 ± 0.001
293.2	0.58 ± 0.02	0.019 ± 0.001
297.2	0.48 ± 0.01	0.023 ± 0.000
298.2	0.51 ± 0.01	0.027 ± 0.001
301.2	0.70 ± 0.02	0.044 ± 0.001

Both k_a and k_d values showed a polynomial trend with the temperature increase (Fig. 4.6).

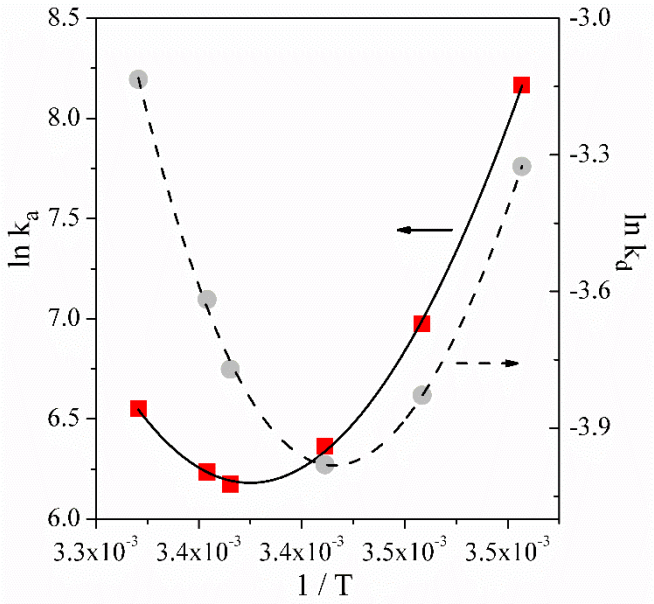

Fig. 4.6. *ln* k_a and *ln* k_d *versus* $1/T$ for BLF-κCG transition complex formation at pH 4. Association (■) and dissociation (●).

To the best of our knowledge, there is no kinetic data in the scientific literature for the interaction between BLF and κCG. However, recently, our research group reported kinetic studies for the interaction of BLF with bioactive molecules, such as dyes (methylene blue (MB) and azure A (AZA)) [45], catechin (epigallocatechin-3-gallate (EGCG)) [47], and flavonoid (naringin (NR)) [46]. At 298.2 K, the number of complexes formed per second (k_a) during the interaction of BLF-MB (5.10 x 10^3 M^{-1} s^{-1}), BLF-AZA (8.10 x 10^3 M^{-1} s^{-1}), BLF-EGCG (1.65 x 10^4 M^{-1} s^{-1}), and BLF-NR (5.00 x 10^4 M^{-1} s^{-1}) was 1 to 2 orders of magnitude higher than for the BLF- κCG interaction (0.51 x 10^3 M^{-1} s^{-1}). Similarly, the fraction of complexes that dissociate per second (k_d) in the binding process of BLF-MB (3.4 x 10^{-2} s^{-1}), BLF-AZA (4.6 x 10^{-1} s^{-1}), BLF-EGCG (1.18 x 10^{-1} s^{-1}), and BLF-NR (3.6 x 10^{-1} s^{-1}) were also higher than for BLF-κCG interaction (2.7 x 10^{-2} s^{-1}). This difference in the k_a and k_d values occurs, probably, due to the size difference between the analytes. Since κCG is a larger molecule, it may be leading to higher conformational changes in the both BLF and κCG structure, during the interaction process.

Studying the energetic of the transition (or activated) complex ($[\mathrm{BLF}-\kappa\mathrm{CG}]^{\ddagger}$)

formation can provide important additional information about the κCG binding event to BLF. This approach helps understanding and evaluating the precise energy landscape of the binding of free species or the thermodynamically stable complex dissociating event, as well as, detecting the exact potential energy barrier (activation energy) dividing the bound and unbound states [48].

The temperature dependence of the $ln\ k_a$ and $ln\ k_d$ rate constants (Fig. 4.6) allows to determine the energetic parameters of $[\mathrm{BLF}-\kappa\mathrm{CG}]^{\ddagger}$ formation from the association (a) of the free molecules (κCG and BLF) or from the dissociation (d) of the BLF-κCG thermodynamically stable complex. That way, the activation energies ($E_x^{\ddagger}$) values were obtained by the Arrhenius plot (Fig. 4.6), by applying Eq. 8. The other energetic parameters (Gibbs free energy change of activation ($\Delta G_x^{\ddagger}$), enthalpy change of activation ($\Delta H_x^{\ddagger}$), and entropy change of activation ($\Delta S_x^{\ddagger}$) were calculated from Eqs. 9, 10 and 11, respectively, and the values are shown in Table 4.4.

$$E_x^{\ddagger}\,(T) = -R\left(\frac{d\ln k_x}{d\,T}\right) \tag{8}$$

$$\Delta G_x^{\ddagger} = -RTln\left(\frac{k_x h}{K_B T}\right) \tag{9}$$

$$\Delta H_x^{\ddagger} = E_x^{\ddagger} - RT \tag{10}$$

$$T\Delta S_x^{\ddagger} = \Delta H_x^{\ddagger} - \Delta G_x^{\ddagger} \tag{11}$$

Where the subscript "x" refers to the events of association (a) or dissociation (d), and R, K_B and h denotes the universal gas, Boltzmann's and the Planck's constants, respectively.

Table 4.4. Energetic parameters for transition complex formation by (a) BLF and κCG association or (d) dissociation of BLF-κCG thermodynamic stable complex, at different temperatures and pH 4.

T	Association step (a)				Dissociation step (d)			
	$E_a^{\ddagger}$	$\Delta H_a^{\ddagger}$	$\Delta G_a^{\ddagger}$	$T\Delta S_a^{\ddagger}$	$E_d^{\ddagger}$	$\Delta H_d^{\ddagger}$	$\Delta G_d^{\ddagger}$	$T\Delta S_d^{\ddagger}$
K	kJ mol^{-1}							
285.2	-236 ± 2	-238 ± 2	50.4 ± 0.1	-289 ± 2	-111.57 ± 0.05	-113.94 ± 0.05	77.61 ± 0.03	-191.55 ± 0.06
289.2	-159 ± 2	-161 ± 2	53.97 ± 0.04	-215 ± 2	-58.07 ± 0.06	-60.47 ± 0.05	79.94 ± 0.02	-140.41 ± 0.05
293.2	-74 ± 1	-76.2 ± 0.7	56.24 ± 0.02	-132.5 ± 0.7	5.0 ± 0.1	2.57 ± 0.02	81.45 ± 0.04	-78.88 ± 0.05
297.2	18.2 ± 0.1	15.70 ± 0.08	57.51 ± 0.04	-41.82 ± 0.09	76.84 ± 0.04	74.37 ± 0.04	82.08 ± 0.04	-7.71 ± 0.06
298.2	42.17 ± 0.02	39.69 ± 0.02	57.56 ± 0.03	-17.90 ± 0.04	96.08 ± 0.03	93.6 ± 0.1	81.98 ± 0.03	11.6 ± 0.1
301.2	117 ± 2	114 ± 1	57.37 ± 0.04	57 ± 1	156.7 ± 0.7	154.2 ± 0.2	81.62 ± 0.02	72.5 ± 0.2

$E_x^{\ddagger}$ and $\Delta H_x^{\ddagger}$ values increased with temperature enhance for both association and dissociation processes, starting with negative values at T < 293.2 K for $E_a^{\ddagger}$ and $\Delta H_a^{\ddagger}$ and T < 289.2 K for $E_d^{\ddagger}$ and $\Delta H_d^{\ddagger}$; assuming positive values at higher temperature. Besides that, for all temperatures the energetic barrier was higher for dissociation processes compared to the association step. This energy barrier occurs because intra- and intermolecular interactions must be broken at the same time as new interactions are formed, when LF interacts with κCG to form the $[\mathrm{BLF}-\kappa\mathrm{CG}]^{\ddagger}$.

$E_x^{\ddagger}$ and $\Delta H_x^{\ddagger}$ values can be attributed to the following sub-processes: I) restructuration of BLF and κCG interacting site solvation shell (for desolvation $E_x^{\ddagger}$ and $\Delta H_x^{\ddagger} > 0$ or for solvation $E_x^{\ddagger}$ and $\Delta H_x^{\ddagger} < 0$), II) electrostatic repulsion between BLF and κCG, promoting electric double layer charge redistribution ($E_x^{\ddagger}$ and $\Delta H_x^{\ddagger} > 0$), III) conformational changes in the macromolecules interaction sites ($E_x^{\ddagger}$ and $\Delta H_x^{\ddagger} > 0$), and IV) direct interaction between κCG and BLF sites ($E_x^{\ddagger}$ and $\Delta H_x^{\ddagger} < 0$). Therefore, at low temperatures, $E_x^{\ddagger}$ and $\Delta H_x^{\ddagger}$ values were negatives because $|\mathrm{IV}| > |\mathrm{I}+\mathrm{II}+\mathrm{III}|$ i.e., the collisional average kinetic energy (3/2 kT) is not high enough to promote higher extension processes associate with: i) the desolvation ii) counterions release from the electric double layer and iii) conformational changes in the protein and polysaccharide site to occur.

However, with the increase in the temperature, the collisional average kinetic energy became higher enough to overcome the energy that maintain the ions trapped in the electric double layer, the conformation of the molecules' sites and the H_2O that solvates the functional groups that participate in the interaction, making $|\mathrm{I}+\mathrm{II}+\mathrm{III}| > |\mathrm{IV}|$, and $E_x^{\ddagger}$ and $\Delta H_x^{\ddagger}$ values positive.

The $[\mathrm{BLF}-\kappa\mathrm{CG}]^{\ddagger}$ formation from the association of κCG and BLF free molecules was found to occur faster than from the dissociation of thermodynamically stable complex ($\Delta G_a^{\ddagger} < \Delta G_d^{\ddagger}$), probably due to the lower energy barrier for the association process ($E_a^{\ddagger}$ and $\Delta H_a^{\ddagger} < E_d^{\ddagger}$ and $\Delta H_d^{\ddagger}$). However, besides $\Delta H_x^{\ddagger}$, the entropic term also contributes to the values of $\Delta G_x^{\ddagger}$, therefore, $T\Delta S_x^{\ddagger}$ analysis is indispensable.

At low temperatures, $T\Delta S_x^{\ddagger}$ values were negative for both processes (association and dissociation), assuming positive values only at T = 301.2 K, for the association, and at T > 297.2 K, for the dissociation. Moreover, similar to E_x and $\Delta H_x^{\ddagger}$, $T\Delta S_x^{\ddagger}$ values were higher for the

thermodynamically stable BLF-κCG complex dissociation than for the BLF and κCG free molecules association.

$T\Delta S_x^{\ddagger}$ also, can be rationalized as the sum of the four molecular sub-processes: I) conformational changes of the protein and polysaccharide binding sites ($T\Delta S_x^{\ddagger} > 0$), II) desolvation of κCG and BLF molecules ($T\Delta S_x^{\ddagger} > 0$), III) release of counterions from the electric double layer of the interacting molecules ($T\Delta S_x^{\ddagger} > 0$) and IV) BLF-κCG complex formation ($T\Delta S_x^{\ddagger} < 0$). The obtained negative $T\Delta S_x^{\ddagger}$ values at low temperature suggests that $|\mathrm{IV}| > |\mathrm{I} + \mathrm{II} + \mathrm{III}|$, probably because at this temperature range the $[\mathrm{BLF} - \kappa\mathrm{CG}]^{\ddagger}$ formation occurs without strong release of H_2O molecules and counterions and with few conformational changes in the macromolecules interaction sites. These results should be attributed mainly because, at low temperature, the κCG molecules binds to BLF surface, maintaining the conformation of the binding sites and the solvation shell of both interacting macromolecules. However, with increasing temperature, $T\Delta S_x^{\ddagger}$ became positive because the increase of collisional average kinetic energy (3/2 kT) promote the flexibility increment of the BLF-binding site during BLF-κCG interaction (I), and increase of H_2O molecules and counterions release from the solvation shell and electric double of macromolecules (II and III), respectively, outweighing the loss of configurational entropy due to complex formation (IV), i.e., $|\mathrm{I} + \mathrm{II} + \mathrm{III}| > |\mathrm{IV}|$.

4.3.2.1.1 Ionic strength effect on the $[\mathrm{BLF} - \kappa\mathrm{CG}]^{\ddagger}$ formation

To understand how the electrostatic interaction contributes for $[\mathrm{BLF} - \kappa\mathrm{CG}]^{\ddagger}$ formation process, the effect of ionic strength change on the BLF-κCG interaction was studied. The sensorgrams for the BLF-κCG interaction, in the presence of KCl (100 mM) at 285.2-301.2 K, are presented in Fig. S.C.4, and from them the kinetic rate constants k_a (Fig. S.C.5) and k_d were obtained, as showed in Table 4.5.

Table 4.5. Kinetic rate constants for the association (k_a) of free BLF and κCG molecules and for dissociation (k_d) of the BLF-κCG thermodynamic stable complexes, in the presence of the KCl (100 mM) and pH 4.

	KCl			
T	0 mM		100 mM	
	k_a	k_d	k_a	k_d
K	10^3 M^{-1} s^{-1}	s^{-1}	10^3 M^{-1} s^{-1}	s^{-1}
285.2	3.52 ± 0.04	0.036 ± 0.000	1.67 ± 0.03	0.024 ± 0.004
289.2	1.07 ± 0.03	0.022 ± 0.001	1.30 ± 0.04	0.029 ± 0.006
293.2	0.58 ± 0.02	0.019 ± 0.001	1.05 ± 0.03	0.034 ± 0.005
297.2	0.48 ± 0.01	0.023 ± 0.000	0.90 ± 0.02	0.039 ± 0.005
298.2	0.51 ± 0.01	0.027 ± 0.001	0.84 ± 0.02	0.042 ± 0.006
301.2	0.70 ± 0.02	0.044 ± 0.001	0.69 ± 0.02	0.046 ± 0.006

The presence of KCl caused an increase in k_a and k_d values, except at 285.2 K in which an opposite effect was observed. A possible molecular mechanism to explain this k_a and k_d behavior can be associated to electric double layer shielding and, consequently, the decrease of electric charge asymmetry of these region, releasing counterions from both macromolecules when the ionic strength is increased.

In order to better comprehend how change in the ionic strength affect the kinetics of the $[\mathrm{BLF} - \kappa\mathrm{CG}]^{\ddagger}$ formation, the determination of KCl effect on the energetic parameters is fundamental. $E_x^{\ddagger}$, $\Delta G_x^{\ddagger}$, $\Delta H_x^{\ddagger}$ and $T\Delta S_x^{\ddagger}$ provide insights about the molecular energetics and dynamics occurring during the BLF-κCG interaction and can be easily obtained by dependence of the k_a and k_d values with temperature (Fig. S.C.6 and Table 4.6).

Table 4.6. Energetic parameters for (a) the formation of the transition complex by κCG and BLF association, and (d) dissociation of the BLF-κCG thermodynamic stable complex, in the presence of KCl (100 mM) and pH 4.

T	Association step (a)				Dissociation step (d)			
	$E_a^{\ddagger}$	$\Delta H_a^{\ddagger}$	$\Delta G_a^{\ddagger}$	$T\Delta S_a^{\ddagger}$	$E_d^{\ddagger}$	$\Delta H_d^{\ddagger}$	$\Delta G_d^{\ddagger}$	$T\Delta S_d^{\ddagger}$
K	kJ mol^{-1}							
0 mM KCl								
285.2	-236 ± 2	-238 ± 2	50.4 ± 0.1	-289 ± 2	-111.57 ± 0.05	-113.94 ± 0.05	77.61 ± 0.03	-191.55 ± 0.06
289.2	-159 ± 2	-161 ± 2	53.97 ± 0.04	-215 ± 2	-58.07 ± 0.06	-60.47 ± 0.05	79.94 ± 0.02	-140.41 ± 0.05
293.2	-74 ± 1	-76.2 ± 0.7	56.24 ± 0.02	-132.5 ± 0.7	5.0 ± 0.1	2.57 ± 0.02	81.45 ± 0.04	-78.88 ± 0.05
297.2	18.2 ± 0.1	15.70 ± 0.08	57.51 ± 0.04	-41.82 ± 0.09	76.84 ± 0.04	74.37 ± 0.04	82.08 ± 0.04	-7.71 ± 0.07
298.2	42.17 ± 0.02	39.69 ± 0.02	57.56 ± 0.03	-17.87 ± 0.04	96.08 ± 0.03	93.6 ± 0.1	81.98 ± 0.03	11.6 ± 0.1
301.2	117 ± 2	114 ± 1	57.37 ± 0.04	57 ± 1	156.7 ± 0.7	154.2 ± 0.2	81.62 ± 0.02	72.5 ± 0.2
100 mM KCl								
285.2	-38 ± 2	-40.1 ± 0.3	52 ± 1	-92 ± 1	28.9 ± 0.8	26.6 ± 0.5	79 ± 1	-52 ± 1
289.2		-40.1 ± 0.5	54 ± 2	-94 ± 2		26.5 ± 0.7	79 ± 2	-53 ± 2
293.2		-40.2 ± 0.5	55 ± 2	-95 ± 2		26.5 ± 0.7	80 ± 2	-54 ± 2
297.2		-40.2 ± 0.5	56 ± 2	-96 ± 2		26.5 ± 0.7	81 ± 2	-54 ± 2
298.2		-40.2 ± 0.5	56 ± 2	-97 ± 2		26.5 ± 0.7	81 ± 2	-54 ± 2
301.2		-40.2 ± 0.5	57 ± 2	-98 ± 2		26.4 ± 0.7	82 ± 2	-55 ± 2

In the absence of KCl, the BLF-κCG interaction was a multi-step process, i.e, the $E_x^{\ddagger}$ values were dependent on the temperature change [49]. However, with the addition of salt, this interaction between these biopolymers became one-step, that is, the $E_x^{\ddagger}$, for both association and dissociation, didn't depended on the temperature change. This behavior indicates that the presence of salt reduces the contribution of complex molecular processes, such as, the conformational change and the release of counterions from the electric double layer, making the $\mathrm{BLF-\kappa CG}$ interaction more direct.

Despite the $[\mathrm{BLF-\kappa CG}]^{\ddagger}$ formation's driving force ($\Delta G_x^{\ddagger}$) was not affected by the ionic strength change, when analyzing its components, $\Delta H_x^{\ddagger}$ and $\mathrm{T}\Delta S_x^{\ddagger}$, a strong effect was observed. For all temperature, in the presence of KCl, $\Delta H_a^{\ddagger}$ values were negative for the association ($-40.1 \leq \Delta H_a^{\ddagger} \leq -40.2$ kJ mol^{-1}) and positive for the dissociation step ($26.6 \leq \Delta H_d^{\ddagger} \leq 26.4$ kJ mol^{-1}), while $\mathrm{T}\Delta S_x^{\ddagger}$ values were negative for both association ($-92 \leq \mathrm{T}\Delta S_a^{\ddagger} \leq -98$ kJ mol^{-1}) and dissociation ($-52 \leq \mathrm{T}\Delta S_d^{\ddagger} \leq -55$ kJ mol^{-1}) step.

In the association step, $\Delta H_a^{\ddagger}$ values were negative probably because the presence of salt causes a shielding of the protein and polysaccharide's electric double layer, resulting in the decrease of the intramolecular electrostatic repulsion, and reduction of the attraction between the electric double layer's ions and biomolecules' surface. These phenomena cause the increase of the binding site's flexibility of both interacting macromolecules due to the electrostatic shielding of the biopolymer's segment-segment intramolecular repulsion. Consequently, the energetic cost of changing the binding site's conformation and restructuring the macromolecules' solvation shell, for the $[\mathrm{BLF-\kappa CG}]^{\ddagger}$ formation, is reduced, making $\Delta H_a^{\ddagger}$ negative.

On the other hand, when the $[\mathrm{BLF-\kappa CG}]^{\ddagger}$ is formed from the thermodynamically stable complex the greatest contribution for $\Delta H_d^{\ddagger}$ comes from the binding site's conformational change. In the presence of salt, the electrostatic shielding releases the counterions from the electric double layer, thus increasing the intramolecular electrostatic repulsion between the biopolymers' segments, making the energetic barrier positive.

The negative $\mathrm{T}\Delta S_x^{\ddagger}$ values, for both association and dissociation step, corroborated with the presented hypothesis. As discussed, the shielding of the biomolecules' electric double layer by the salt causes the release of counterions from this region, consequently, less counterions are available to be released during the formation of the $[\mathrm{BLF-\kappa CG}]^{\ddagger}$ resulting in a decrease of configurational entropy of the system.

4.3.2.2 Thermodynamic study

To compare surface-based thermodynamic parameters with the values determined in solution using fluorescence spectroscopy (FS), the K_b^{SPR}, ΔG_{SPR}^o, ΔH_{SPR}^o, and $T\Delta S_{SPR}^o$ values for the BLF-κCG complex formation was determined by SPR. On the basis of the obtained k_a and k_d kinetic rate constants, the equilibrium binding constant was calculated:

$$K_b^{SPR} = \frac{k_a}{k_d} \tag{12}$$

Additionally, the temperature dependence of K_b^{SPR} (Fig. S.C.7) was used to calculate the ΔH^o values, using the van't Hoff equation (Eq. 4). While ΔG^o and $T\Delta S^o$ values were calculated from Eqs. 3 and 5, respectively.

The thermodynamic parameters of BLF-κCG complex formation obtained by SPR, at pH 4 and different temperature, are showed in Table 4.7.

Table 4.7. Thermodynamic parameters (ΔG_{SPR}^o, ΔH_{SPR}^o, and $T\Delta S_{SPR}^o$) for the BLF-κCG complex formation at different temperatures (T) and pH 4. Data obtained from SPR measurements.

T	K_b^{SPR}	ΔH_{SPR}^o	ΔG_{SPR}^o	$T\Delta S_{SPR}^o$
K	10^4 M^{-1}		kJ mol^{-1}	
285.2	9.8 ± 0.1	-81 ± 3	-27.2 ± 0.3	-54 ± 3
289.2	5.0 ± 0.1		-26.0 ± 0.7	-55 ± 3
293.2	3.11 ± 0.09		-25.2 ± 0.7	-56 ± 3
297.2	2.08 ± 0.04		-24.6 ± 0.4	-56 ± 3
298.2	1.90 ± 0.04		-24.4 ± 0.6	-57 ± 3
301.2	1.61 ± 0.04		-24.3 ± 0.7	-57 ± 3

Similar to FS ($1.54 \times 10^4 \leq K_b^{FS} \leq 1.21 \times 10^4$ M^{-1}), K_b^{SPR} values obtained by SPR were in the order of 10^4 M^{-1} and they also decreased with temperature increment, showing that less BLF-κCG complexes were formed at higher temperatures. Besides that, ΔG_{SPR}^o values were consistent with the obtained by FS thermodynamic studies ($-23.10 \leq \Delta G_{FS}^o \leq -24.5$ kJ mol^{-1}), confirming that the complex (BLF-κCG) was favored in relation to the free ligands (BLF and κCG) in the equilibrium $BLF + \kappa CG \rightleftharpoons B LF - \kappa CG$. However, ΔH^o and $T\Delta S^o$ values obtained

from both techniques were very different. ΔH^o_{SPR} values (-81 kJ mol^{-1}), although also negative, was around ten times greater than the determined by FS (ΔH^o_{FS} =-8.07 kJ mol^{-1}), while, the entropic term ($T\Delta S^o$) was negative when obtained by SPR ($-54 \leq T\Delta S^o_{SPR} \leq$ -57 kJ mol^{-1}) and positive when determined by FS ($15.03 \leq T\Delta S^o_{FS} \leq$16.4 kJ mol^{-1}), at all temperatures.

These differences in the parameters obtained by these two techniques are likely due to different measurement approaches. SPR requires protein immobilization, and detects interactions that occur in all BLF sites, while FS monitors the interactions between chemical species in solution, in which only the binding that occurs near site the Trp residues can be detected. Therefore, the more negative ΔH^o_{SPR} value obtained by SPR shows the BLF-κCG interaction occurs in other BLF's binding sites beyond the ones close to the Trp residue, releasing more energy than detected by FS. On the other hand, negative $T\Delta S^o_{SPR}$ values suggest that, due to BLF immobilization on the CM5 chip surface, a decrease the BLF translational degree of freedom occurs, diminishing the contribution of the BLF configurational entropy to $T\Delta S^o_{SPR}$, making them negative.

Despite of differences in the thermodynamic parameters obtained by SPR and FS, the negative values of ΔH^o_{SPR} and $T\Delta S^o_{SPR}$ generally suggest the formation of van der Waals forces and hydrogen bond between interacting species [50], which was proposed by FS thermodynamic analysis.

4.3.2.2.1 Ionic strength effect on the formation of the BLF-κCG thermodynamic stable complex

It is well known that protein-polysaccharide interactions can occur via a variety of intermolecular forces including electrostatic interactions, hydrogen bonds, van der Waals and hydrophobic forces [41]. Therefore, these interactions can be modified by varying the pH, ionic strength and/or dielectric constant of the solvent phase.

To study the impact of ionic strength change on the thermodynamics of BLF-κCG thermodynamic stable complex formation processes, the thermodynamic parameters (K_b^{SPR}, ΔG^o_{SPR}, ΔH^o_{SPR}, and $T\Delta S^o_{SPR}$) were calculated in the presence of KCl (100 mM), by using equations 12, 3, 4 and 5, respectively. The van't Hoff plots for the interaction between BLF and κCG in the presence of KCl are presented in (Fig. S.C.8).

The K_b^{SPR}, ΔG^o_{SPR}, ΔH^o_{SPR}, and $T\Delta S^o_{SPR}$ values in the salt presence, at different temperatures, are shown in Table 4.8.

Table 4.8. Thermodynamic parameters (ΔG^o_{SPR}, ΔH^o_{SPR}, and $T\Delta S^o_{SPR}$) for the BLF-κCG complex formation, in the presence of KCl (100 mM) and pH 4. Data obtained from SPR measurements.

T	K_b^{SPR}	ΔH^o_{SPR}	ΔG^o_{SPR}	$T\Delta S^o_{SPR}$
K	10^4 M^{-1}		kJ mol^{-1}	
		0 mM KCl		
285.2	9.8 ± 0.1	-81 ± 3	-27.2 ± 0.3	-54 ± 3
289.2	4.9 ± 0.1		-26.0 ± 0.7	-55 ± 3
293.2	3.11 ± 0.09		-25.2 ± 0.7	-56 ± 3
297.2	2.08 ± 0.04		-24.6 ± 0.4	-56 ± 3
298.2	1.90 ± 0.04		-24.4 ± 0.9	-57 ± 3
301.2	1.61 ± 0.04		-24.3 ± 0.7	-57 ± 3
		100 mM KCl		
285.2	7.0 ± 0.2	-67 ± 2	-26.4 ± 0.5	-40 ± 2
289.2	4.5 ± 0.6		-25.8 ± 0.7	-41 ± 2
293.2	3.1 ± 0.3		-25.2 ± 0.6	-41 ± 2
297.2	2.3 ± 0.5		-24.8 ± 0.6	-42 ± 2
298.2	2.0 ± 0.3		-24.6 ± 0.7	-42 ± 2
301.2	1.5 ± 0.2		-24.1 ± 0.6	-43 ± 2

The change of the medium's ionic strength caused a decrease in the K_b^{SPR} values, and consequently an increase in that of ΔG^o_{SPR} values. Furthermore, in the presence of KCl, ΔH^o_{SPR}, and $T\Delta S^o_{SPR}$ values became less negative.

As previously discussed for the kinetic parameters, in the presence of salt, the shielding and subsequent release of ions from the double electric layer of BLF and κCG occur. In this scenario, the formation of the BLF-κCG complex must occur with the approximation of the protein and polysaccharide's positively charged segments causing the increase of electrostatic repulsive interaction, which causes the decrease of the energy released (ΔH^o_{SPR}) during the interaction process. At the same time, the shielding of the biopolymers' intramolecular repulsion increases the BLF and κCG binding site's flexibility, resulting in an increase of $T\Delta S^o_{SPR}$ values.

4.4 Conclusions

Both SPR and FS study showed that BLF interact with κCG forming a 1:1 complex in an aqueous media and at pH 4, which was mainly driven by van der Waals forces and hydrogen bonds that overcome electrostatic repulsion between the biopolymers. Although the increase of the ionic strength causes the electrostatic repulsion shielding, the complex stability is not altered. In addition, SPR kinetic measurements indicated that BLF-κCG interaction occurred through a multi-step process and with the formation of transition complex ($[\mathrm{BLF}-\kappa\mathrm{CG}]^{\ddagger}$). The $[\mathrm{BLF}-\kappa\mathrm{CG}]^{\ddagger}$ formation from the association of κCG and BLF free molecules was found to occur faster ($\Delta G_a^{\ddagger} < \Delta G_d^{\ddagger}$) and with higher $\Delta H_a^{\ddagger}$ and $T\Delta S_a^{\ddagger}$ values than from the dissociation of thermodynamically stable complex. The ionic strength change affected the kinetics of BLF-κCG interaction, making it a one-step process due, probably, to the macromolecules' electric double layer shielding, and the consequent release of counterions from this region. Our results show the importance of using complementary techniques for a complete characterization of the energy and dynamics of protein-polysaccharide complexes formation, which is a fundamental for designing new bionanostructures with therapeutic/technological applications.

References

[1] M. Semenova, Protein–polysaccharide associative interactions in the design of tailor-made colloidal particles, Curr. Opin. Colloid Interface Sci. 28 (2017) 15–21. doi:10.1016/j.cocis.2016.12.003.

[2] S.L. Turgeon, C. Schmitt, C. Sanchez, Protein–polysaccharide complexes and coacervates, Curr. Opin. Colloid Interface Sci. 12 (2007) 166–178. doi:10.1016/j.cocis.2007.07.007.

[3] C.G. (Kees De Kruif, R. Tuinier, Polysaccharide protein interactions, 2001. doi:10.1016/S0268-005X(01)00076-5.

[4] F. Liu, C. Ma, D.J. McClements, Y. Gao, Development of polyphenol-protein-polysaccharide ternary complexes as emulsifiers for nutraceutical emulsions: Impact on formation, stability, and bioaccessibility of β-carotene emulsions, Food Hydrocoll. 61 (2016) 578–588. doi:10.1016/j.foodhyd.2016.05.031.

[5] X. Huang, X. Huang, Y. Gong, H. Xiao, D.J. McClements, K. Hu, Enhancement of curcumin water dispersibility and antioxidant activity using core–shell protein–polysaccharide nanoparticles, Food Res. Int. 87 (2016) 1–9. doi:10.1016/j.foodres.2016.06.009.

[6] S. Sellimi, A. Benslima, V. Barragan-Montero, M. Hajji, M. Nasri, Polyphenolic-protein-polysaccharide ternary conjugates from Cystoseira barbata Tunisian seaweed as potential biopreservatives: Chemical, antioxidant and antimicrobial properties, Int. J. Biol. Macromol. (2017). doi:10.1016/j.ijbiomac.2017.08.007.

[7] M.E. Wall, S.C. Gallagher, J. Trewhella, L Arger P Roteins and M Olecular, Annu. Rev. Phys. Chem. 51 (2000) 355–380.

[8] X. Pang, H. Zhou, Rate Constants and Mechanisms of Protein- Ligand Binding, Annu. Rev. Biophys. 46 (2017) 105–130. doi:10.1146/annurev-biophys-070816-033639.

[9] J. Doublier, C. Garnier, D. Renarda, C. Sanchezb, Protein-polysaccharide interactions, Curr. Opin. Colloid Interface Sci. 5 (2000) 202–214.

[10] Y.A. Antonov, I.L. Zhuravleva, R. Cardinaels, P. Moldenaers, Macromolecular complexes of lysozyme with kappa carrageenan, Food Hydrocoll. 74 (2018) 227–238. doi:10.1016/j.foodhyd.2017.07.022.

[11] G. Sason, A. Nussinovitch, Characterization of k -carrageenan gels immersed in ethanol solutions, Food Hydrocoll. 79 (2018) 136–144. doi:10.1016/j.foodhyd.2017.12.025.

[12] S.R. Derkach, S.O. Ilyin, A.A. Maklakova, V.G. Kulichikhin, A.Y. Malkin, The rheology of gelatin hydrogels modi fi ed by k-carrageenan, LWT - Food Sci. Technol. 63 (2015) 612–619. doi:10.1016/j.lwt.2015.03.024.

[13] R.I. Baeza, D.J. Carpw, O.E. Pérezz, A.M.R. Pilosof, k -Carrageenan F Protein Interactions : Effect of Proteins on Polysaccharide Gelling and Textural Properties, Leb. u.-Technol. 35 (2002) 741–747. doi:10.1006/fstl.2002.0938.

[14] J. Liu, X. Zhan, J. Wan, Y. Wang, C. Wang, Review for carrageenan-based pharmaceutical biomaterials : Favourable physical features versus adverse biological effects, Carbohydr. Polym. 121 (2015) 27–36. doi:10.1016/j.carbpol.2014.11.063.

[15] W. Liang, X. Mao, X. Peng, S. Tang, Effects of sulfate group in red seaweed polysaccharides on anticoagulant activity and cytotoxicity, Carbohydr. Polym. 101 (2014) 776–785. doi:10.1016/j.carbpol.2013.10.010.

[16] L. Li, R. Ni, Y. Shao, S. Mao, Carrageenan and its applications in drug delivery, Carbohydr. Polym. 103 (2014) 1–11. doi:10.1016/j.carbpol.2013.12.008.

[17] S. Selvakumaran, I.I. Muhamad, S.I.A. Razak, Evaluation of kappa carrageenan as potential carrier for floating drug delivery system : Effect of pore forming agents, Carbohydr. Polym. 135 (2016) 207–214. doi:10.1016/j.carbpol.2015.08.051.

[18] V.L. Campo, D.F. Kawano, D.B. da Silva Jr., I. Carvalho, Carrageenans : Biological properties , chemical modifications and structural analysis – A review, Carbohydr. Polym. 77 (2009) 167–180. doi:10.1016/j.carbpol.2009.01.020.

[19] J. Necas, L. Bartosikova, Carrageenan : a review, Vet. Med. (Praha). 4 (2013) 187–205.

[20] V.B. Galazka, D.A. Ledward, I.G. Sumner, E. Dickinson, Influence of High Pressure on Bovine Serum Albumin and Its Complex with Dextran Sulfate, J. Agric. Food Chem. 45 (1997) 3465–3471. doi:10.1021/jf9700642.

[21] E.S. Gul, M.F. De Campos, E.E. Garcia-rojas, Polymeric complexes obtained from the interaction of bovine serum albumin and k -carrageenan, Food Hydrocoll. 45 (2015) 286–290. doi:10.1016/j.foodhyd.2014.10.023.

[22] S. Bourriot, C. Garnier, J. Doublier, Micellar-casein – k -carrageenan mixtures . I . Phase separation and ultrastructure, Carbohydr. Polym. 40 (1999) 145–157.

[23] C. Garnier, C. Michon, S. Durand, G. Cuvelier, J.-L. Doublier, B. Launay, Iota-carrageenan / casein micelles interactions : e v idence at different scales, Colloids Surfaces B Biointerfaces. 31 (2003) 177–184. doi:10.1016/S0927-7765(03)00137-1.

[24] K. Ozawa, R. Niki, S. Arima, Interaction of β -Casein and κ-Carrageenan . I . Viscosity and Turbidity under Non-gelling Conditions, Agric. Bioi. Chern. 48 (1984) 627–632. doi:10.1080/00021369.1984.10866195.

[25] M.M.O. Eleya, S.L. Turgeon, The effects of pH on the rheology of b -lactoglobulin / k -carrageenan mixed gels, Food Hydrocoll. 14 (2000) 245–251.

[26] M.M.O. Eleya, S.L. Turgeon, Rheology of k -carrageenan and b -lactoglobulin mixed gels, Food Hydrocoll. 14 (2000) 29–40.

[27] Y.A. Antonov, I.L. Zhuravleva, R. Cardinaels, P. Moldenaers, Food Hydrocolloids Speci fi c effect of the linear charge density of the acid polysaccharide on thermal aggregation / disaggregation processes in complex carrageenan / lysozyme systems, Food Hydrocoll. 70 (2017) 8–13. doi:10.1016/j.foodhyd.2017.03.017.

[28] Y.A. Antonov, I.L. Zhuravleva, R. Cardinaels, P. Moldenaers, Food Hydrocolloids Macromolecular complexes of lysozyme with kappa carrageenan, Food Hydrocoll. 74 (2018) 227–238. doi:10.1016/j.foodhyd.2017.07.022.

[29] I.A. García-montoya, T.S. Cendón, S. Arévalo-gallegos, Q. Rascón-cruz, Lactoferrin a multiple bioactive protein : An overview, BBA - Gen. Subj. 1820 (2012) 226–236. doi:10.1016/j.bbagen.2011.06.018.

[30] O.M. Conneely, Antiinflammatory Activities of Lactoferrin, J. Am. Coll. Nutr. 20 (2001) 389S–395S. doi:10.1080/07315724.2001.10719173.

[31] I.A. García-Montoya, T.S. Cendón, S. Arévalo-Gallegos, Q. Rascón-Cruz, Lactoferrin a multiple bioactive protein: An overview, Biochim. Biophys. Acta - Gen. Subj. 1820 (2012) 226–236. doi:10.1016/j.bbagen.2011.06.018.

[32] F. Liu, S. Zhang, J. Li, D. Julian, X. Liu, Recent development of lactoferrin-based vehicles for the delivery of bioactive compounds : Complexes , emulsions , and nanoparticles, Trends Food Sci. Technol. 79 (2018) 67–77. doi:10.1016/j.tifs.2018.06.013.

[33] Y. Yan, G. Marriott, Analysis of protein interactions using fluorescence technologies, Curr. Opin. Chem. Biol. 7 (2003) 635–640. doi:10.1016/j.cbpa.2003.08.017.

[34] J.R. Lakowicz, Principles of Fluorescence Spectroscopy, Trird edit, Maryland, USA, 2006. doi:10.1007/978-0-387-46312-4.

[35] N. Stănciuc, I. Aprodu, G. Râpeanu, I. van der Plancken, G. Bahrim, M. Hendrickx, Analysis of the Thermally Induced Structural Changes of Bovine Lactoferrin, J. Agric. Food Chem. 61 (2013) 2234–2243. doi:10.1021/jf305178s.

[36] J.R.Albani, Chapter 4 FLUORESCENCE QUENCHING, in: Struct. Dyn. Macromol. Absorpt. Fluoresc. Stud., 2004: pp. 141–192. doi:10.1016/B978-044451449-3/50004-6.

[37] X.L. Wei, J.B. Xiao, Y. Wang, Y. Bai, Which model based on fluorescence quenching is suitable to study the interaction between trans -resveratrol and BSA ?, Spectrochim. Acta Part A Mol. Biomol. Spectrosc. 75 (2010) 299–304. doi:10.1016/j.saa.2009.10.027.

[38] P.L. Xavier, K. Chaudhari, P.K. Verma, S.K. Pal, T. Pradeep, Luminescent quantum clusters of gold in transferrin family protein, lactoferrin exhibiting FRET, Nanoscale. 2 (2010) 2769–2776. doi:10.1039/c0nr00377h.

[39] M. Van De Weert, L. Stella, Fluorescence quenching and ligand binding: A critical discussion of a popular methodology, J. Mol. Struct. 998 (2011) 145–150. doi:10.1016/j.molstruc.2011.05.023.

[40] D. Stan, I. Matei, C. Mihailescu, M. Savin, M. Hillebrand, I. Baciu, M. Matache, Spectroscopic investigations of the binding interaction of a new indanedione derivative with human and bovine serum albumins., Molecules. 14 (2009) 1614–1626. doi:10.3390/molecules14041614.

[41] P.D. Ross, S. Subramanian, Thermodynamics of Protein Association Reactions: Forces Contributing to Stability, Biochemistry. 20 (1981) 3096–3102. doi:10.1021/bi00514a017.

[42] H. Babazada, T. Alekberli, P. Hajieva, E. Farajov, Biosensor-based kinetic and thermodynamic characterization of opioids interaction with human μ-opioid receptor, Eur. J. Pharm. Sci. 138 (2019) 105017. doi:10.1016/j.ejps.2019.105017.

[43] M. Bernetti, M. Masetti, W. Rocchia, A. Cavalli, Kinetics of Drug Binding and Residence Time, Annu. Rev. OfPhysical Chem. 70 (2019) 143–171.

[44] D.G. Drescher, D. Selvakumar, M.J. Drescher, Analysis of Protein Interactions by Surface Plasmon Resonance, in: Adv. Protein Chem. Struct. Biol., 1st ed., Elsevier Inc., 2017: pp. 1–30. doi:10.1016/bs.apcsb.2017.07.003.

[45] Y.L. Coelho, H.M.C. de Paula, A.J.P. Agudelo, A.S.B. de Castro, E.A. Hudson, A.C.S. Pires, L.H.M. da Silva, Lactoferrin-phenothiazine dye interactions : Thermodynamic and kinetic approach, Int. J. Biol. Macromol. 136 (2019) 559–569. doi:10.1016/j.ijbiomac.2019.06.097.

[46] N.M. Nunes, H.M.C. de Paula, Y.L. Coelho, L.H.M. da Silva, A.C.S. Pires, Surface plasmon resonance study of interaction between lactoferrin and naringin, Food Chem. 297 (2019) 125022. doi:10.1016/j.foodchem.2019.125022.

[47] J. de P. Rezende, E.A. Hudson, H.M.C. de Paula, Y.L. Coelho, L.H.M. da Silva, A.C. dos S. Pires, Thermodynamic and kinetic study of epigallocatechin-3-gallate-bovine lactoferrin complex formation determined by surface plasmon resonance (SPR): A comparative study with fluorescence spectroscopy, Food Hydrocoll. 95 (2019) 526–532. doi:10.1016/j.foodhyd.2019.04.065.

[48] J.R. Horn, T.R. Sosnick, A.A. Kossiakoff, Principal determinants leading to transition state formation of a protein – protein complex , orientation trumps side-chain interactions, Proc. Natl. Acad. Sci. 106 (2009) 2559–2564.

[49] W. Wang, C.J. Roberts, Non-Arrhenius Protein Aggregation, AAPS J. 15 (2013) 840–851. doi:10.1208/s12248-013-9485-3.

[50] P.D. Ross, S. Subramanian, Thermodynamics of Protein Association Reactions : Forces

Contributing to Stability, Biochemistry. 20 (1981) 3096–3102.
doi:10.1021/bi00514a017.

CONCLUSÕES GERAIS

Diferentes tipos de interações moleculares dirigem e/ou modulam a máquina da vida. Portanto, elucidar os mecanismos que governam a energética e a dinâmica da interação entre proteínas e diferentes ligantes tem sido uma meta científica importante, pois permite o controle sobre as propriedades fundamentais desse tipo de sistema, bem como sua aplicação nos diversos campos das ciências. Este trabalho teve este objetivo fundamental e forneceu importantes descobertas sobre a formação de complexos supramoleculares entre a lactoferrina e diferentes moléculas. Além disso, as determinações termodinâmicas e cinéticas dos sistemas nanoestruturados supramoleculares apresentados neste trabalho demonstraram a eficiência e a potencialidade da abordagem experimental e teórica dos resultados obtidos.

A caracterização da energética e da dinâmica de formação dos complexos entre a lactoferrina e os corantes fenotiazínicos realizada neste trabalho forneceu uma visão detalhada das interações dos corantes AZA e MB com essa importante transferrina, o que pode ser muito útil para entender como esses candidatos a fármacos interagem com seus alvos macromoleculares. O resultado mais surpreendente neste trabalho foi, sem dúvida, o valor de variação de entalpia encontrado por calorimetria. Embora as técnicas de SPR e fluorescência indicassem que os fatores entrópicos eram as únicas forças motrizes para a formação dos complexos BLF-corantes fenotiazínicos, a calorimetria mostrou que existe uma forte contribuição entálpica associada à interação desses corantes com a holo-BLF. Além disso, os dados cinéticos revelaram que embora a formação dos complexos de transição BLF-MB e BLF-AZA a partir da associação dos ligantes livres exija parâmetros de ativação muito semelhantes, a dissociação dos complexos termodinamicamente estáveis para formar os complexos de transição é muito dependente da estrutura química do corante.

Em contrapartida, o estudo da interação entre a lactoferrina e a carboximetilcelulose revelou que a CMC se liga fortemente à proteína, formando complexos solúveis. Curiosamente, embora as interações eletrostáticas tenham contribuído para a formação dos complexos BLF-CMC, forças não polieletrolíticas dominaram o processo de interação. As medidas de SPR mostraram também que a formação dos complexos entre a BLF e a CMC ocorre através de um complexo intermediário e sem alterações conformacionais intensas nos biopolímeros. Este estudo forneceu informações inéditas sobre a formação de complexos solúveis entre proteínas e polissacarídeos, o que poderia facilitar a utilização destes sistemas no encapsulamento funcional de ingredientes em diferentes áreas industriais.

Por fim, foi investigada a dinâmica e a energética de formação dos complexos supramoleculares entre a lactoferrina e a kappa-carragena, um polissacarídeo com características estruturais bastante distintas da CMC. Adicionalmente, foi avaliado o efeito da força iônica sobre os parâmetros termodinâmicos e cinéticos de formação destes complexos. Nossos resultados mostraram que apesar da ocorrência da repulsão eletrostática entre a BLF e a κCG, a interação entre estes biopolímeros foi impulsionada principalmente por forças de van der Waals e ligações de hidrogênio. Além disso, as medidas cinéticas indicaram que a interação BLF-κCG ocorreu por meio de um processo multietapas e com a formação de um complexo de transição. Curiosamente, embora a mudança na força iônica não tenha alterado a estabilidade dos complexos termodinamicamente estáveis, ela afetou a cinética da interação BLF-κCG, tornando-a um processo de uma única etapa, provavelmente, devido à blindagem da dupla camada elétrica e à consequente liberação de contra íons dessa região.

Diante destes resultados, reconhecemos a importância do uso de técnicas complementares para uma caracterização completa da energética e da dinâmica de formação de complexos entre proteínas e polissacarídeos, bem como, entre proteínas e pequenas moléculas, o que é fundamental para estabelecer uma base teórica forte acerca destes sistemas, bem como, proporcionar ferramentas para o desenvolvimento e aprimoramento de bionanoestruturas com aplicações estratégicas. Além disso, estamos certos da importância de trabalhos fundamentais como os realizados nesta tese para a compreensão profunda de sistemas complexos, como são os formados por proteína-corante e proteína-polissacarídeo.

Apêndice A

Supporting Information of the Article 1:

Lactoferrin-phenothiazine dye interactions: thermodynamic and kinetic approach

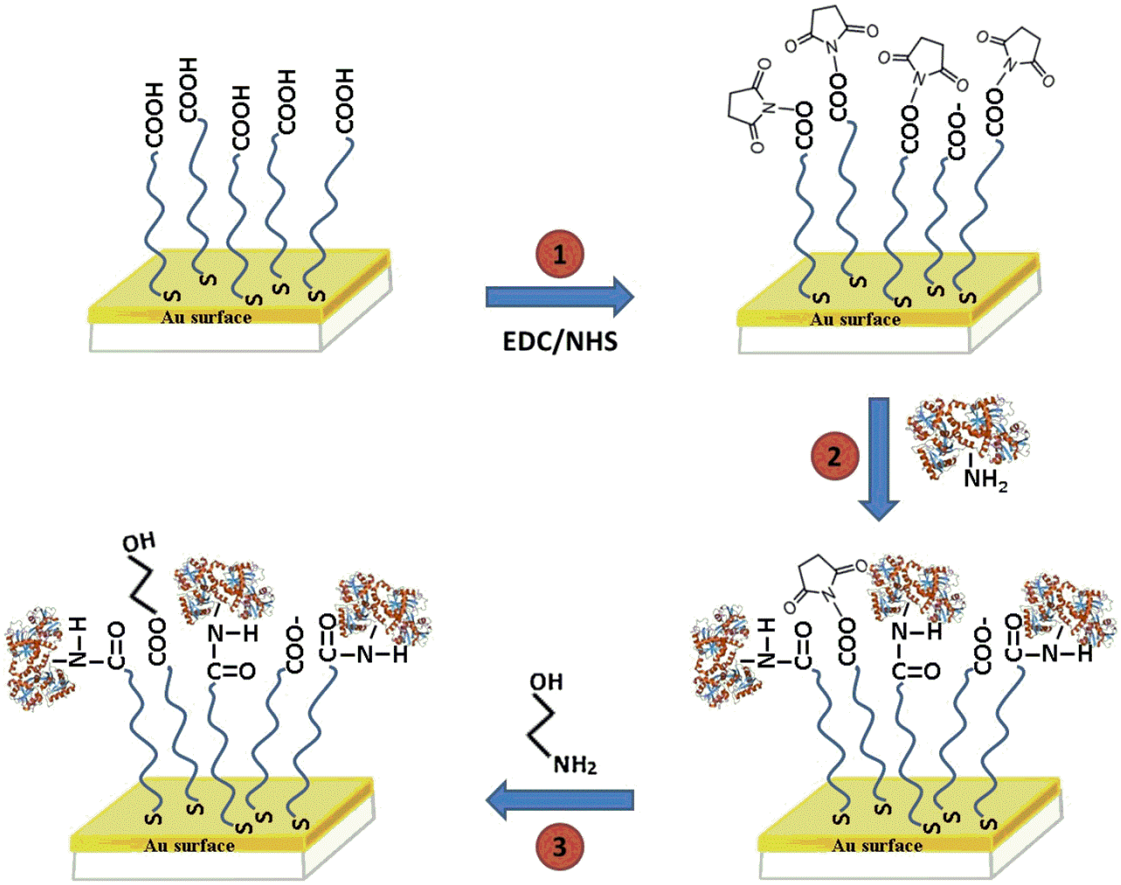

Fig. S.A.1. Schematic illustration of BLF immobilization by amine coupling: (1) activation of -COOH in CM5 sensorchip by EDC/NHS, (2) immobilization of the BLF through covalent bond formation, and (3) deactivation of unreacted activated ester sites by ethanolamines.

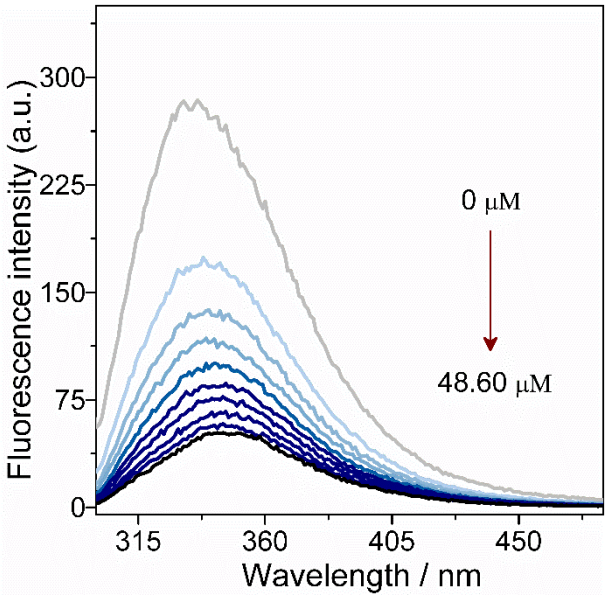

Fig. S.A.2. Steady state fluorescence emission spectrum of BLF (20 μM) titrated with AZA (0-48.60 μM). All experiments were done in phosphate buffer pH 7.4 at 298.2 K.

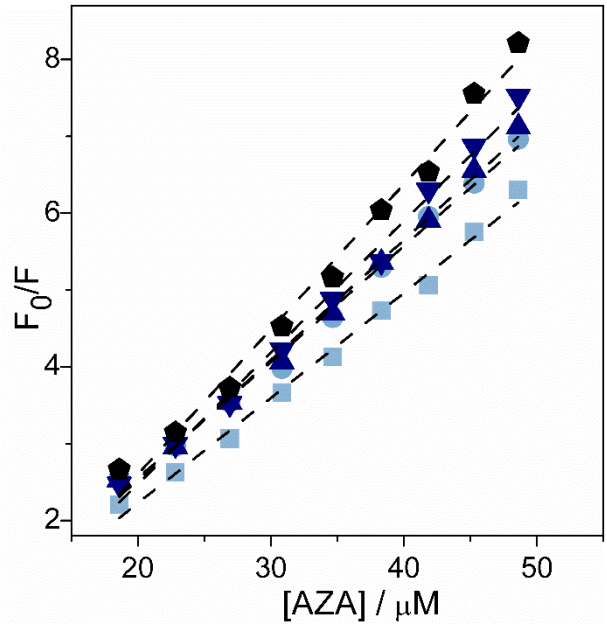

Fig. S.A.3. Stern-Volmer plots for the BLF fluorescence quenching due to binding with AZA, at (■) 283.2 K; (●) 293.2 K; (▲) 298.2 K; (▼) 303.2 K; (⬟) 313.2 K. and pH 7.4.

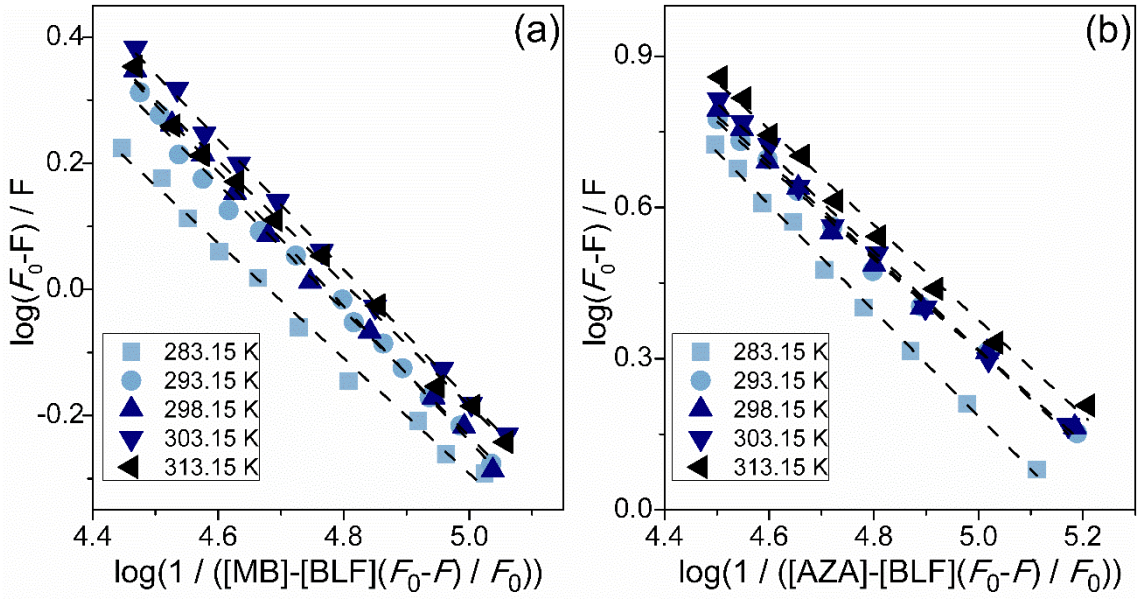

Fig. S.A.4. Plot of $log(F_0 - F)/F$ *versus* $log(1/([Q_T] - (F_0 - F)[BLF]/F_0))$ for the determination of the K_b and n values of the complex between: (a) BLF-MB and b) BLF-AZA.

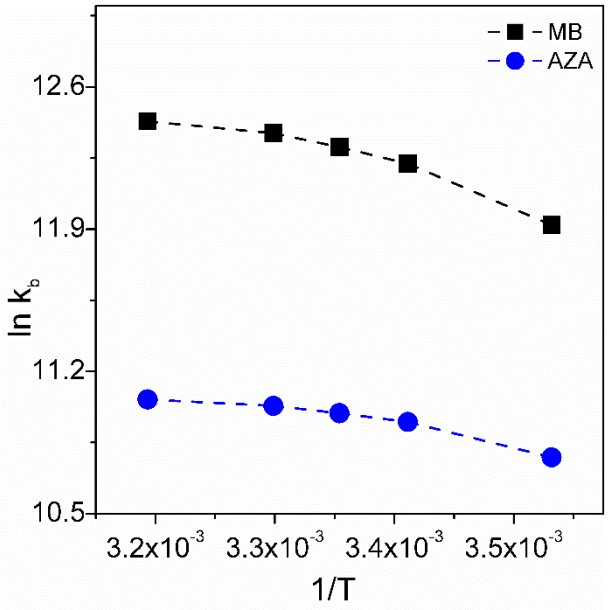

Fig. S.A.5. Plot of $ln\ K_b$ *versus* 1/T (van't Hoff approach) for the interaction of: (■) BLF-MB and (●) BLF-AZA obtained from fluorescence experiments. (r^2 = 0.99).

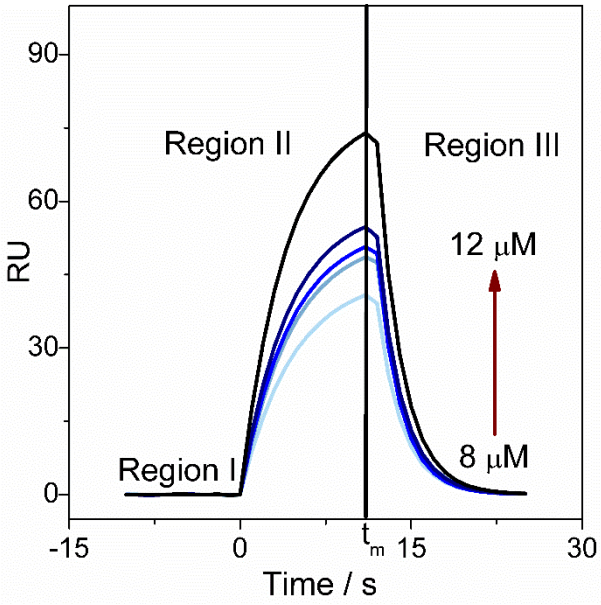

Fig. S.A.6. Sensorgram obtained from injection of AZA (8-12 μM) flowing over a CM5 low-density BLF-immobilized sensor-chip surface (3890 RU) at 298.2 K and pH 7.4. The arrows indicate increasing of concentrations de AZA solution.

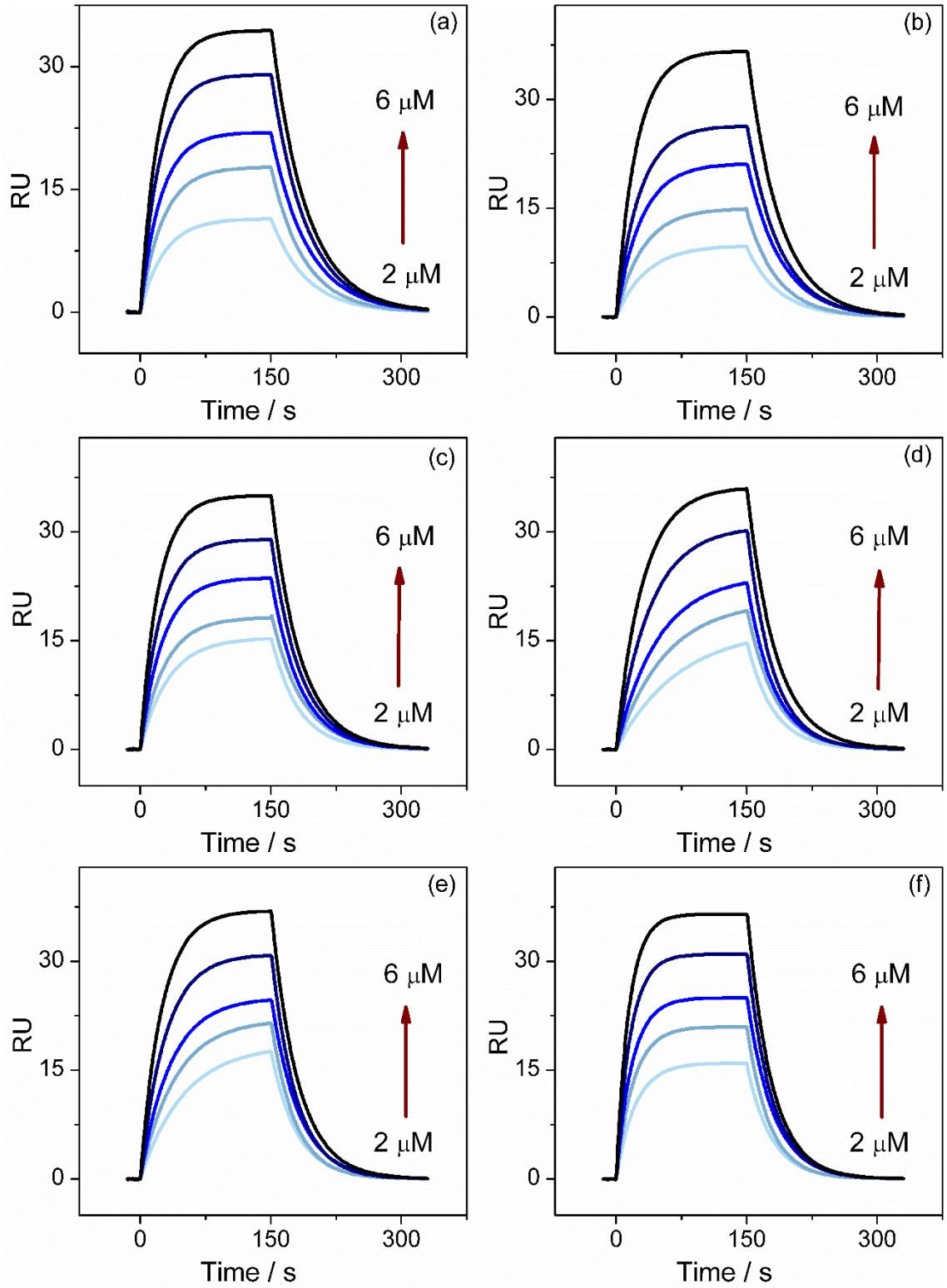

Fig. S.A.7. Sensorgrams (RU x time) for 2-6 μM MB interaction kinetic with BLF at different temperatures: (a) 285.2 K, (b) 289.2 K, (c) 293.2 K, (d) 297.2 K, (e) 298. 2 K, (f) 301. 2 K. The arrows indicate increasing of concentrations de MB solution.

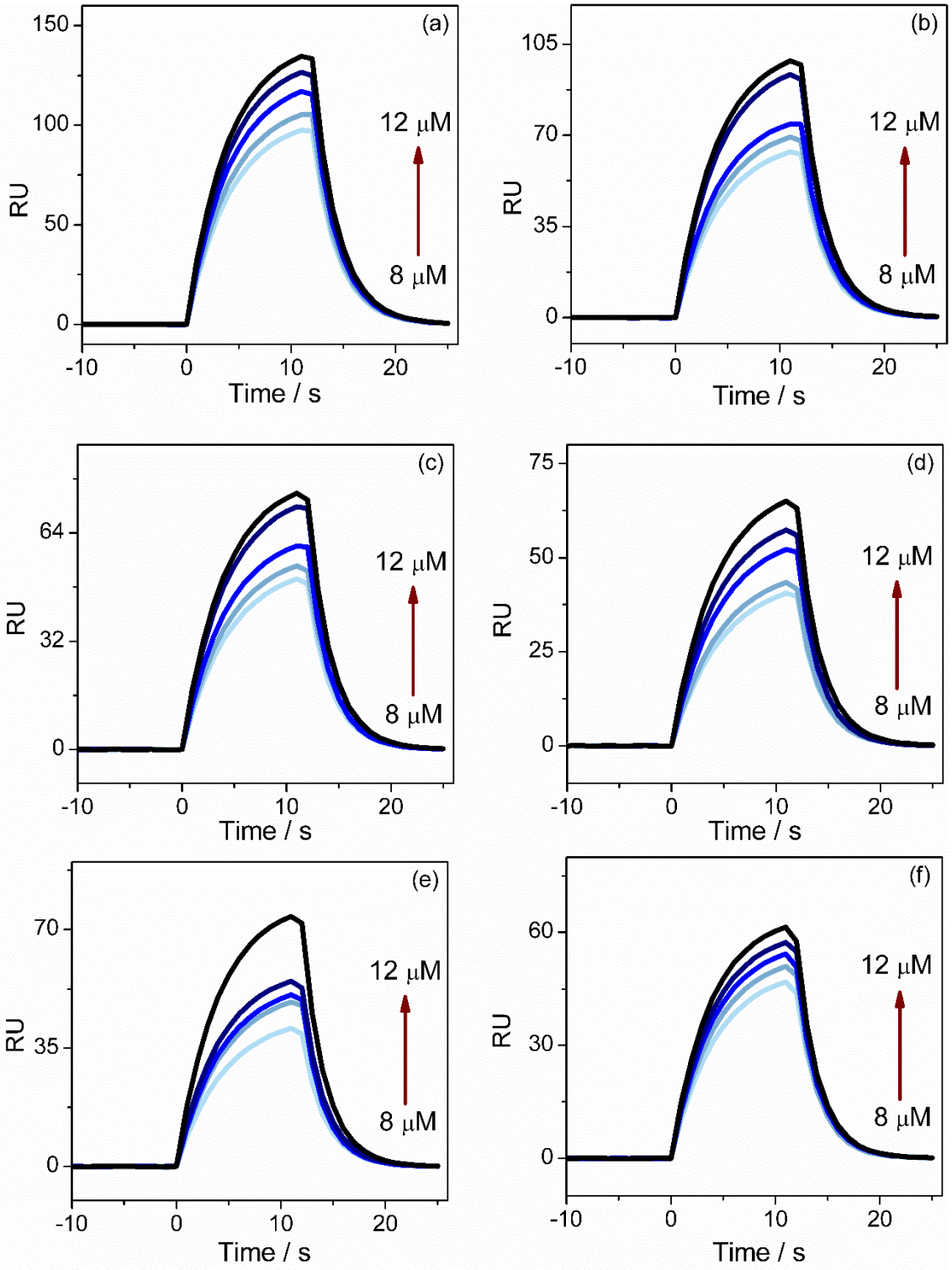

Fig. S.A.8. Sensorgrams (RU x time) for 8-12 μM AZA interaction kinetic with BLF at different temperatures: (a) 285.2 K, (b) 289.2 K, (c) 293.2 K, (d) 297.2 K, (e) 298.2 K, (f) 301.2 K. The arrows indicate increasing of concentrations de AZA solution.

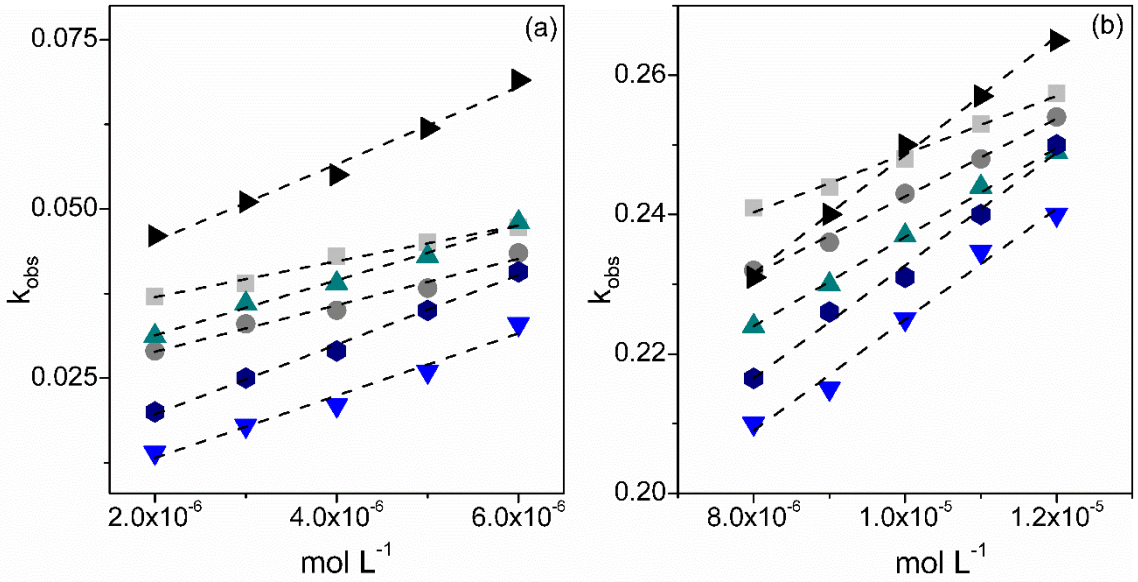

Fig. S.A.9. Plot of k_{obs} as a function of AM (a) or AZA (b) concentration, used to determine k_a at temperatures: (■) 285.2 K, (●) 289.2 K, (▲) 293.2 K, (▼) 297.2 K, (⬢) 298.2 K and (▶) 301.2 K.

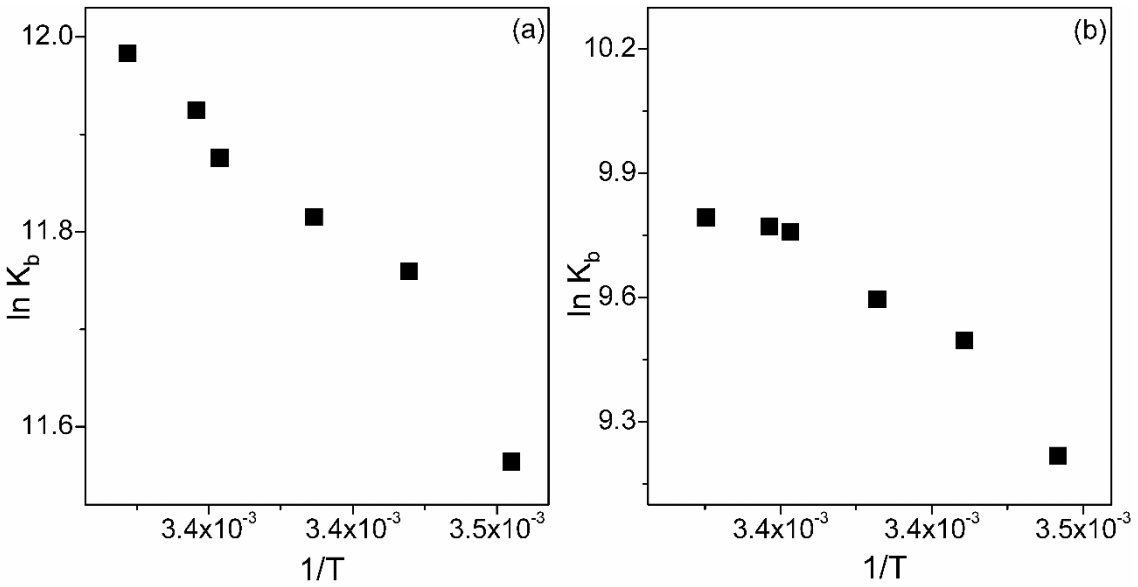

Fig. S.A.10. Plot of *ln* K_b *versus* 1/*T* (van't Hoff approach) for the interaction of: (a) BLF-MB and (b) BLF-AZA obtained from SPR experiments.

Table S.A.1. Values of $\Delta G_a^{\ddagger}$ and $\Delta G_d^{\ddagger}$ for the BLF-MB and BLF-AZA interactions at different temperatures obtained from SPR experiments.

T	BLF-MB		BLF-AZA	
	$\Delta G_a^{\ddagger}$	$\Delta G_d^{\ddagger}$	$\Delta G_a^{\ddagger}$	$\Delta G_d^{\ddagger}$
K	kJ mol^{-1}		kJ mol^{-1}	
285.2	51.0 ± 0.1	78.5 ± 0.1	50.0 ± 0.2	71.8 ± 0.2
289.2	51.2 ± 0.2	79.4 ± 0.2	49.99 ± 0.05	72.82 ± 0.07
293.2	51.5 ± 0.1	80.30 ± 0.08	50.4 ± 0.1	73.8 ± 0.2
297.2	51.93 ± 0.03	81.27 ± 0.08	50.6 ± 0.2	74.7 ± 0.1
298.2	51.84 ± 0.05	81.4 ± 0.2	50.7 ± 0.2	74.93 ± 0.08
301.2	52.1 ± 0.1	82.1 ± 0.2	51.1 ± 0.2	75.7 ± 0.1

Table S.A.2. $\Delta H^{\ddagger}$ and $T\Delta S^{\ddagger}$ values of association and dissociation processes for the BLF-MB and BLF-AZA interactions at different temperatures obtained from SPR experiments.

T	BLF-MB				BLF-AZA			
	$\Delta H_a^{\ddagger}$	$\Delta H_d^{\ddagger}$	$T\Delta S_a^{\ddagger}$	$T\Delta S_d^{\ddagger}$	$\Delta H_a^{\ddagger}$	$\Delta H_d^{\ddagger}$	$T\Delta S_a^{\ddagger}$	$T\Delta S_d^{\ddagger}$
K	kJ mol^{-1}				kJ mol^{-1}			
285.2	31 ± 2	14 ± 1	-20 ± 2	-65 ± 1	30 ± 2	4.0 ± 0.6	-20 ± 2	-67.8 ± 0.7
289.2	31 ± 2	14 ± 1	-20 ± 2	-66 ± 1	30 ± 2	4.0 ± 0.6	-20 ± 2	-68.8 ± 0.6
293.2	31 ± 2	14 ± 1	-21 ± 2	-67 ± 1	30 ± 2	4.0 ± 0.6	-21 ± 2	-69.8 ± 0.6
297.2	31 ± 2	14 ± 1	-21 ± 2	-68 ± 1	30 ± 2	3.9 ± 0.6	-21 ± 2	-70.8 ± 0.6
298.2	31 ± 2	14 ± 1	-21 ± 2	-68 ± 1	30 ± 2	3.9 ± 0.6	-21 ± 2	-71.0 ± 0.6
301.2	31 ± 2	14 ± 1	-21 ± 2	-68 ± 1	30 ± 2	3.9 ± 0.6	-22 ± 2	-71.8 ± 0.6

Apêndice B

Supporting Information of the Article 2:

Energetic characterization of supramolecular structure formation between carboxymethylcellulose and lactoferrin

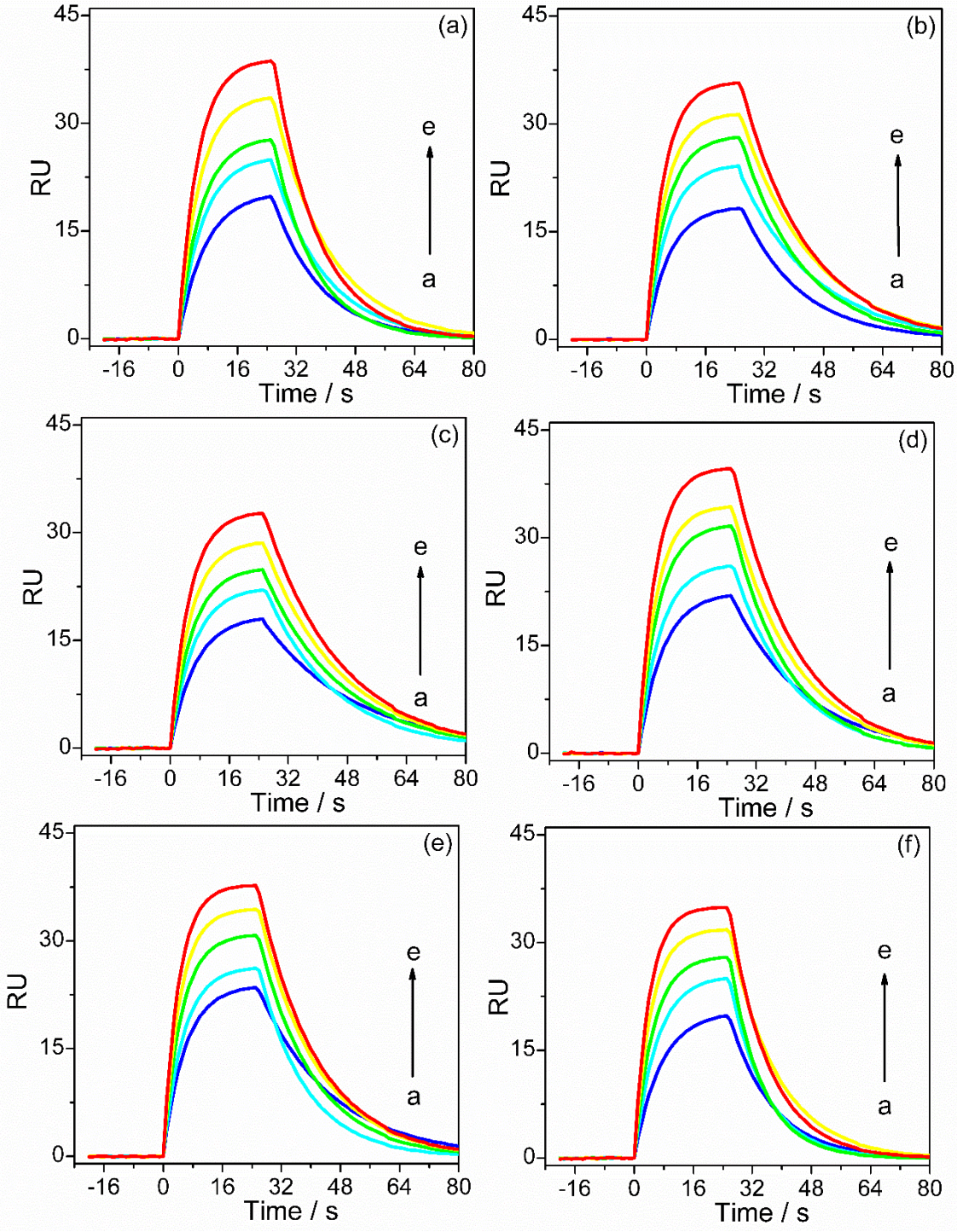

Fig. S.B.1. Sensorgrams for BLF interacting with CMC at different concentrations (a-e: 3 x 10^{-6} – 3.4 x 10^{-6} mol L^{-1}), pH 4, and different temperatures: (a) 285.2 K, (b) 289.2 K, (c) 293.2 K, (d) 297.2 K, (e) 298.2 K, (f) 301.2 K.

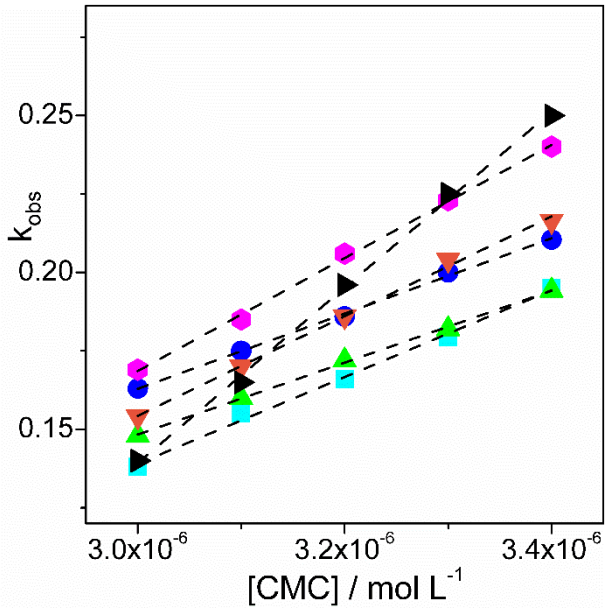

Fig. S.B.2. Plot of k_{obs} as a function of CMC concentration, used to determine k_a at temperatures: (■) 285.2 K, (●) 289.2 K, (▲) 293.2 K, (▼) 297.2 K, (⬢) 298.2 K and (▶) 301.2 K.

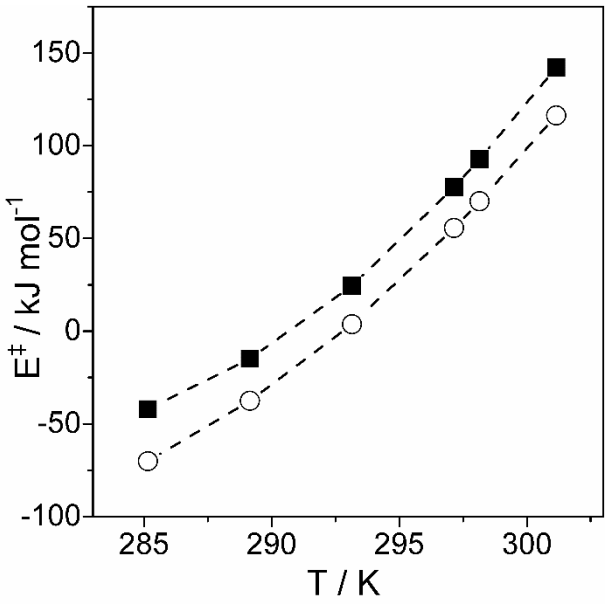

Fig. S.B.3. Activation energy *versus* temperature plot to form activated complex from: (■) association of free BLF and CMC biomolecules and (○) dissociation of BLF-CMC stable complex.

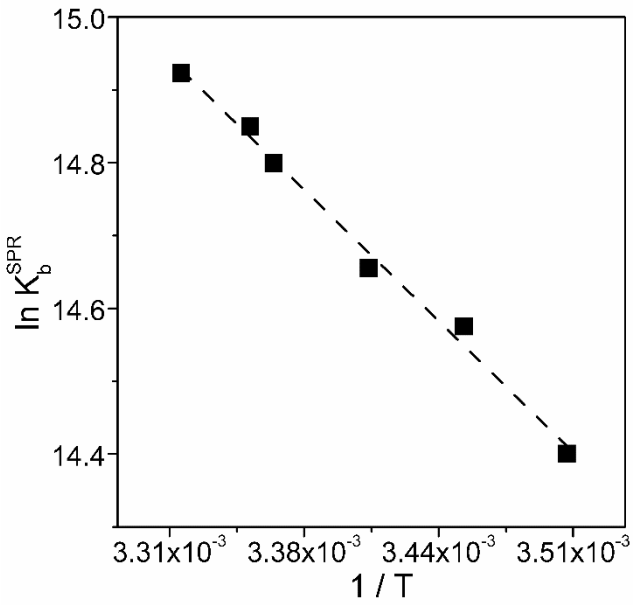

Fig. S.B.4. Van't Hoff plot (ln K_b^{SPR} as a function of $1/T$) for the interaction between BLF and CMC studied by SPR at pH 4.

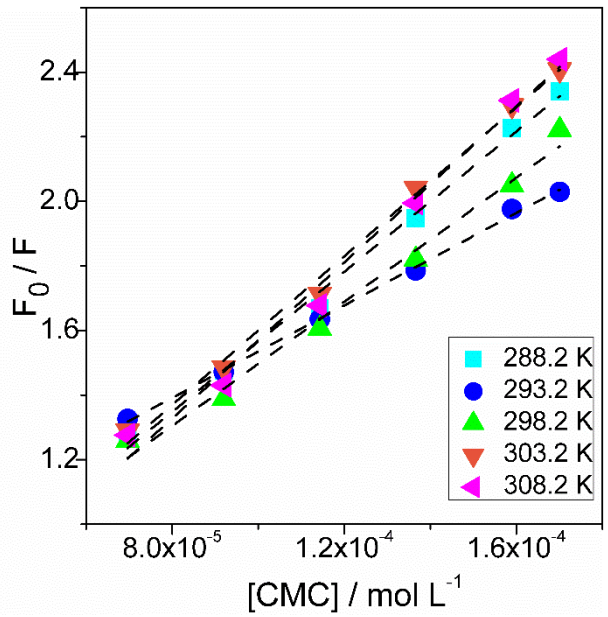

Fig. S.B.5. Stern-Volmer plots for the BLF fluorescence quenching due to binding with CMC, at pH 4.

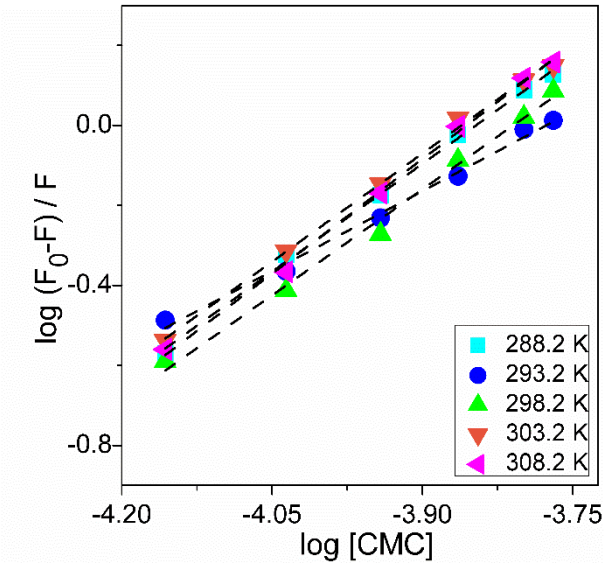

Fig. S.B.6. Plot for the determination of K_b^{FS} and n values of the complex between BLF and CMC at pH 4.

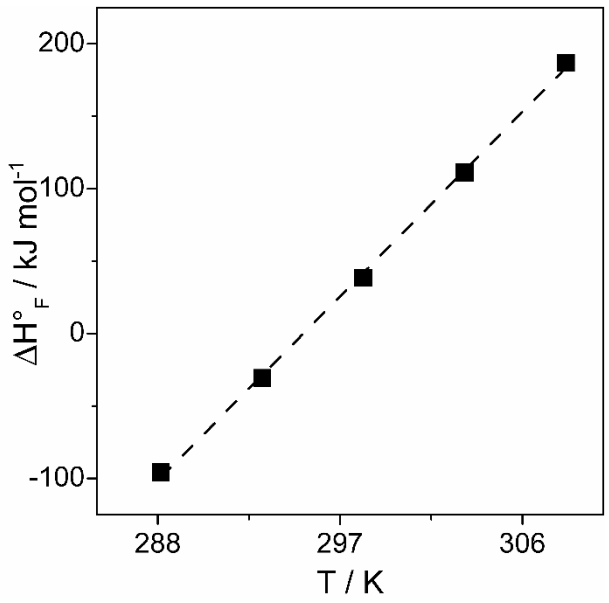

Fig. S.B.7. ΔH_{FS}^{o} *versus* T plot for BLF-CMC interaction obtained by fluorescence spectroscopy.

Apêndice C

Supporting Information of the Article 3:

Complexation between lactoferrin and κ-carrageenan: molecular insights obtained by surface plasmon resonance and fluorescence spectroscopy

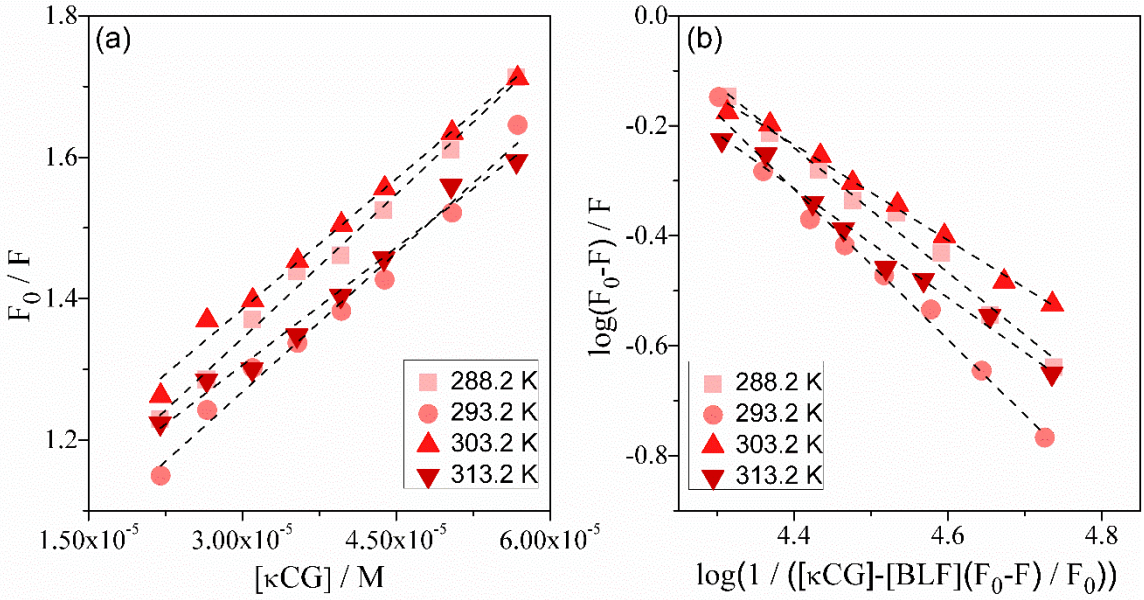

Fig. S.C.1. Plots for determination of the interaction parameters between native BLF and κCG, according to (a) Stern-Volmer and (b) modified double logarithm models, obtained and different temperatures and pH 4.

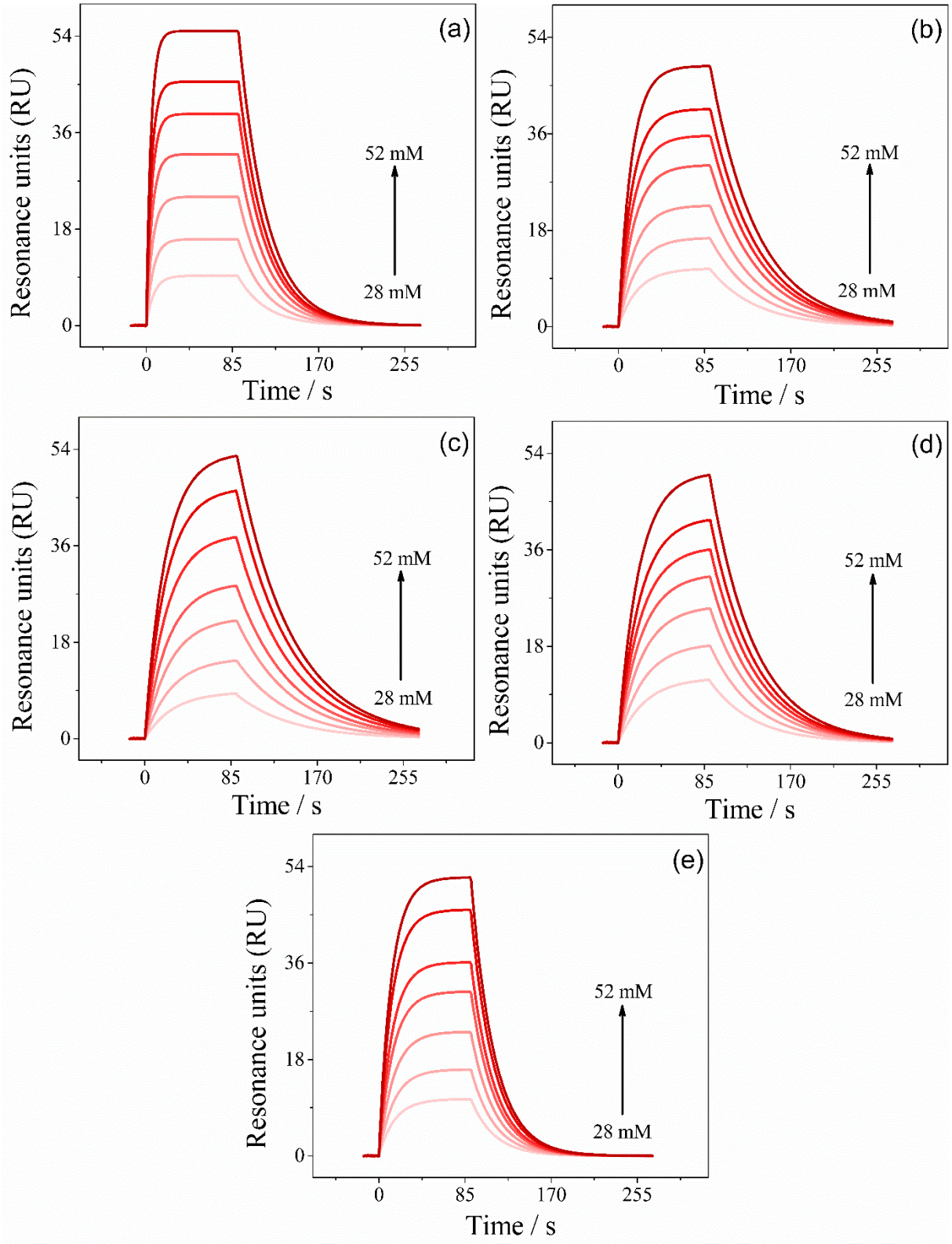

Fig. S.C.2. Sensorgrams for BLF interacting with κCG at different concentrations (28 mM - 52 mM), pH 4, and different temperatures: (a) 285.2 K, (b) 289.2 K, (c) 293.2 K, (d) 297.2 K, (e) 301.2 K.

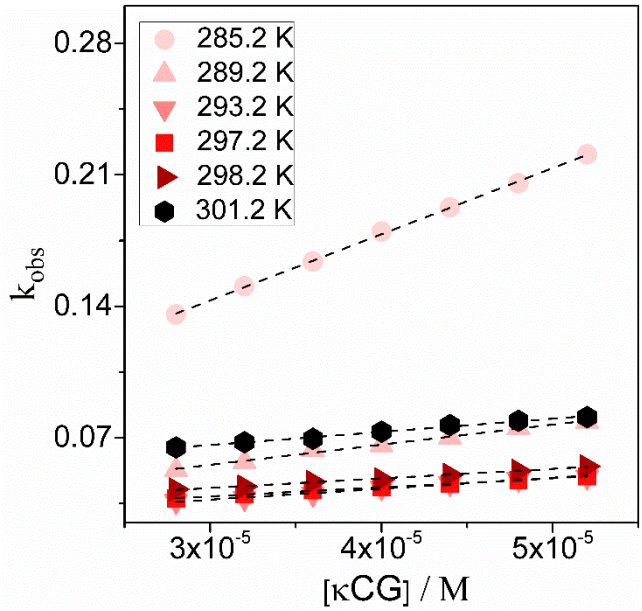

Fig. S.C.3. Plot of k_{obs} as a function of κCG concentration, used to determine k_a at temperatures and pH 4.

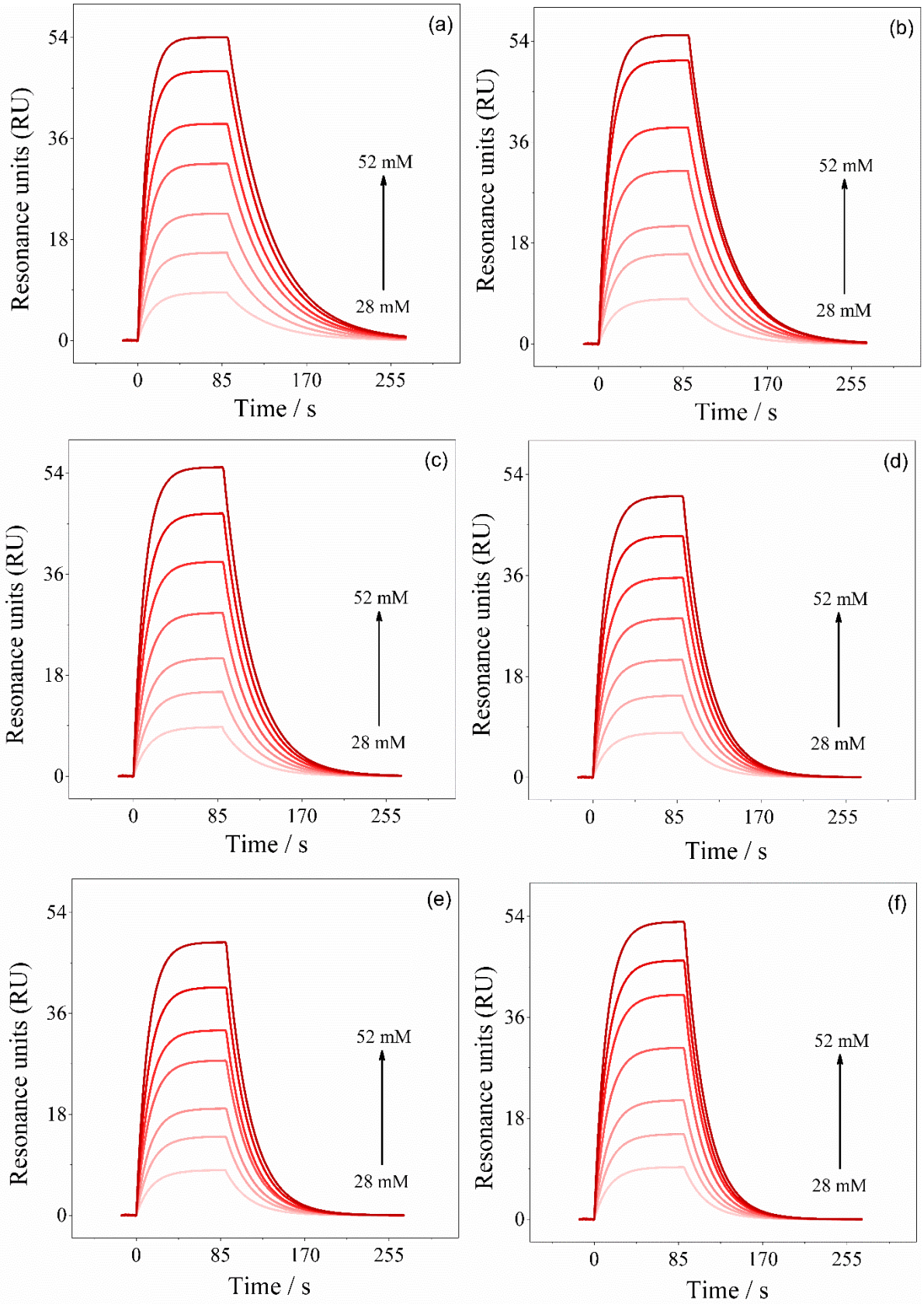

Fig. S.C.4. Sensorgrams for BLF interacting with κCG at different concentrations (28 mM - 52 mM), in the presence of the KCl (100 mM), pH 4, and different temperatures: (a) 285.2 K, (b) 289.2 K, (c) 293.2 K, (d) 297.2 K, (e) 301.2 K.

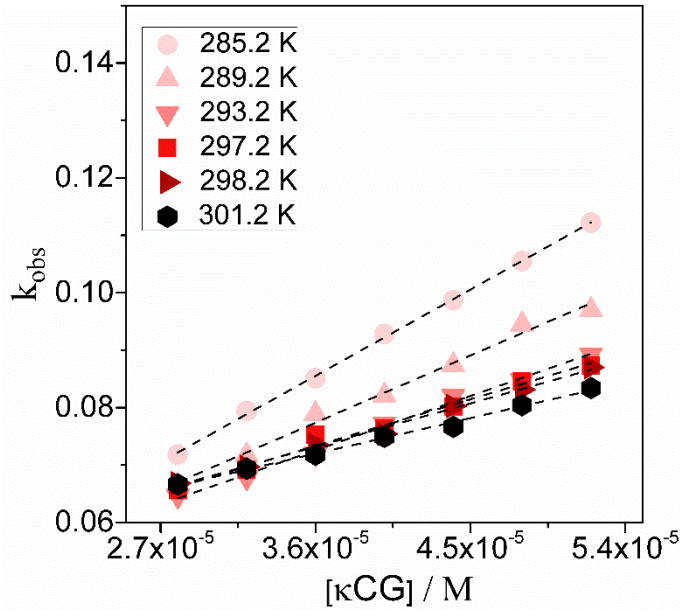

Fig. S.C.5. Plot of k_{obs} as a function of κCG concentration, used to determine k_a in the presence of the KCl (100 mM) and pH 4.

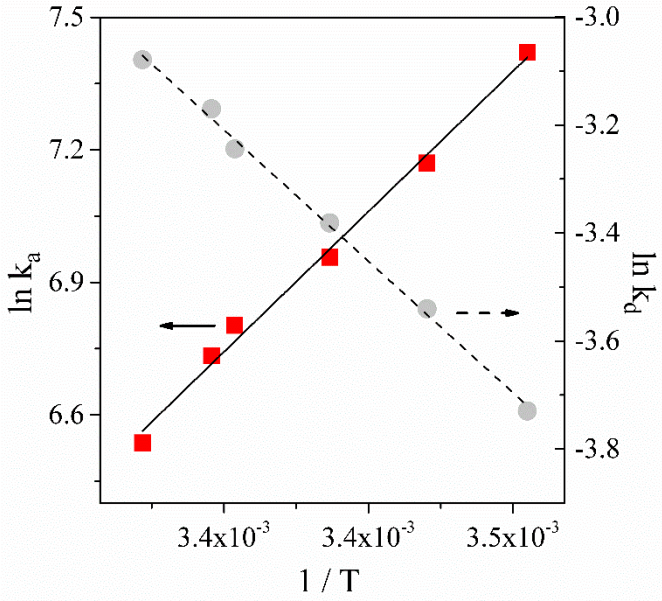

Fig. S.C.6. $ln\ k_a$ and $ln\ k_d$ *versus* $1/T$ for BLF-κCG transition complex formation in the presence of the KCl (100 mM) and pH 4. Association (■) and dissociation (●).

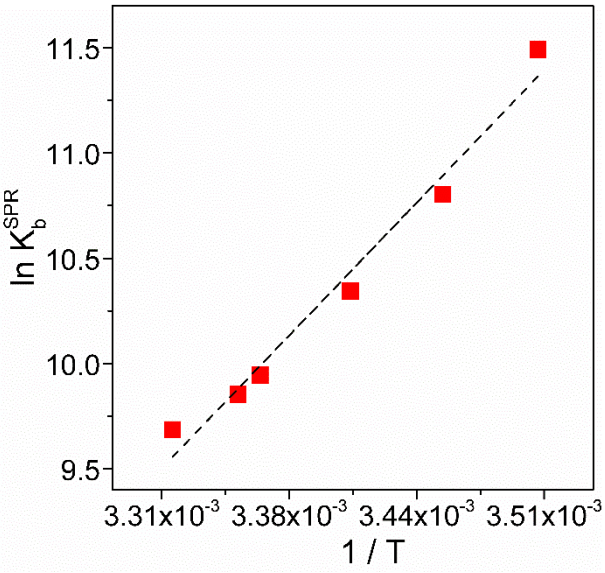

Fig. S.C.7. Van't Hoff plot (ln K_b^{SPR} as a function of $1/T$) for the interaction between BLF and κCG studied by SPR at pH 4.

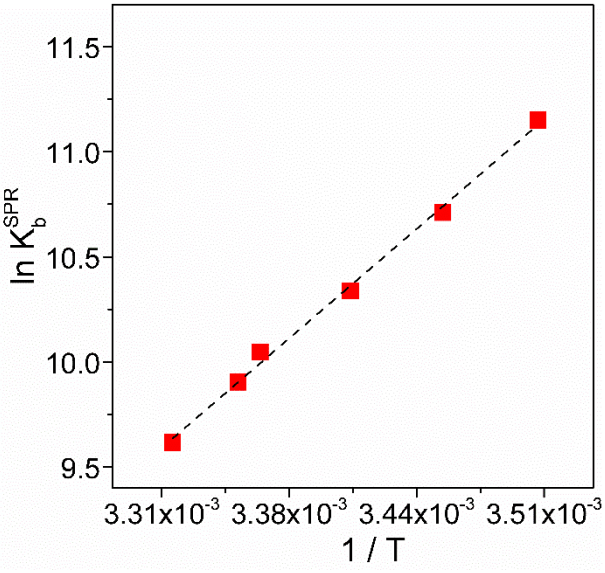

Fig. S.C.8. Van't Hoff plot (ln K_b^{SPR} as a function of $1/T$) for the interaction between BLF and κCG studied by SPR in the presence of the KCl (100 mM) and pH 4.

Apêndice D

Produção Científica

Artigos completos publicados em periódicos

1. PAIVA, PAULO HENRIQUE C.; **COELHO, YARA L.**; DA SILVA, LUIS HENRIQUE M.; PINTO, MAXIMILIANO S.; VIDIGAL, MÁRCIA CRISTINA T.R.; PIRES, ANA CLARISSA DOS S. Influence of protein conformation and selected Hofmeister salts on bovine serum albumin/lutein complex formation. FOOD CHEMISTRY JCR, v. 305, p. 125463, 2020. https://doi.org/10.1016/j.foodchem.2019.125463

2. CASTRILLON, ELKIN DARIO C.; **COELHO, YARA L.**; AGUDELO, ÁLVARO JAVIER P.; MARQUES, ISABELA A.; HUDSON, ELIARA A.; PIRES, ANA CLARISSA S.; DA SILVA, LUIS HENRIQUE M. Contribution of different chemical groups to the driving forces for the partition of phenylmethane dyes in the PEO1500 + MgSO4 + H2O aqueous two-phase system. FLUID PHASE EQUILIBRIA JCR, v. 508, p. 112451, 2020. https://doi.org/10.1016/j.fluid.2019.112451

3. AGUDELO, ÁLVARO JAVIER PATIÑO; FERREIRA, GUILHERME MAX DIAS; FERREIRA, GABRIEL MAX DIAS; **COELHO, YARA LUIZA**; HUDSON, ELIARA ACIPRESTE; PIRES, ANA CLARISSA DOS SANTOS; DA SILVA, LUIS HENRIQUE MENDES. Aggregation of sodium dodecylbenzene sulfonate: Weak molecular interactions modulated by imidazolium cation of short alkyl chain length. COLLOIDS AND SURFACES A-PHYSICOCHEMICAL AND ENGINEERING ASPECTS JCR, v. 589, p. 124435, 2020. https://doi.org/10.1016/j.colsurfa.2020.124435

4. LELIS, C. A. ; NUNE, N. M.; CAMPOS, H. M.; **COELHO, YARA LUIZA**; DA SILVA, L. H. M.; PIRES, A. C. S. Insights into protein-curcumin interactions: Kinetics and thermodynamics of curcumin and lactoferrin binding. FOOD HYDROCOLLOIDS JCR, p. 105825, 2020. https://doi.org/10.1016/j.foodhyd.2020.105825

5. REZENDE, JAQUELINE DE PAULA; PACHECO, ANA FLÁVIA COELHO; MAGALHÃES, OTÁVIO FERNANDES; **COELHO, YARA LUIZA**; VIDIGAL, MÁRCIA CRISTINA TEIXEIRA RIBEIRO; DA SILVA, LUIS HENRIQUE MENDES; PIRES, ANA CLARISSA DOS SANTOS. Polydiacetylene/triblock copolymer/surfactant nanoblend: A simple and rapid method for the colorimetric screening of enrofloxacin residue. FOOD CHEMISTRY JCR, v. 280, p. 1-7, 2019. https://doi.org/10.1016/j.foodchem.2018.12.033

6. REZENDE, JAQUELINE DE PAULA; HUDSON, ELIARA ACIPRESTE; DE PAULA, HAUSTER MAXIMILER CAMPOS; **COELHO, YARA LUIZA**; DA SILVA, LUIS HENRIQUE MENDES; PIRES, ANA CLARISSA DOS SANTOS. Thermodynamic and kinetic study of epigallocatechin-3-gallate-bovine lactoferrin complex formation determined by surface plasmon resonance (SPR): A comparative study with fluorescence spectroscopy. FOOD HYDROCOLLOIDS JCR, v. 95, p. 526-532, 2019. https://doi.org/10.1016/j.foodhyd.2019.04.065

7. **COELHO, Y. L.**; CAMPOS, H. M. ; AGUDELO, ALVARO JAVIER PATIÑO; BENHAMEA, A. S. ; HUDSON, E. A.; PIRES, A. C. S.; DA SILVA, L. H. M. Lactoferrin-phenothiazine dye interactions: Thermodynamic and kinetic approach. INTERNATIONAL JOURNAL OF BIOLOGICAL MACROMOLECULES JCR, v. 136, p. 559-569, 2019. https://doi.org/10.1016/j.ijbiomac.2019.06.097

8. NUNE, N. M.; CAMPOS, H. M.; **COELHO, Y. L.**; DA SILVA, L. H. M.; PIRES, A. C. S. Surface Plasmon Resonance Study of Interaction Between Lactoferrin and Naringin. FOOD CHEMISTRY JCR, v. 297, p. 125022, 2019. https://doi.org/10.1016/j.foodchem.2019.125022

9. AGUDELO, A. J. P.; **COELHO, Y. L.**; FERREIRA, G. M. D.; FERREIRA, G. M. D.; HUDSON, E. A.; PIRES, A. C. S.; DA SILVA, L. H. M. Solvophobic effect of 1-alkyl-3-methylimidazolium chloride on the thermodynamic of complexation between β-cyclodextrin and dodecylpyridinium cation. COLLOIDS AND SURFACES A-PHYSICOCHEMICAL AND ENGINEERING ASPECTS JCR, v. 582, p. 123850, 2019. https://doi.org/10.1016/j.colsurfa.2019.123850

10. HUDSON, E. A.; REZENDE, J. P.; CAMPOS, H. M.; **COELHO, YARA LUÍZA**; DA SILVA, L. H. M.; PIRES, A. C. S. Energetic parameters of β-casein/quercetin activated and thermodynamically stable complex formation accessed by Surface Plasmon Resonance. COLLOIDS AND SURFACES B-BIOINTERFACES JCR, p. 798-805, 2019. https://doi.org/10.1016/j.colsurfb.2019.06.048

11. DE PAULA, HAUSTER MAXIMILER CAMPOS; **COELHO, YARA LUIZA**; AGUDELO, ALVARO JAVIER PATIÑO; REZENDE, JAQUELINE DE PAULA; FERREIRA, GABRIEL MAX DIAS; FERREIRA, GUILHERME MAX DIAS; PIRES, ANA CLARISSA DOS SANTOS; DA SILVA, LUIS HENRIQUE MENDES. Kinetics and thermodynamics of bovine serum albumin interactions with Congo red dye. COLLOIDS AND SURFACES B-BIOINTERFACES JCR, v. 159, p. 737-742, 2017. https://doi.org/10.1016/j.colsurfb.2017.08.036

12. PATRÍCIO, PAMELA R.; CUNHA, ROSELAINE C.; RODRIGUEZ VARGAS, SILVIA J.; **COELHO, YARA L.**; MENDES DA SILVA, LUIS H.; HESPANHOL DA SILVA, MARIA C. Chromium speciation using aqueous biphasic systems: Development and mechanistic aspects. SEPARATION AND PURIFICATION TECHNOLOGY JCR, v. 158, p. 144-154, 2015. https://doi.org/10.1016/j.seppur.2015.12.013

Artigos completos aceitos para publicação em periódicos

1. COELHO, Y. L.; AGUDELO, A. J. P.; FERREIRA, G. M. D.; FERREIRA, G. M. D.; BENHAMEA, A. S.; HUDSON, E. A.; PIRES, A. C. S. ; DA SILVA, L. H. M. Insights into the Partitioning of Phenothiazine Dyes in Aqueous Two-Phase Systems. JOURNAL OF THE BRAZILIAN CHEMICAL SOCIETY JCR, 2020.